Rate Constants for Charge Transfer Across the Semiconductor/Liquid Interface

Thesis by

Arnel M. Fajardo

In Partial Fulfillment of the Requirements for the Degree of Doctor of Philosophy

California Institute of Technology

Pasadena, California

1999

(Submitted 14 September 1998)

Copyright © 1999

Arnel M. Fajardo

All rights reserved

Acknowledgments

First of all, I would like to thank Nate for his professional guidance during my doctoral development. One of Nate's true strengths is his scientific rigor, and this relentless pursuit of fact is one of the distinguishing hallmarks of the Lewis Group. The other part of Nate's character that I would like to recognize is his ability to teach and to communicate ideas on an elementary level. I've been fortunate to witness these two traits on display, and I hope that I've picked up those traits myself in the five years that I've been at Caltech. The final criterion of one's graduate experience is whether one would "do it all over again," and I have absolutely no regrets about joining the Lewis Group in 1993.

Speaking of which, I'd like to acknowledge the Lewis Group for making the last five years a truly entertaining experience. First, the old guard. Ashish Bansal and Gary Shreve showed me the ropes of doing research in 217 and 221 Noyes. Mark Lonergan gave me a chance to think out and discuss plenty of scientific concepts.

The Lewis Group of September 1998 is replete with an entire cast of characters that would be the envy of any primetime sitcom. While mostly everyone has helped me at some point (I've probably borrowed a book off your desk or used some of your office supplies), I'd like to recognize a few individuals. Will Royea, prankster and wiseass extraordinaire, has bailed me out of many a jam since he's been here. I've also had some great conversations with him on everything from band bending to Nate's ever-changing public popularity level. For the real weighty topics, I could always rely on George Coia for valuable insight, incisive commentary, and maybe even a humorous anecdote or two. Chris Claypool has provided lots of useful advice, whether it involved professional career paths or Super Bowl wagers. Rob Rossi has continually found generous ways to help out, ranging from fixing instruments to clarifying the nature of interfacial electric fields.

Finally, I'd like to thank Kathleen Williams for her love, patience and support.

Abstract

The interface between a semiconductor and a solution is relevant not only to various technological applications but also to the study of fundamental heterogeneous charge-transfer processes. The rate constants for charge transfer from a semiconductor electrode to an outer-sphere redox couple in solution were examined using standard electrochemical methods. Differential capacitance-potential measurements provided information on the interfacial electric field, which in turn quantified the concentration of relevant charge carriers at the surface of the semiconductor. Current density-potential measurements characterized the kinetic flux of charge carriers across the interface. The first section of this thesis presents results on the upper limits for electron-transfer rate constants at the n-Si/methanol-dimethylferrocene$^{+/0}$ and n-GaAs/acetonitrile-ferrocene$^{+/0}$ contacts. Magnitudes of the empirical upper limits were fully consistent with the theoretical maximum rate constants. The second section describes the measurement of electron-transfer rate constants as a function of the free-energy change at the n-Si/bipyridinium$^{2+/+}$ interface and compares these kinetic results to a theoretical treatment based on Marcus theory. Excellent agreement was found between the experimental values and the predictions of several charge-transfer theories. The third section outlines an attempt to compare the hole-transfer rate constants at p-InP/methanol junctions with the electron-transfer rate constants at n-InP/methanol contacts. Nonideal electrical behavior, likely orginiating from surface electrical traps, prevented any kinetic characterization of the p-InP/methanol system.

Table of Contents

Chapter One 1

Introduction to Interfacial Charge-Transfer Rate Constants

References 21

Chapter Two 26

Experimental Upper Bounds on the Rate Constants for Electron Transfer Across the n-Si/CH_3OH-Dimethylferrocene$^{+/0}$ and n-GaAs/CH_3CN-Ferrocene$^{+/0}$ Interfaces

References 50

Chapter Three 55

Free-Energy Dependence of Electron-Transfer Rate Constants at Silicon/Liquid Interfaces

References 117

Chapter Four 122

Bohr Radius Effects on the Majority-Carrier Charge-Transfer Rate Constants at InP/CH_3OH Interfaces

References 158

List of Illustrations and Tables

Chapter One

Scheme 1. Electric field formation at the semiconductor/liquid interface. 2

Scheme 2. Thermodynamic and kinetic parameters of a metal/liquid interface. 7

Scheme 3. Thermodynamic and kinetic parameters of a semiconductor/liquid interface. 10

Scheme 4. Charge recombination pathways at a semiconductor/liquid interface. 16

Chapter Two

Figure 1. Bode plot of a n-Si/CH_3OH-$Me_2Fc^{+/0}$ junction. 39

Figure 2. Mott-Schottky plot of a n-Si/CH_3OH-$Me_2Fc^{+/0}$ junction. 41

Figure 3. Mott-Schottky plot of a n-GaAs/CH_3CN-$Fc^{+/0}$ junction. 45

Chapter Three

Figure 1. Structures of seven bipyridnium redox compounds. 62

Table I. Formal reduction potentials of bipyridinium$^{2+/+}$ compounds. 64

Figure 2. Representative Bode plots for the n-Si/CH_3OH junction. 71

Figure 3. Mott-Schottky plots for junctions between n-Si and compounds **II-VII**. 74

Table II. Impedance data for n-Si/CH_3OH interfaces. 76

Table III. Barrier height results for n-Si/CH_3OH interfaces. 79

Figure 4. A plot of the barrier height vs the Nernstian solution potential. 81

Figure 5. Current density-potential behavior for n-Si/bipyridinium$^{2+/+}$ junctions. 83

Figure 6. Dark J-E_{corr} characteristics for compounds **II-VII**. 87

Table IV. Current density-potential data for n-Si/CH_3OH interfaces. 90

Figure 7. Dark J-E properties for compound **I** at different redox concentrations. 93

Figure 8. Plots of k_{et} as a function of the driving force for electron transfer. 96

Scheme 1. Two possible mechanisms for interfacial electron transfer. 102

Figure 9. A plot of k_{et} as a function of the driving force for electron transfer, with the upper limit on k_{et} for the n-Si/CH_3OH-$Me_2Fc^{+/0}$ interface 113

Chapter Four

Figure 1. Representative Bode plots for the p-InP/CH_3OH interface. 134

Figure 2. Mott-Schottky plots of the p-InP/CH_3OH interface. 138

Table I. Barrier height results for p-InP/CH_3OH interfaces. 145

Figure 3. A plot of the barrier height vs the Nernstian solution potential. 146

Figure 4. Dark ln J-E_{corr} characteristics for p-InP/CH_3OH junctions. 149

Figure 5. Dark J-E_{corr} data for the p-InP/CH_3OH-$DCEV^{2+/+}$ system. 154

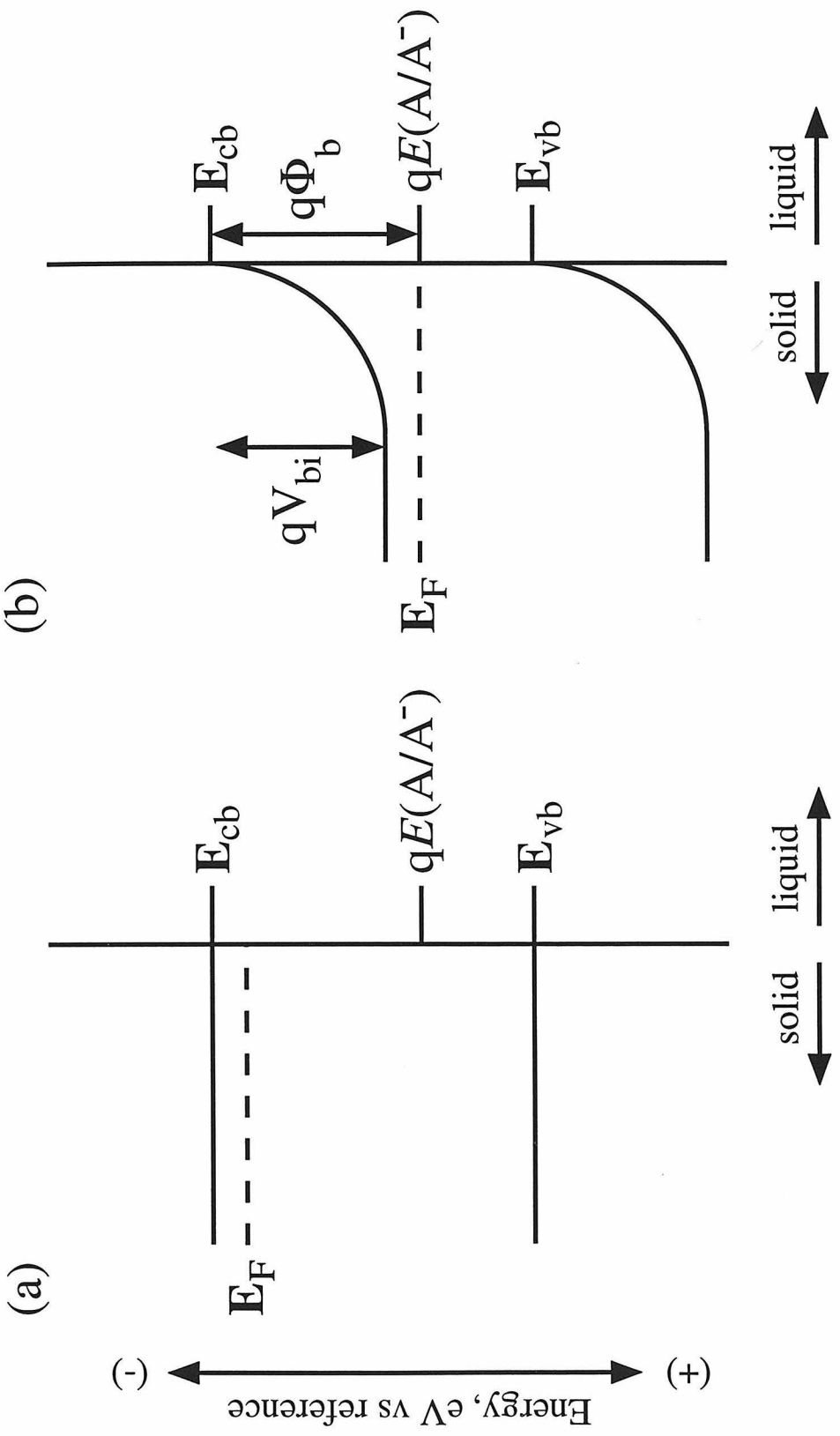
Chapter One

Introduction to Interfacial Charge-Transfer Rate Constants

The interface between a semiconductor electrode and an electrolyte solution is a system that is relevant to various technologies, of which the most notable is solar energy conversion.[1-10] In light of the incipient shortage of nonrenewable fossil fuels, the prospect of inexpensive solar cells based on the semiconductor/liquid interface has stimulated extensive research on such systems. Recent advances in dye-sensitized nanocrystalline TiO_2 particles that drive the inexpensive generation of electricity,[11,12] and p-$GaInP_2$/GaAs electrodes that reduce water to hydrogen gas,[13] represent not only the ongoing interest in this field but also two promising avenues for future development. Semiconductor/liquid junctions have also been applied to heterogeneous photocatalysis,[14] degradation of organic pollutants in waste water streams,[15,16] semiconductor processing,[17] and chemical sensors.[18-20]

One of the attractive features of the semiconductor/liquid interface is the ease with which a rectifying electrical junction may be created. Mere immersion of a semiconductor electrode into an electrolyte solution results in an interfacial electric field, which can separate photogenerated charge carriers of opposite sign.[1] Electric field formation proceeds because of the difference between the electrochemical potential of the semiconductor, i. e., the Fermi level, and the electrochemical potential of the solution, i. e., the Nernstian solution potential (Scheme 1). This difference induces partial charge transfer between the two phases in order to equilibrate their electrochemical potentials.[1] The excess charge in the electrolyte phase, essentially confined to the inner Helmholtz plane, resides within 3 Å of the interface. In contrast, the excess charge in a nondegenerately doped semiconductor is dispersed over a thickness on the order of 10^3 Å, since it is located on the easily ionized,

Scheme 1. The process of electric field formation at the semiconductor/liquid interface. $\mathbf{E}_F$ is the Fermi level of the semiconductor, q is the electronic charge, $E(A/A^-)$ is the Nernstian potential of the solution, $\mathbf{E}_{cb}$ is the conduction band edge energy at the surface, $\mathbf{E}_{vb}$ is the valence band edge energy at the surface, V_{bi} is the built-in potential, and ϕ_b is the barrier height. Provided that $E(A/A^-)$ serves as the reference potential, $V_{bi} = - E_{fb}$. (a) Before equilibration, the Fermi level of the n-type semiconductor is higher than the Nernstian potential energy of the solution. Since $\mathbf{E}_F$ and $qE(A/A^-)$ are effectively electrochemical potentials, electrons will flow from the solid to the liquid until $\mathbf{E}_F = qE(A/A^-)$ at the interface. (b) After equilibration, an electric field exists within the semiconductor, as indicated by the "band bending." The dopant atoms near the interface are depleted of electrons, creating a region of positive charge that is thick relative to the corresponding region of negative charge in the liquid. In the absence of electrical traps at the semiconductor surface, all of the equilibrating charge originates from dopant atoms and the band edge energies appear fixed.


(a)
(b)
Energy, eV vs reference
(-)
(+)
E_F
E_{cb}
$qE(A/A^-)$
E_{vb}
qV_{bi}
$q\Phi_b$
solid
liquid

but sparsely distributed, dopant atoms. This latter thickness, known as the depletion width, is sufficiently large that it imposes an electric potential gradient but prevents charge carriers in the semiconductor from tunnelling through the electric field, which occurs in the case of a metal/liquid junction. Because a comprehensive review of electric field formation, and indeed of all other aspects of the semiconductor/liquid interface, is assuredly beyond the scope of this thesis -- the reader is advised to consult several excellent reviews[1,21-23] that address the historical background, theoretical basis, experimental parameters, and technological applications of the semiconductor/liquid electrochemical system -- it should be noted explicitly that quantification of the equilibrium electric field is not only important for device optimization, but as will be seen in the following chapters, crucial to the understanding of interfacial kinetics.

Even without a detailed prologue on the fine points of semiconductor electrochemistry, it is evident that the rate constant for transfer of charge from the semiconductor electrode to the charge acceptor in solution is a fundamental parameter that dictates the performance of the system. Within the context of photoelectrochemical energy conversion devices, very large charge-transfer rate constants of majority carriers in the semiconductor can lead to significant levels of recombination and efficiency losses, whereas very small interfacial rate constants would be undesirable because they could prevent efficient collection of photogenerated minority charge carriers by redox ions in the solution. The open-circuit voltage, an empirical parameter that indicates the voltage output for a given illumination intensity, depends in part on the interplay between the rate constants of majority and minority carriers.[24] Generating higher voltages which can drive larger electrical loads therefore requires a working knowledge of the interfacial kinetic mechanisms.

However, despite its significance to device technology, charge transfer across the semiconductor/liquid interface has been investigated almost exclusively for its basic

scientific value. Unlike homogeneous electron transfer between donor and acceptor molecules, which has been extensively studied with the reactants dispersed in solution,[25-28] linked via rigid hydrocarbon spacers,[29-40] or attached to proteins,[41-44] heterogeneous electron transfer across an interface has not been as fully explored. Experimental work in this arena has historically approached the subject through the use of metal electrodes in contact with electrolyte solutions.[45] These electrochemical kinetic studies have continued since 1924,[46] yet only recently have researchers adequately characterized the charge transfer across the metal/liquid junction, by the ingenious use of insulating monolayers to access lower currents that are not limited by mass transport through the solution.[47] Furthermore, the solid/liquid interface may not be best probed with a metal as the solid. Gerischer has asserted that semiconductor electrodes possess significant advantages over metal electrodes in addressing many of the primary predictions of interfacial electron-transfer theories.[48] Notably, although this rationale was published more than 40 years ago, relatively few robust kinetic measurements have been reported for charge transfer from semiconductor electrodes to one-electron, outer-sphere redox species.[49-55] This thesis describes experimental results on the measurement of rate constants for charge transfer across the semiconductor/liquid interface, and it places these results within the context of existing models for interfacial charge transfer.

A. Comparison Between the Kinetic Behavior of Metal and Semiconductor Electrodes

Because kinetic measurements at semiconductor electrodes have not been emphasized in the literature relative to measurements at metal electrodes, it is useful to compare the behavior expected for the two different types of solid/liquid junctions. Summarized below are the theoretical predictions for a metal electrode in contact with a redox solution, followed by those for a semiconductor electrode in a similar situation.

1. Metal Electrodes

For reduction of an acceptor at a metal electrode, the rate law for current flow is:[45,56]

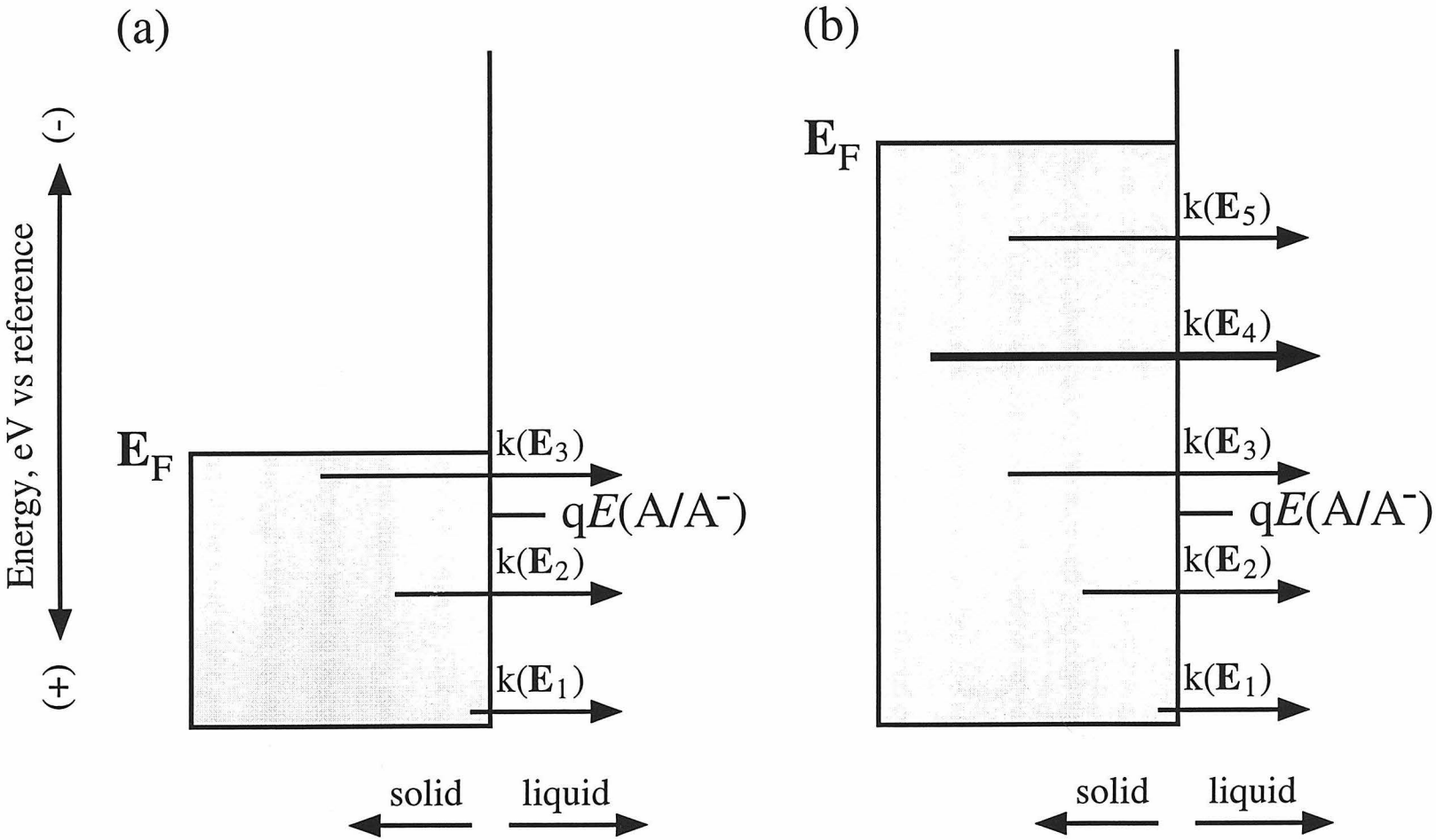
$$J(E) = - q\, k_m(E)\, [A] \qquad (1)$$

where J is the interfacial current density at an electrode potential E, q is the charge on the electron, [A] is the concentration (in units of molecules cm^{-3}) of redox acceptors at the interface, and $k_m(E)$ is the charge-transfer rate constant at the potential E. The rate constant $k_m(E)$ has units of cm s^{-1}. In this well-known rate law, the electron concentration at the surface of the metal, $n_{s,m}$, is not directly determined experimentally and is instead implicitly contained in the value of $k_m(E)$.

The measured rate constant $k_m(E)$ is actually a summation of the energy-dependent rate constants that describe interfacial charge transfer from every occupied electronic state in the metal to the acceptor species in the solution phase. Every energy-dependent rate constant has its own activation energy and implicitly includes the electron concentration at the surface of the metal at that specific energy (Scheme 2a). Although neither the individual energy-dependent rate constants nor the electron concentrations included in these $k_m(E)$ values have been measured to date, the Marcus theory nevertheless does predict a functional form for the dependence of $k_m(E)$ on E, if the density of states in the metal is assumed to be independent of energy and if the electronic coupling between the charge carrier in the solid and the acceptor in the solution is also independent of energy.[57,58] Recent kinetic studies for redox species immobilized at a fixed distance in a self-assembled monolayer on a gold surface[39,57-59] and for freely diffusing species through insulating barrier layers on electrode surfaces[47] have verified this prediction, subject to these assumptions, in satisfying detail.

Another consequence of the kinetic behavior of a metal/electrolyte interface is that, at optimal exoergicity for a freely diffusing redox species at such a contact, the interfacial

Scheme 2. Thermodynamic and kinetic parameters of a metal/liquid interface. $\mathbf{E}_F$ is the Fermi level of the metal, q is the electronic charge, and $E(A/A^-)$ is the electrochemical potential of the solution. k(**E**) is the electron-transfer rate constant at an energy **E**, and the length of each associated arrow denotes the relative magnitude of the rate constant. The shaded area indicates occupied electronic states in the metal electrode. (a) In the normal Marcus regime, an increase in potential effects a larger observed rate, since larger rate constants are continually accessed. (b) In the inverted Marcus regime, an increase in potential does not result in a smaller observed rate, since the rate constant at optimal exoergicity (here represented by $k(\mathbf{E}_4)$) dominates the electron-transfer process.


(a)
Energy, eV vs reference
(-)
(+)
$\mathbf{E}_F$
k($\mathbf{E}_3$)
qE(A/A$^-$)
k($\mathbf{E}_2$)
k($\mathbf{E}_1$)
solid
liquid
(b)
$\mathbf{E}_F$
k($\mathbf{E}_5$)
k($\mathbf{E}_4$)
k($\mathbf{E}_3$)
qE(A/A$^-$)
k($\mathbf{E}_2$)
k($\mathbf{E}_1$)
solid
liquid

flux is always controlled by mass transport, not by kinetics. Because the electrode surface has such a large concentration of electrons that can participate in the interfacial charge-transfer process, the current density expected theoretically at optimal exoergicity far exceeds the mass-transport-limited flux of redox species to the electrode surface. This precludes direct measurement of $k_m(E)$ for such systems and requires either surface immobilization of the redox reagent[57] or the formation of insulating, nearly pinhole-free overlayers on the metal[47] in order to access the required rate constant regime. Also, Marcus inverted behavior for the individual energy-dependent values of $k_m(E)$ cannot be directly observed at a metal/electrolyte interface, because there are always occupied electronic states at optimal exoergicity that dominate the interfacial current flow and maintain the optimal rate of charge transfer to the acceptor in the solution (Scheme 2b).

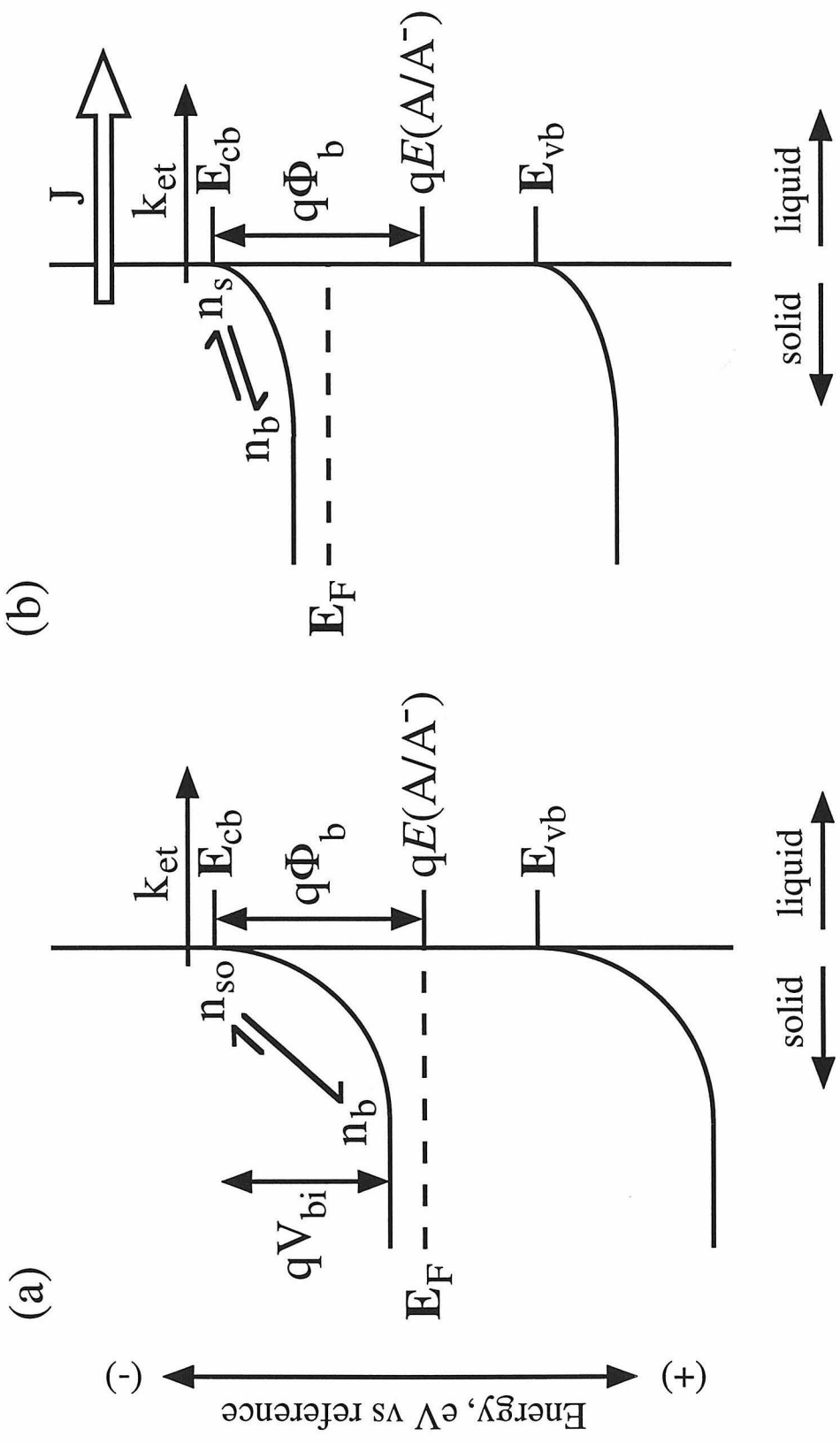
2. Semiconductor Electrodes

For a semiconductor electrode, the situation is quite different. For an n-type semiconductor in contact with a redox system A/A^- of formal electrochemical potential $E^{\circ\prime}(A/A^-)$, it is generally possible to identify systems in which the energies of the conduction and valence band edges at the surface of the semiconductor, $\mathbf{E}_{cb}$ and $\mathbf{E}_{vb}$ respectively, are very different from the value of $qE^{\circ\prime}(A/A^-)$. Since no electronic states are available in the forbidden energy gap of the semiconductor, only electrons that are thermally excited into the conduction band of the solid need to be considered in the kinetic rate expression for electron flow from the semiconductor into the solution (Scheme 3a). For electron transfer from the conduction band of the solid to the acceptor species in the solution, the charge-transfer rate law is therefore:[21,55]

$$J(E) = - q\, k_{et}\, n_s\, [A] \qquad (2)$$

where k_{et} is the second-order rate constant and n_s is the electron concentration at the surface of the semiconductor. Although not directly discussed in this chapter, hole transfer from

Scheme 3. Thermodynamic and kinetic parameters of a semiconductor/liquid interface. $\mathbf{E}_{cb}$ and $\mathbf{E}_{vb}$ are respectively the conduction and valence band edge energies at the surface of the semiconductor, V_{bi} is the built-in voltage of the semiconductor/liquid contact, ϕ_b is the barrier height, and k_{et} is the electron-transfer rate constant. (a) At equilibrium, a Boltzmann distribution relates the electron concentration in the bulk of the semiconductor (n_b) to the equilibrium electron concentration at the surface (n_{so}). (b) As the junction is biased away from equilibrium, a current density (J) is observed because the electron concentration at the surface of the semiconductor (n_s) is larger than n_{so}. Unlike electron transfer across a metal/liquid interface, the experimental rate constant is invariant with potential.


(a)
(b)
Energy, eV vs reference
(-)
(+)
solid
liquid
solid
liquid
E_F
qV_{bi}
n_b
n_{so}
n_s
k_{et}
J
E_{cb}
$q\Phi_b$
$qE(A/A^-)$
E_{vb}

the semiconductor to the redox donor may be described with an analogous expression. Dimensional analysis of eq 2 indicates that the units of k_{et} are $cm^4\ s^{-1}$, as $J(E)$ has units of A cm^{-2} and both n_s and [A] have units of cm^{-3}.

This kinetic behavior differs in several important aspects from that of a metal electrode. First, n_s is explicitly contained in the rate law and thus is not included in the value of k_{et}. The value of n_s can be determined experimentally, and is related to the electron concentration in the bulk, n_b, through a Boltzmann relation:[60]

$$n_s = n_b \exp\{q(E_{fb} - E)/kT\} \qquad (3)$$

where k is Boltzmann's constant, T is temperature and E_{fb} is the flat-band potential of the semiconductor. The value of the potential drop in the semiconductor electrode can be determined through a variety of methods,[60-63] and n_b can be measured from knowledge of the resistivity and mobility of carriers in the solid.[60,64,65] Therefore, n_s is known in principle for any specific semiconductor/liquid interface. Since the diffusion coefficient of electrons in the semiconductor is much larger than the diffusion coefficient of ions in the solution phase,[45] exchange of electrons between the bulk and surface regions of the solid occurs very rapidly relative to interfacial charge transfer.[62,66] In fact, a limiting current density of 10^7 A cm^{-2} could, in principle, be supported before transport of charge carriers in the solid becomes rate-limiting.[60] Since this is much larger than any experimentally accessible current density in an electrochemical experiment, the charge carrier transport process can be viewed chemically as a rapid pre-equilibrium followed by a rate-determining charge-transfer step. In this framework, the potential dropped in the semiconductor determines the electron concentration of the rate-determining process, n_s, in terms of its value in the bulk, n_b, through eq 3.

Secondly, the electrons available for charge transfer at a semiconductor/liquid contact are contained in a narrow region of defined, experimentally determinable energies. Because the valence electrons of dopant atoms must undergo thermal excitation to produce

free carriers in the solid, to an excellent approximation only electronic states with energies of $\mathbf{E}_{cb}$ - 3kT < **E** < $\mathbf{E}_{cb}$ are occupied by free carriers.[67] Only these carriers can therefore contribute to the interfacial current flow that determines the value of k_{et}. The measured k_{et} for a semiconductor electrode thus corresponds more closely to a microscopic, individual-energy, interfacial charge-transfer rate constant than does $k_m(E)$ for a metal electrode, since the latter is integrated over a much wider energy range of occupied electronic states.

Thirdly, changing the electrode potential does not affect the driving force for charge transfer at a semiconductor/liquid contact, and thus k_{et} is essentially independent of *E*. Because the differential capacitance of a nondegenerately doped semiconductor electrode is much smaller than that of the Helmholtz layer in the electrolyte, an applied potential drops almost exclusively across the semiconductor electrode instead of across the double layer of such solid/liquid contacts.[7,21,45,60,68,69] Changing the electrode potential of a semiconductor/liquid contact therefore primarily affects the value of n_s and does not perturb k_{et} (Scheme 3b). In this fashion, the potential dependence of the current density at a semiconductor electrode allows direct evaluation of the first-order dependence of J on n_s (eq 2), and allows explicit removal of n_s from the observed kinetic rate to obtain a value for k_{et}. However, it is not possible to investigate the driving-force dependence of k_{et} through manipulation of the electrode potential; instead the value of $\mathbf{E}_{cb}$ or of the formal reduction potential of the redox couple, $E^{\circ\prime}(A/A^-)$, must be manipulated at the semiconductor/liquid contact.

Fourth, because the electron concentration at the surface of the semiconductor electrode can be very small, typically 6 to 8 orders of magnitude less than the atomic density of the solid, even charge-transfer events that proceed at optimal exoergicity produce very small absolute interfacial charge carrier fluxes. For example, at an n-Si/liquid contact with $\mathbf{E}_{cb} - qE^{\circ\prime}(A/A^-) = -0.5$ eV, charge transfer at an optimally exoergic rate constant of 10^{-16} cm^4 s^{-1} would produce an exchange current density of only 9.6 μA cm^{-2} at [A] = 10

mM. This is far smaller than the mass-transport-limited value of 1900 $\mu A\ cm^{-2}$ that would be obtained for this redox system at a rotating disk electrode of rotation velocity 100 rev min^{-1}.[45,70] Rate constants at optimal exoergicity therefore can be determined at semiconductor electrodes without interference from mass-transport limitations, which prevent measurement of the analogous kinetic processes at metal/liquid interfaces.

Finally, because of the limited energetic range of the occupied electronic states in the solid, it should be possible to observe directly the Marcus inverted region for interfacial charge transfer at a semiconductor/liquid interface. In fact, Fujishima *et al.* have interpreted the current-potential behavior at deuterated vs nondeuterated thianthrene cation radicals at ZnO electrodes within this type of inverted-region framework.[71] Transient absorbance data at the TiO_2-$Fe^{III}(CN)_5(ligand)^{x+}$ interface have also been cited as evidence for the Marcus inverted region.[72]

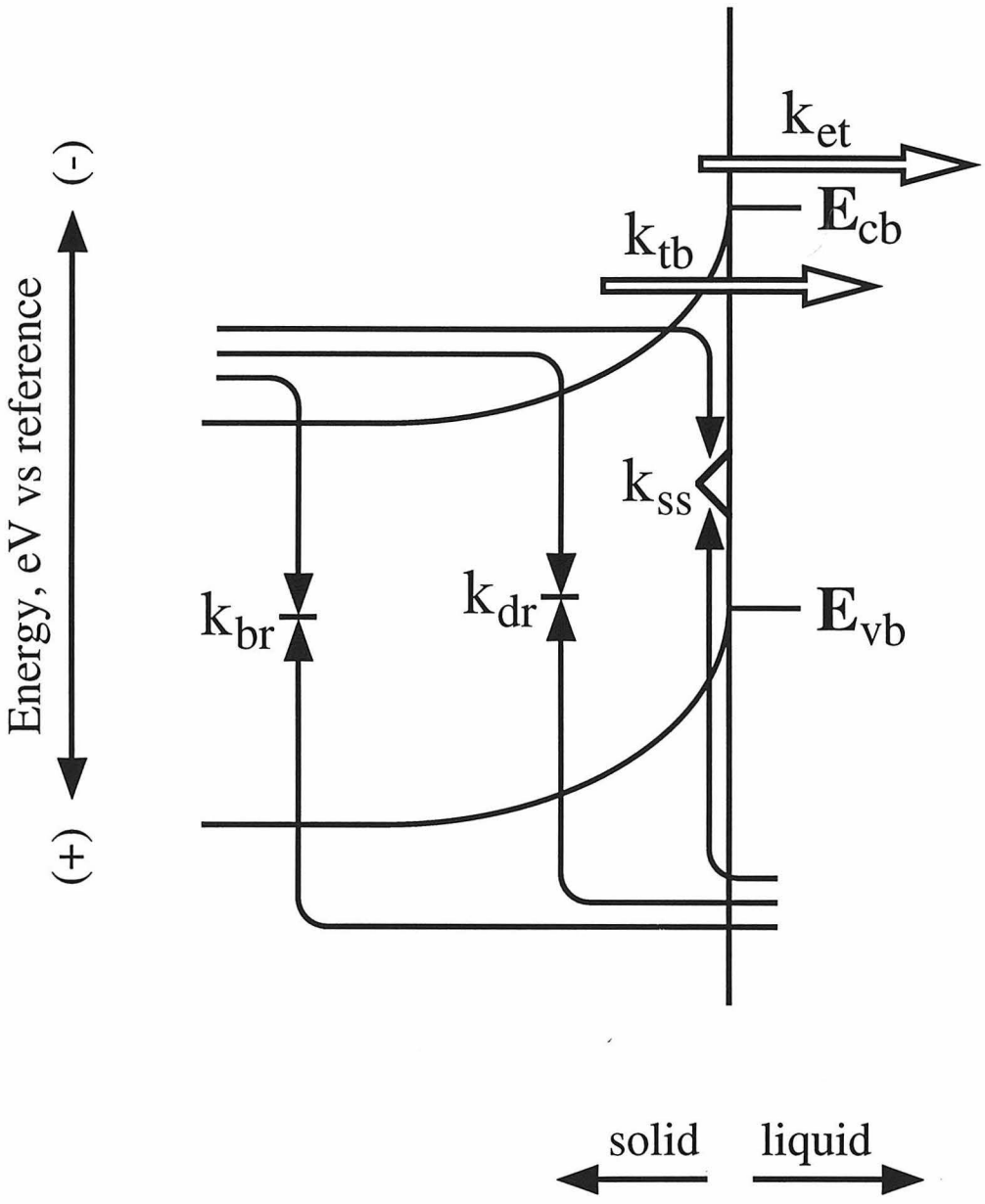
B. Requirements for the Experimental Determination of Charge-Transfer Rate Constants at the Semiconductor/Liquid Interface

The accurate determination of the electron-transfer rate constant k_{et} requires (1) the reliable measurement of the quantities $J(E)$, [A], and n_s in the rate law of eq 2; and (2) the verification that this second-order rate law adequately describes the observed electrochemistry. In practice, the measurement of $J(E)$ is readily performed through the use of a three-electrode electrochemical setup, wherein E is controlled potentiostatically. The measurement of [A] is likewise straightforward. According to the Frumkin corrections for the concentration of a cationic redox species A in the vicinity of a charged electrode under depletion conditions, the low dielectric constant of the semiconductor, relative to the dielectric constant of the electrolyte medium, causes the concentration of A at the outer Helmholtz plane of the electrode to be within 1% of its concentration in the bulk solution.[69]

The surface electron concentration, unlike the current density and the acceptor concentration at the interface, has traditionally eluded exact characterization. The principal culprit of reliable n_s information has been the difficulty of accurately measuring the value of E_{fb} (eq 3).[55] Various experimental techniques have been devised to measure this parameter, but each has its own shortcomings. Photocurrent onset, which relies on the hypothesis that a measurable photocurrent requires a finite interfacial electric field, is of dubious quality because the field is unlikely to be eliminated exclusively by an applied bias.[73] Estimates of E_{fb} have also been obtained by increasing the illumination intensity on a semiconductor electrode until the open-circuit voltage saturates. The ultimate voltage has been claimed to approximate E_{fb} closely,[74] but again it is unclear whether the interfacial electric field can be eliminated by the incident light.[75] Moreover, effects such as nonlinear light response and local heating render the results inaccurate at best and deceiving at worst.[75] Measurement of the semiconductor conductivity parallel to the interface has been proven to be a viable method for quantifying junction energetics,[76] but elaborate device fabrication is necessary and only select systems can be characterized. Differential capacitance measurements are the most feasible and general technique for reliable E_{fb} determinations, but even with this distinction, material imperfections can effect dependence on the input ac voltage signal frequency and thus limit the accuracy of the final E_{fb} results.[21,55,61]

The second requirement for determining the electron-transfer rate constant is the empirical adherence to the second-order rate law of eq 2. On an experimental level, the current density must be shown to increase concomitantly with either the surface electron concentration or the acceptor concentration. On a theoretical level, forward-bias currents at the semiconductor/liquid junction may originate from majority carriers, as with the aforementioned electron transfer or else by tunneling through the potential barrier, or from minority carriers, as with bulk recombination, depletion region recombination, or surface

Scheme 4. The five charge recombination pathways at the interface between an n-type semiconductor and an electrolyte solution. In all cases, the net outcome is the reduction of the redox acceptor, whether the process occurs by electron emission from the conduction band (majority-carrier recombination, depicted as white arrows) or by hole injection into the valence band (minority-carrier recombination, depicted as black arrows). Electrons leaving the semiconductor may react from the band-edge energy (k_{et}) or may tunnel through the potential barrier (k_{tb}). Holes injected by the redox acceptor may recombine with electrons in the bulk of the semiconductor (k_{br}), in the depletion region (k_{dr}), or at surface states (k_{ss}).


Energy, eV vs reference
(-)
(+)
k_{et}
E_{cb}
k_{tb}
k_{ss}
k_{br}
k_{dr}
E_{vb}
solid
liquid

state recombination (Scheme 4).[77] In fact all of these processes occur in concert at all times, but a single mechanism typically dominates over a given potential regime, or more importantly, over certain combinations of semiconductor and solution.[77] What usually thwarts a rate constant measurement for a semiconductor/liquid interface is that its recombination current is not dominated by direct electron transfer from the conduction band to the redox acceptor.[22,55] This apparent lack of suitable junctions originates largely from the engineering impulses of investigators; in their efforts to improve photoelectrochemical device quality, scientists in this field have dismissed possible electron-transfer-limited systems as inefficient and have instead devoted attention to junctions limited by recombination in the bulk or at the surface.[10,73,78-81] Although other laboratories have recently found several interfaces whose recombination currents obey eq 2,[50,52,82] discovering additional systems of this type still calls for a blend of insight and intuition from the researcher.

C. Outline of Thesis

The remainder of this thesis is organized according to the chronological order in which these experiments were performed. The text, tables and illustrations of the thesis have been adapted primarily from three publications. Chapters 1 and 3 use material from "Rate Constants for Charge Transfer Across Semiconductor/Liquid Interfaces," [Fajardo, A. M.; Lewis, N. S. *Science* **1996**, *262*, 969] and "Free-Energy Dependence of Electron-Transfer Rate Constants at Si/Liquid Interfaces" [Fajardo, A. M.; Lewis, N. S. *J. Phys. Chem. B* **1997**, *101*, 11131]. Chapter 2 incorporates text and illustrations from "Theoretical and Experimental Upper Bounds on Interfacial Charge-Transfer Rate Constants between Semiconducting Solids and Outer-Sphere Redox Couples" [Pomykal, K. E.; Fajardo, A. M.; Lewis, N. S. *J. Phys. Chem.* **1996**, *100*, 5289].

Chapter 2 discusses the upper limits on the rate constants for electron transfer across the n-Si/dimethylferrocene$^{+/0}$ ($Me_2Fc^{+/0}$) and n-GaAs/ferrocene$^{+/0}$ ($Fc^{+/0}$) interfaces. In these two systems, the rate law of eq 2 does not represent the dominant recombination mechanism. Minority-carrier pathways govern the recombination currents across both junctions: bulk recombination for n-Si/$Me_2Fc^{+/0}$ and surface-state recombination for n-GaAs/$Fc^{+/0}$. Consequently, measurements of J(E), [A], and n_s result only in upper limits for the magnitude of the electron-transfer rate constant. Current density-potential data were obtained from photocurrent density-photovoltage measurements, which are more easily analyzed than measurements in the dark since the absence of current at open ciruit obviates the need for overpotential and resistance corrections. Differential capacitance methods were employed to determine E_{fb} and hence n_s. The upper limits that were calculated from these data are fully consistent with the magnitudes predicted by theory.

Chapter 3 presents the experimental characterization of the interfacial kinetics of the n-Si/bipyridinium$^{2+/+}$ system. In contrast to the n-Si/$Me_2Fc^{+/0}$ and n-GaAs/$Fc^{+/0}$ junctions described in Chapter 2, the n-Si/bipyridinium$^{2+/+}$ junction displays electrical behavior consistent with a second-order rate law. Forward-bias current density-potential data were acquired in the dark and corrected for concentration overpotential and cell resistance in order to quantify the interfacial charge flux. Differential capacitance-potential measurements, refined to yield minimal frequency dispersion in the E_{fb} results, supplied the corresponding information on junction energetics. The responses of the current density to shifts in the surface electron concentration and in the acceptor concentration confirmed that a second-order kinetic mechanism governs the electrical behavior. Interfaces with seven different bipyridinium compounds, having reduction potentials that vary over a 0.4 V range, all exhibited this second-order kinetic behavior. The variation of the free-energy change for the electron-transfer reaction, in conjunction with the roughly invariant

reorganization energy of this homologous series of redox couples, permitted a comparison to the predictions of Marcus theory. The experimental k_{et} values spanned more than one order of magnitude, and the calculated fit to these results yielded a reorganization energy of 0.7 eV and a maximum rate constant of 6×10^{-17} cm^4 s^{-1}. The former value agrees with a prior, independent measurement of the reorganization energy of methyl viologen, whereas the latter value corroborates several theoretical treatments of charge transfer from a semiconductor to a one-electron, outer-sphere redox species in an electrolyte solution.

Chapter 4 describes the investigation attempted in this laboratory to determine the hole-transfer rate constants at the p-InP/CH_3OH interface and to compare the results with the electron-transfer rate constants previously measured at the n-InP/CH_3OH interface. As in Chapter 3, the objective of this effort was to ascertain how the rate constant varied as one of its theoretical components was modified. Instead of the free-energy change, which is an interfacial property, the experiments in this chapter probed the Bohr radius, which is specific to the semiconductor. The Bohr radius is hypothesized to reflect the degree of charge delocalization, and therefore it should influence the extent of electronic coupling between a charge carrier in the solid and a redox molecule in the solution. Four outer-sphere redox couples were examined using current density-potential and differential capacitance-potential techniques in order to characterize the kinetic flux and junction energetics, respectively. While the flat-band potentials of the p-InP/CH_3OH interfaces were quantifiable (albeit with slightly larger standard deviations than those of the systems discussed in Chapters 2 and 3), the current densities of these junctions never exhibited a first-order dependence on the redox donor concentration. Furthermore, the p-InP/CH_3OH system displayed partial Fermi level pinning, since negative shifts in the Nernstian solution potential did not result in equivalent increases in the magnitude of E_{fb}. No rate constant results were extractable, and the role of carrier delocalization in charge transfer across the semiconductor/liquid interface remains experimentally unknown.

REFERENCES

(1) Tan, M. X.; Laibinis, P. E.; Nguyen, S. T.; Kesselman, J. M.; Stanton, C. E.; Lewis, N. S. *Prog. Inorg. Chem.* **1994**, *41*, 21.

(2) Bard, A. J.; Fox, M. A. *Acc. Chem. Res.* **1995**, *28*, 141.

(3) Bard, A. J. *J. Phys. Chem.* **1982**, *86*, 172.

(4) Gerischer, H. In *Solar Energy Conversion. Solid-State Physics Aspects*; B. O. Seraphin, Ed.; Springer-Verlag: Berlin, 1979; Vol. 31.

(5) Heller, A. *Acc. Chem. Res.* **1981**, *14*, 154.

(6) Hodes, G.; Howell, I. D. J.; Peter, L. M. *J. Electrochem. Soc.* **1992**, *139*, 3136.

(7) Memming, R. In *Electrochemistry II*; E. Steckhan, Ed.; Springer Verlag: New York, 1988; Vol. 143.

(8) Nozik, A. J. *Ann. Rev. Phys. Chem.* **1978**, *29*, 189.

(9) Rajeshwar, K.; Singh, P.; DuBow, J. *Electrochim. Acta* **1978**, *23*, 1117.

(10) Wrighton, M. S. *Acc. Chem. Res.* **1979**, *12*, 303.

(11) Moser, J. E.; Bonnote, P.; Grätzel, M. *Coord. Chem. Rev.* **1998**, *171*, 245.

(12) Gerfin, T.; Grätzel, M.; Walder, L. *Prog. Inorg. Chem.* **1997**, *44*, 345.

(13) Khaselev, O.; Turner, J. A. *Science* **1998**, *280*, 425.

(14) Fox, M. A. In *Photocatalysis: Fundamentals and Applications*; N. Serpone and E. Pelizzetti, Ed.; John Wiley & Sons: New York, 1989.

(15) Ollis, D. F.; Pelizzetti, E.; Serpone, N. In *Photocatalysis: Fundamentals and Applications*; N. Serpone and E. Pelizzetti, Ed.; Wiley: New York, 1989.

(16) Hoffmann, M. R.; Martin, S. T.; Choi, W. Y.; Bahnemann, D. W. *Chem. Rev.* **1995**, *95*, 69.

(17) O'Brien, S. C. *Chem. Soc. Rev.* **1996**, *25*, 393.

(18) Poznyak, S. K.; Kulak, A. I. *Sens. Actuators B* **1994**, *22*, 97.

(19) Moore, D. E.; Lisensky, G. C.; Ellis, A. B. *J. Am. Chem. Soc.* **1994**, *116*, 9487.

(20) Hirota, K.; Miyayama, M.; Nakamura, Y.; Yanagida, H. *Chem. Lett.* **1994**, 1793.

(21) Morrison, S. R. *Electrochemistry at Semiconductor and Oxidized Metal Electrodes*; Plenum: New York, 1980.

(22) Koval, C. A.; Howard, J. N. *Chem. Rev.* **1992**, *92*, 411.

(23) Nozik, A. J.; Memming, R. *J. Phys. Chem.* **1996**, *100*, 13061.

(24) Rosenbluth, M. L.; Lewis, N. S. *J. Phys. Chem.* **1989**, *93*, 3735.

(25) Closs, G. L.; Calcaterra, L. T.; Green, N. J.; Penfield, K. W.; Miller, J. R. *J. Phys. Chem.* **1986**, *90*, 3673.

(26) McLendon, G.; Miller, J. R. *J. Am. Chem. Soc.* **1985**, *107*, 7811.

(27) Marcus, R. A.; Sutin, N. *Biochim. Biophys. Acta* **1985**, *811*, 265.

(28) Fox, L. S.; Kozik, M.; Winkler, J. R.; Gray, H. B. *Science* **1990**, *247*, 1069.

(29) Oevering, H.; Paddon-Row, M. N.; Heppener, M.; Oliver, A. M.; Cotsaris, E.; Verhoeven, J. W.; Hush, N. S. *J. Am. Chem. Soc.* **1987**, *109*, 3258.

(30) Paddon-Row, M. N.; Oliver, A. M.; Warman, J. M.; Smit, K. J.; de Haas, M. P.; Oevering, H.; Verhoeven, J. W. *J. Phys. Chem.* **1988**, *92*, 6958.

(31) Closs, G. L.; Miller, J. R. *Science* **1988**, *240*, 440.

(32) Penfield, K. W.; Miller, J. R.; Paddon-Row, M. N.; Cotsaris, E.; Oliver, A. M.; Hush, N. S. *J. Am. Chem. Soc.* **1987**, *109*, 5061.

(33) Isied, S. S.; Vassilian, A.; Wishart, J. F.; Creutz, C.; Schwarz, H. A.; Sutin, N. *J. Am. Chem. Soc.* **1988**, *110*, 635.

(34) Schanze, K. S.; Sauer, K. *J. Am. Chem. Soc.* **1988**, *110*, 1180.

(35) Leland, B. A.; Joran, A. D.; Felker, P. M.; Hopfield, J. J.; Zewail, A. H.; Dervan, P. B. *J. Phys. Chem.* **1985**, *89*, 5571.

(36) Geno, M. J. K.; Dawson, J. H. *Inorg. Chem.* **1984**, *23*, 1182.

(37) Finckh, P.; Heitele, H.; Volk, M.; Michelbeyerle, M. E. *J. Phys. Chem.* **1988**, *92*, 6584.

(38) Woitellier, S.; Launay, J. P.; Spangler, C. W. *Inorg. Chem.* **1989**, *28*, 758.

(39) Finklea, H. O.; Hanshew, D. D. *J. Am. Chem. Soc.* **1992**, *114*, 3173.

(40) Carter, M. T.; Rowe, G. K.; Richardson, J. N.; Tender, L. M.; Terrill, R. H.; Murray, R. W. *J. Am. Chem. Soc.* **1995**, *117*, 2896.

(41) Bowler, B. E.; Raphael, A. L.; Gray, H. B. *Prog. Inorg. Chem.* **1990**, *38*, 259.

(42) Axup, A. W.; Albin, M.; Mayo, S. L.; Crutchley, R. J.; Gray, H. B. *J. Am. Chem. Soc.* **1988**, *110*, 435.

(43) Elias, H.; Chou, M. H.; Winkler, J. R. *J. Am. Chem. Soc.* **1988**, *110*, 429.

(44) Mayo, S. L.; Ellis, W. R.; Crutchley, R. J.; Gray, H. B. *Science* **1986**, *233*, 948.

(45) Bard, A. J.; Faulkner, L. R. *Electrochemical Methods: Fundamentals and Applications*; Wiley: New York, 1980.

(46) Butler, J. A. V. *Trans. Faraday Soc.* **1924**, *19*, 729 and 734.

(47) Terrettaz, S.; Becka, A. M.; Traub, M. J.; Fettinger, J. C.; Miller, C. J. *J. Phys. Chem.* **1995**, *99*, 11216.

(48) Gerischer, H.; Beck, F. *Z. Phys. Chem., N. F.* **1957**, *13*, 389.

(49) Morrison, S. R. *Surf. Sci.* **1969**, *15*, 363.

(50) Horrocks, B. R.; Mirkin, M. V.; Bard, A. J. *J. Phys. Chem.* **1994**, *98*, 9106.

(51) Howard, J. N.; Koval, C. A. *Anal. Chem.* **1994**, *66*, 4525.

(52) Uhlendorf, I.; Reineke-Koch, R.; Memming, R. *J. Phys. Chem.* **1996**, *100*, 4930.

(53) Fajardo, A. M.; Lewis, N. S. *Science* **1996**, *274*, 969.

(54) Pomykal, K. E.; Lewis, N. S. *J. Phys. Chem. B* **1997**, *101*, 2476.

(55) Lewis, N. S. *Annu. Rev. Phys. Chem.* **1991**, *42*, 543.

(56) Marcus, R. A. *Annu. Rev. Phys. Chem.* **1964**, *15*, 155.

(57) Chidsey, C. E. D. *Science* **1991**, *251*, 919.

(58) Smalley, J. F.; Feldberg, S. W.; Chidsey, C. E. D.; Linford, M. R.; Newton, M. D.; Liu, Y. P. *J. Phys. Chem.* **1995**, *99*, 13141.

(59) Richardson, J. N.; Peck, S. R.; Curtin, L. S.; Tender, L. M.; Terrill, R. H.; Carter, M. T.; Murray, R. W.; Rowe, G. K.; Creager, S. E. *J. Phys. Chem.* **1995**, *99*, 766.

(60) Sze, S. M. *Physics of Semiconductor Devices;* 2nd ed.; Wiley: New York, 1981.

(61) Chazalviel, J.-N. *Electrochim. Acta* **1988**, *33*, 461.

(62) Fonash, S. J. *Solar Cell Device Physics*; Academic: New York, 1981.

(63) Fahrenbruch, A. L.; Bube, R. H. *Fundamentals of Solar Cells: Photovoltaic Solar Energy Conversion*; Academic: New York, 1983.

(64) Kittel, C. *Introduction to Solid State Physics;* 6^{th} ed.; Wiley: New York, 1986.

(65) Thurber, W. R.; Mattis, R. L.; Liu, Y. M.; Filliben, J. J. *J. Electrochem. Soc.* **1980**, *127*, 1807.

(66) Sze, S. M.; Irvin, J. C. *Solid State Electron.* **1968**, *11*, 599.

(67) *Modular Series on Solid State Devices*; 2 ed.; Neudeck, G. W.; Pierret, R., Ed.; Addison-Wesley: Reading, Massachusetts, 1989; Vol. 2.

(68) Gerischer, H. In *Adv. Electrochem. Electrochem. Eng.*; P. Delahay, Ed.; Wiley Interscience: New York, 1961; Vol. 1.

(69) Royea, W. J.; Krüger, O.; Lewis, N. S. *J. Electroanal. Chem.* **1997**, *438*, 191.

(70) Levich, V. G. *Acta Physicochim. URSS* **1942**, *17*, 257.

(71) Nakabayashi, S.; Itoh, K.; Fujishima, A.; Honda, K. *J. Phys. Chem.* **1983**, *87*, 5301.

(72) Lu, H.; Prieskorn, J. N.; Hupp, J. T. *J. Am. Chem. Soc.* **1993**, *115*, 4927.

(73) Finklea, H. O. *Semiconductor Electrodes*; Elsevier: New York, 1988.

(74) Bard, A. J.; Bocarsly, A. B.; Fan, F.-R. F.; Walton, E. G.; Wrighton, M. S. *J. Am. Chem. Soc.* **1980**, *102*, 3671.

(75) Lewis, N. S. *Ann. Rev. Mater. Sci.* **1984**, *14*, 95.

(76) Laibinis, P. E.; Stanton, C. E.; Lewis, N. S. *J. Phys. Chem.* **1994**, *98*, 8765.

(77) Lewis, N. S.; Rosenbluth, M. L. In *Photocatalysis: Fundamentals and Applications*; N. Serpone and E. Pelizzetti, Ed.; Wiley: New York, 1989.

(78) Gronet, C. M.; Lewis, N. S.; Cogan, G.; Gibbons, J. *Proc. Natl. Acad. Sci. USA* **1983**, *80*, 1152.

(79) Gronet, C. M.; Lewis, N. S. *Appl. Phys. Lett.* **1983**, *43*, 115.

(80) Lieber, C. M.; Gronet, C. M.; Lewis, N. S. *Nature* **1984**, *307*, 533.

(81) Rajeshwar, K. *J. Appl. Electrochem.* **1985**, *15*, 1.

(82) Rosenwaks, Y.; Thacker, B. R.; Bertness, K.; Nozik, A. J. *J. Phys. Chem.* **1995**, *99*, 7871.

Chapter Two

Experimental Upper Bounds on the Rate Constants for Electron Transfer Across the n-Si/CH_3OH-Dimethylferrocene$^{+/0}$ and n-GaAs/CH_3CN-Ferrocene$^{+/0}$ Interfaces

ABSTRACT

An experimental upper bound on the interfacial electron-transfer rate constant has been obtained through the determination of key energetic and kinetic measurements for stable semiconductor electrodes in contact with outer-sphere redox species. For this purpose, n-Si/CH_3OH-dimethylferrocenium-dimethylferrocene and n-GaAs/CH_3CN-ferrocenium-ferrocene contacts were investigated using a combination of differential capacitance-potential and current density-potential methods. Differential capacitance measurements indicated the magnitude of the interfacial electric field at equilibrium, and thus permitted the calculation of the concentration of electrons at the surface of the semiconducting phase from knowledge of the dopant density and the applied potential. Current density-potential techniques, specifically measurements of the photocurrent density and the corresponding open-circuit voltage, afforded information on the reaction rate and the effective applied potential. Because the dominant recombination mechanisms of the two semiconductor/liquid interfaces examined in this work have been previously established as minority-carrier pathways, the rate of electron transfer from the conduction band of the semiconductor to the acceptor in solution must be less than the observed rate. The upper limits for the interfacial charge-transfer rate constant at these semiconductor/liquid contacts were found to be consistent with the upper limits predicted by theory.

I. INTRODUCTION

One of the fundamental steps in the electrochemical reaction of a semiconductor is the process of charge transfer across the solid/liquid interface. The rate at which charge crosses the interface can influence the amount of current flow through the system, the rate of corrosion of the semiconductor, and the magnitude of any photogenerated voltage. As a result, an understanding of the rate constants for interfacial charge transfer across the semiconductor/liquid interface is distinctly germane to improving the stability and energy conversion efficiency of photoelectrochemical cells. For electron-transfer processes between molecular donor and molecular acceptor reagents in homogeneous solution, the theoretical behavior predicted by Marcus has been widely verified by experiment.[1-4] In addition, data on metal electrodes have yielded insight into heterogeneous charge-transfer processes.[5-9] In contrast, relatively little linkage between theory and experiment has been attained for delocalized carriers in a semiconducting solid transferring into localized, molecular acceptors dissolved in an electrolyte solution.[10-17]

Recent theoretical treatments of charge-transfer processes at semiconductor/liquid interfaces have yielded expressions for the electron-transfer rate constant, k_{et}, between an electron in the conduction band of the semiconductor and an outer-sphere redox acceptor in the electrolyte solution.[14] Using Marcus' treatment for liquid-liquid interfaces,[18] and modifying the result to describe the situation in which one species is a delocalized electron in the semiconducting solid and the other is an electron acceptor dissolved in a homogeneous solution, yields:[14]

$$k_{et} = \nu_n \kappa_{el} \kappa_n \tag{1}$$

with

$$\kappa_{el} = \pi\left[\frac{2(r_e + r_A)}{\beta^3} + \frac{6}{\beta^4}\right] \tag{2}$$

and

$$\kappa_n = \exp\left\{\frac{-(\lambda + \Delta G^{\circ\prime})^2}{4\lambda kT}\right\} \qquad (3)$$

The attempt frequency, ν_n, in this transition-state-theory description of the interfacial rate constant is the relevant nuclear vibrational frequency, with ν_n taken to be approximately 10^{13} s^{-1}. κ_{el} is the electronic term that defines the coupling between the wavefunctions of the donor and of the acceptor, whereas κ_n is the nuclear term that accounts for isoenergetic electron transfer between reactants. In the expression for κ_{el}, r_e and r_A are the effective radii of the electron in the solid and the acceptor in solution, respectively, and β is the electronic coupling decay constant. These values allow evaulation of the electronic coupling component of the rate constant for a given concentration of electrons at the surface of the solid and for a given concentration of electron acceptors in the liquid phase.[14] In the expression for κ_n, λ is the total reorganization energy of the system, $\Delta G^{\circ\prime}$ is the free energy of the electron-transfer reaction, k is the Boltzmann constant, and T is the temperature.

An estimate for the maximum value of the rate constant, $k_{et,max}$, can be obtained by setting the total reorganization energy equal to $-\Delta G^{\circ\prime}$, so that $\kappa_n = 1.0$ in eq 3 and the condition of optimal exoergicity for k_{et} is attained. The numerical value of $k_{et,max}$ in this case depends on the value of κ_{el}. To arrive at the expression for κ_{el} in eq 2, the distance dependence of the electronic coupling term is taken to be

$$\kappa_{el}(R) = \kappa_{el,0} \exp\left\{-\beta\left(R - r_e - r_A\right)\right\} \qquad (4)$$

where $\kappa_{el,0}$ is the electronic term at the distance of closest approach of the reactants and R is the distance between the electron in the solid and the acceptor in solution.[18] Integration of $\kappa_{el}(R)$ may then be performed over the relevant distances and angles to describe properly a random distribution of acceptors confined to the liquid phase and a random distribution of electrons confined to the semiconducting phase.[14,18]

In the semiquantitative treatment of such processes presented previously in the literature, r_e is approximated as the Bohr radius of an electron in the solid, and β is assumed to be $\approx 1 \times 10^{-8}$ cm^{-1}. The value for the Bohr radius is well-documented from theory and experiment on Si, GaAs and other semiconducting solids,[19] while the assumed value for β is consistent with values reported previously for the experimentally determined distance dependence of $\kappa_{el}(R)$ through hydrocarbon glasses,[20,21] as well as through proteins[22-25] and other non-conjugated chemical linkages.[26-37] Inserting $\beta = 1 \times 10^{-8}$ cm^{-1}, $r_A = 3 \times 10^{-8}$ cm, and $r_e = 2 \times 10^{-7}$ cm for Si into eq 2 and substituting the resulting κ_{el} value into eq 1 yields an estimate of $k_{et,max} = 10^{-17}$ cm^4 s^{-1}. Although k_{et} is theoretically sensitive to the third power of the decay constant β, the assumed value for β is unlikely to be in error by one order of magnitude, so the uncertainty in $k_{et,max}$ is estimated to be less than a factor of 10^2. A somewhat different derivation, which uses an effective reaction zone for the electron-transfer process and assumes that this process occurs with a single, average rate constant for all electron-acceptor pairs in the reaction zone, yields a similar value for the estimate of the maximum rate constant: $k_{et,max} = 10^{-16}$ cm^4 s^{-1}.[38]

Some data on charge-transfer rate constants across semiconductor/liquid interfaces appear to support this theoretical model. In the few systems amenable to experimental investigation to date, measured k_{et} values, or upper limits on k_{et}, have been established as $k_{et} \leq 10^{-16}$ cm^4 s^{-1}.[15,39-43] However, it has been suggested recently that the prior theoretical treatments may underestimate $k_{et,max}$ by as much as 4 to 5 orders of magnitude.[17] This suggestion was based on experimental data that have been interpreted to indicate that k_{et} values exceeded 10^{-12} cm^4 s^{-1} for p-InP/liquid and p-GaAs/liquid contacts.[17] In addition, it has been suggested that significant increases in $k_{et,max}$ would be obtained theoretically if adiabaticity in the electron-transfer process were explicitly included into the pair-weighted averaging procedure that was used to calculate κ_{el} from the functional form of $\kappa_{el}(R)$ (eq 4).[44]

In this work, we present experimental results that have allowed us to investigate whether k_{et} values in the range $k_{et} \approx 10^{-13}$-10^{-12} cm^4 s^{-1} are generally characteristic of semiconductor/liquid contacts. We have specifically investigated electron-transfer processes involving nonadsorbing, outer-sphere redox reagents at semiconductor/liquid contacts that provide efficient energy conversion systems. Because the electron-transfer theory that is described above was developed for this type of interface, any experimental validation requires the study of these junctions. In these systems, interfacial electron transfer is not the rate-determining recombination step, so the observed steady-state interfacial current density cannot yield a direct value for k_{et}. However, for each of these junctions, measurements of the total interfacial recombination flux at a specific potential, combined with energetic information on the barrier height of the semiconductor/liquid contact, can yield an experimentally rigorous upper bound for k_{et} for that contact. The measurements in this chapter have been performed on semiconductor/liquid junctions with $\kappa_n \approx 1.0$, so that any upper bounds on k_{et} should also establish upper bounds on $k_{et,max}$ at these contacts. Finally, this chapter also explores analytically the implications of k_{et} values far larger than $k_{et} = 10^{-16}$ cm^4 s^{-1} for the construction of efficient photoelectrochemical energy conversion devices.

II. THEORY

A. Establishing an Upper Bound for Rate Constants for Charge Transfer of Majority Carriers Across Semiconductor/Liquid Contacts

Current density vs potential measurements, in conjunction with energetic information obtained from differential capacitance vs potential measurements, can provide useful information on the value of k_{et} for various semiconductor/liquid contacts. For specificity, the theoretical discussion will focus on interfacial electron-transfer processes for an n-type semiconductor/liquid contact under illumination. Similar expressions for p-

type semiconductor/liquid contacts can be derived in terms of hole-transfer rate constants, with appropriate changes in sign due to the change in direction of rectification at the semiconductor/liquid contact.

In general, the interfacial current density can be separated into a photocurrent density, $J_{ph}(E)$, and a recombination current density, $J_{rec}(E)$:[10,45,46]

$$J(E)= J_{rec}(E) - J_{ph}(E) \quad (5)$$

The potential, E, is measured relative to the Nernstian potential of the cell. The sign convention in eq 5 arises because the photocurrent density $J_{ph}(E)$ produces a net flow of electrons from the liquid into the solid, whereas $J_{rec}(E)$ represents all processes that produce a net flow of electrons from the solid into the liquid (resulting from the voltage developed by illumination of the solid).

The charge-transfer process related to k_{et} involves transfer of electrons from the conduction band of the n-type semiconductor into the acceptor ions of the liquid electrolyte. At an applied potential E, the expression for the current density resulting from this kinetic process is[10,14]

$$J_{et}(E) = -q\, k_{et}\, n_s(E)\, [A] \quad (6)$$

where [A] is the concentration of acceptors in the interfacial region. The negative sign appears in eq 6 because cathodic current flow through the interface is assigned as a negative current density by convention. If the built-in voltage, V_{bi}, of the semiconductor/liquid contact is known experimentally, $n_s(E)$ can be computed from the dopant density, N_d, of the semiconductor:[47]

$$n_s(E) = N_d \exp\left[\frac{-q\left(V_{bi} + E\right)}{kT}\right] \quad (7)$$

Thus

$$J_{et}(E) = J_{et}(0)\exp\left(\frac{-qE}{kT}\right) \quad (8)$$

where

$$J_{et}(0) = -qk_{et}[A]N_d \exp\left(\frac{-qV_{bi}}{kT}\right) \quad (9)$$

In general, other kinetic processes will also contribute to the interfacial current flow. These processes include tunneling of majority carriers through the depletion region, with a current density $J_{tun}(E)$.[45] In addition, several processes resulting from interfacial transfer of minority carriers, including surface recombination, with a current density $J_{ss}(E)$, recombination in the depletion region, with a current density $J_{dr}(E)$, and bulk recombination/diffusion, with a current density $J_{br}(E)$, must all be considered as possible rate-determining recombination processes.[45,47-49] The total interfacial recombination current density can then be written as

$$J_{rec}(E) = J_{et}(E) + J_{tun}(E) + J_{dr}(E) + J_{ss}(E) + J_{br}(E) \quad (10)$$

If the total measured recombination current density is dominated by $J_{et}(E)$ (i.e., $J_{et}(E) \approx J_{rec}(E)$), then measurement of $J_{rec}(E)$ provides a direct measurement of k_{et} through use of eq 6, provided that $n_s(E)$ (i.e., either V_{bi} or the barrier height $\phi_b = V_{bi} + (kT/q)(\ln N_c/N_d)$,[47] where N_c is the effective density of states in the conduction band) is known. Otherwise, if it can be shown that $J_{rec}(E)$ is not limited by $J_{et}(E)$ (i.e., $|J_{rec}(E)| >> |J_{et}(E)|$), then measurement of $J_{rec}(E)$ can be used with eqs 6 and 7 to establish an upper limit on the value of $J_{et}(E)$. Under these conditions, use of eqs 6 and 7 allows establishment of an upper bound for k_{et} of the semiconductor/liquid interface of concern.

Prior work from several laboratories has shown that, in contrast to directly measuring $J_{rec}(E)$, it is experimentally advantageous to measure the magnitude of the voltage at open circuit, V_{oc}, developed by a cell at a given photocurrent density.[50,51] Measurement of V_{oc} is advantageous because negligible net current flows through the interface during the measurement, so effects of uncompensated ohmic resistance losses, mass transport overpotentials, kinetic overpotentials, and other significant corrections to

$J_{rec}(E)$ are minimized at J = 0 (i.e., at $E = -V_{oc}$ for an n-type semiconductor).[52] When J = 0 and $J_{rec}(E)$ $J_{et}(E)$ (and $V_{oc} >> kT/q$), eqs 6 and 8 yield

$$V_{oc} = \left(\frac{kT}{q}\right)\left[\ln\left(\frac{J_{ph}}{-J_{et}(0)}\right)\right] \tag{11}$$

or equivalently

$$V_{oc} = \left(\frac{kT}{q}\right)\left[\ln\left(\frac{J_{ph}}{N_d k_{et}[A]}\right)\right] + V_{bi} \tag{12}$$

Under these conditions, measurement of V_{oc} at a known value of J_{ph} directly yields a value for k_{et} if N_d and V_{bi} are known.

Alternatively, if it can be established that $|J_{et}(E)| << |J_{rec}(E)|$, then the inequality in eq 13 must hold:

$$V_{oc} < \left(\frac{kT}{q}\right)\left[\ln\left(\frac{J_{ph}}{qN_d k_{et}[A]}\right)\right] + V_{bi} \tag{13}$$

In other words, when another recombination mechanism dominates V_{oc}, the experimentally determined open-circuit voltage allows establishment of an upper limit on the magnitude of the direct interfacial charge-transfer current density, $|J_{et}(E)|$. This upper limit of $|J_{et}(E)|$ then provides an upper limit on k_{et}, if V_{bi} is known. Measurement of V_{oc} at a known cell temperature and photocurrent density can therefore be used to either establish k_{et} directly (eq 12) or can be used to establish an upper bound on the possible value of k_{et} (eq 13).

III. EXPERIMENTAL

A. Electrodes and Materials

All semiconductor electrodes were fashioned using the general procedure described below. After making an ohmic contact, each sample was attached to a Sn:Cu wire with Ag print (GC Electronics). The wire was enclosed in glass tubing, and after mounting the sample onto the wire, the back and edges of the electrode assembly were insulated from the solution by white epoxy (Dexter Corp.). Electrode areas were quantified by photographing

the electrodes concurrently with a microruler, followed by magnifying the images and digitizing them.

Phosphorus-doped n-type (100)-oriented silicon wafers were obtained from Silicon Sense, Inc. (Nashua, NH) with a dopant density of 9 x 10^{16} cm^{-3}. A Ga:In eutectic provided ohmic contacts to the back sides of these wafers.[53] Immediately before use in an electrochemical cell, the Si electrode was etched by immersion into a 48% HF(aq) solution (Mallinckrodt) twice for 30 s, followed by rinsing with 18 M cm resistivity H_2O obtained from a Barnstead NANOpure filter system. After each etching step, the electrode was dried under a stream of N_2(g).

The n-type gallium arsenide wafers ((100) orientation, selenium-doped; Laser Diode Co.) had dopant densities of (0.9-1.9) x 10^{17} cm^{-3}. Ohmic contacts were made by evaporation of 1000 Å of an 88:12 alloy of Au:Ge, followed by annealing at 480°C for 5 min under forming gas.[54] The GaAs electrodes were etched in a solution of 0.05% (v/v) Br_2 in CH_3OH followed by immersion in 1.0 M KOH(aq). The etching protocol of such electrodes was identical to that described in prior reports from this laboratory.[55]

Methanol (EM Science) and acetonitrile (EM Science) were dried before use and distilled under N_2(g). Methanol was dried over Mg filings, while acetonitrile was predried over CaH_2 and then dried over P_2O_5. Ferrocene (Fc, Aldrich) and dimethylferrocene (Me_2Fc, Strem) were purified by sublimation before use. $FcBF_4$ and Me_2FcBF_4 were prepared as previously described[56] and were dried under active vacuum for at least 4 h at room temperature. Lithium perchlorate (Aldrich) was dried by fusing at 280°C under active vacuum. All reagents listed above were stored in a N_2(g)-purged drybox until use.

B. Electrochemical Cells and Instrumentation

All solids were introduced into the cell vessel inside the drybox. For n-Si/CH_3OH-$Me_2Fc^{+/0}$ contacts, the cells were then removed from the drybox and CH_3OH was added

by syringe under nitrogen. The electrodes were then introduced into the cell under a $N_2(g)$ purge. After introduction of the electrodes, the cell remained sealed over the course of each set of experiments. The n-GaAs cells were sufficiently sensitive to air that the above procedure yielded instability in the curves of current density vs potential. The solids and solvents for these cells were instead separately transferred into a nitrogen flushbox that contained less than 10 ppm of O_2 (as monitored by the fuming of $(CH_3CH_2)_2Zn$). The solids were dissolved in an appropriate solvent, and the electrodes were etched within the flushbox and added to the cell. All electrochemical experiments with these systems were then conducted within the flushbox.

All cells utilized a three-electrode potentiostatic setup, with a Pt wire reference electrode poised at the Nernstian solution potential and a Pt foil or Pt gauze counter electrode. The area of the counter electrode was at least ten times larger than that of the working electrode, to minimize any set-up related impedance losses and to minimize mass transport overpotentials at the counterelectrode. For the n-Si junctions, the concentrations of the cell components were typically 0.100 M of the reduced form of the redox couple (A^-), 0.010 M of the oxidized form of the redox couple (A), and 1.00 M of electrolyte. The composition of n-GaAs cell solutions differed only in the concentration of electrolyte, which was limited to 0.70 M by solubility constraints. These precautions (large counterelectrode, high concentrations of both forms of the redox couple, large working electrode areas, etc.) were essential to obtaining highly reproducible, minimal frequency dispersion of the differential capacitance of the semiconductor/liquid contacts studied in this work. This minimal frequency dispersion contrasts with prior reports of the impedance properties of many of these same photoelectrode systems, which apparently contained non-linearities and/or frequency-dependent features that arose from an unoptimized experimental configuration of the cells and measurement apparatus and/or unoptimal electrode etching and surface preparation.[57-59]

All current density vs potential experiments were performed using an EG&G Princeton Applied Research (PAR) Model 173 Potentiostat in conjunction with a Houston Instruments Omnigraphic 2000 recorder and an EG&G PAR Model 175 Universal Programmer. Light intensities were controlled by the use of an ENH-type W-halogen bulb in conjunction with neutral density filters. Impedance spectra were obtained on a computer-controlled Schlumberger Model 1260 Frequency Response Analyzer equipped with a Model 1286 Electrochemical Interface.

C. Built-in Voltage Measurements and Rate Constant Calculations

For experiments with semiconductors in non-aqueous electrolytes, the current density vs potential (J-*E*) behavior of each electrode was initially measured as a function of the incident light intensity. The J-*E* data were obtained at a scan rate of 50 mV s^{-1}, and direct measurements of V_{oc} and J_{sc} (where J_{sc} is the current density at short circuit and is assumed to be equal to J_{ph}) were taken at each light intensity by reading the appropriate quantities through a digital multimeter that had been connected to the electrochemical cell. These J-*E* measurements were repeated after each set of impedance measurements to verify that the properties of the electrode remained constant over the time scale of the impedance measurements.

The built-in voltages, V_{bi}, of the various semiconductor/liquid junctions were calculated from electrochemical impedance data. An impedance measurement consisted of 11 or 13 frequency sweeps, each with an ac voltage of 10 mV rms amplitude. Each sweep was performed at a different dc potential in reverse bias. The ac frequency range was varied for each semiconductor/liquid system in order to identify the region of purely capacitive behavior of the semiconductor/liquid contact. Impedance data were fit to an equivalent circuit consisting of a resistor R_{sc} (representing the resistance to Faradaic charge transfer) in parallel with a capacitor C_{sc} (representing the differential capacitance of the

semiconductor space charge region), both of which were in series with a resistance R_s (representing resistive losses through the solution, leads, etc.). This model assumes that the measured differential capacitance (C_{diff}) equals C_{sc}. The differential space-charge capacitance was computed from the impedance data using the equation[60]

$$2\pi f C_{diff} = \frac{1+(1-4(Z_{im}/R_{sc})^2)^{1/2}}{2Z_{im}} \quad (14)$$

where f is the frequency of the ac voltage and Z_{im} is the imaginary part of the measured impedance, Z, at the dc bias of interest. R_{sc} values were taken as the diameter of a semicircular fit to a Nyquist plot (Z_{im} vs Z_{real} as a function of f, where Z_{real} is the real part of the measured impedance) at each dc bias. The differential capacitance was then related to the built-in voltage of the semiconductor/liquid junction by the Mott-Schottky equation:[10]

$$C_{sc}^{-2} = \frac{2}{q\varepsilon\varepsilon_0 N_d A_s^2}(E - V_{bi} - \frac{kT}{q}) \quad (15)$$

Here ε is the dielectric constant of the semiconductor, ε_0 is the permittivity of free space, and A_s is the area of the semiconductor electrode. A plot of E vs C_{diff}^{-2}, followed by extrapolation of the data to infinite capacitance and application of the correction factor (kT/q) (eq 15), yielded the built-in voltage of the solid/liquid contact. The validity of the equivalent circuit model used in this work was assessed by computing the slopes of the lines of C_{sc}^{-2} vs E at each frequency of the ac voltage and comparing these slopes to those expected from the known dopant density, area, and dielectric constant of the electrode in question. Within a data set, only data which exhibited linear C_{diff}^{-2} vs E ($R^2 \geq 0.999$, where R is the correlation coefficient) plots having slopes which corresponded to the measured dopant density to within 50% were considered. Electrodes that yielded non-linear or frequency-dependent plots for all frequency values were considered defective and were not included in the analysis.

IV. RESULTS

A. Differential Capacitance vs Voltage Data and Barrier Heights for n-Si/CH_3OH-$Me_2Fc^{+/0}$ Contacts

Previous measurements have shown that n-Si/CH_3OH-$Me_2Fc^{+/0}$ contacts exhibit *J-E* properties that are limited only by minority carrier (hole injection) currents.[50] In these systems, the open-circuit voltage has been quantitatively described by the Shockley diode equation for bulk minority carrier diffusion/recombination processes;[50] thus, $J_{rec}(E) = J_{br}(E)$. This observation, combined with the lack of dependence of V_{oc} on $[Me_2Fc^+]$,[50] implies that transfer of electrons from the Si conduction band to the Me_2Fc^+ acceptor ion is not rate-limiting. Thus $|J_{br}| >> |J_{et}|$ for $[Me_2Fc^+] \leq 0.10$ M at n-Si/CH_3OH-$Me_2Fc^{+/0}$ contacts.

For Si samples with the minimum value of $|J_{br}(V_{oc})|$ investigated to date under 1 Sun illumination (i.e., samples with the minimum value of the quantity $(n_i^2/L_p N_d)$, where n_i is the intrinsic carrier concentration of the semiconductor and L_p is the minority carrier diffusion length), $V_{oc} = 0.670$ V at $J_{ph} = 20$ mA cm^{-2} and T = 300 K.[50] The value of $|J_{et}|$ must therefore be less than 20 mA cm^{-2} at $E = 0.670$ V and [A] = 0.10 M. Since $|J_{et}(0)| <$ 9.5 x 10^{-14} A cm^{-2} from eq 8, an upper bound for k_{et} can then be established from the inequality of eq 13 if V_{bi} can be determined.

Differential capacitance vs potential data were used to measure V_{bi} for n-Si/CH_3OH-$Me_2Fc^{+/0}$ contacts. Figure 1 displays the measured circuit impedance as a function of frequency, in Bode plot form (log $|\mathbf{Z}|$ vs log f, where $|\mathbf{Z}|$ is the magnitude of the impedance vector), for an electrode potential of 0.30 V vs $E(A/A^-)$. For 5 kHz < f < 100 kHz, the slope of the Bode plot was -0.984±0.003; i.e., the differential capacitance was essentially independent of the measurement frequency. Similar behavior was observed for all potentials in reverse bias, with 0.00 V < *E* < 0.50 V vs $E(A/A^-)$.

Figure 2a displays a plot of C_{diff}^{-2} vs *E* at six different measurement frequencies, and Figure 2b shows the extrapolated linear fits to these data. For this electrode, the

Figure 1. Bode plot of a n-Si/CH_3OH-$Me_2Fc^{+/0}$ junction. The cell solution consisted of 0.100 M Me_2Fc, 0.014 M Me_2FcBF_4, and 1.00 M $LiClO_4$. This plot was taken at +0.30 V vs $E(A/A^-)$. The electrode area was 0.864 cm^2, and its N_d calculated from four-point probe measurements was 9.26 x 10^{16} cm^{-3}.

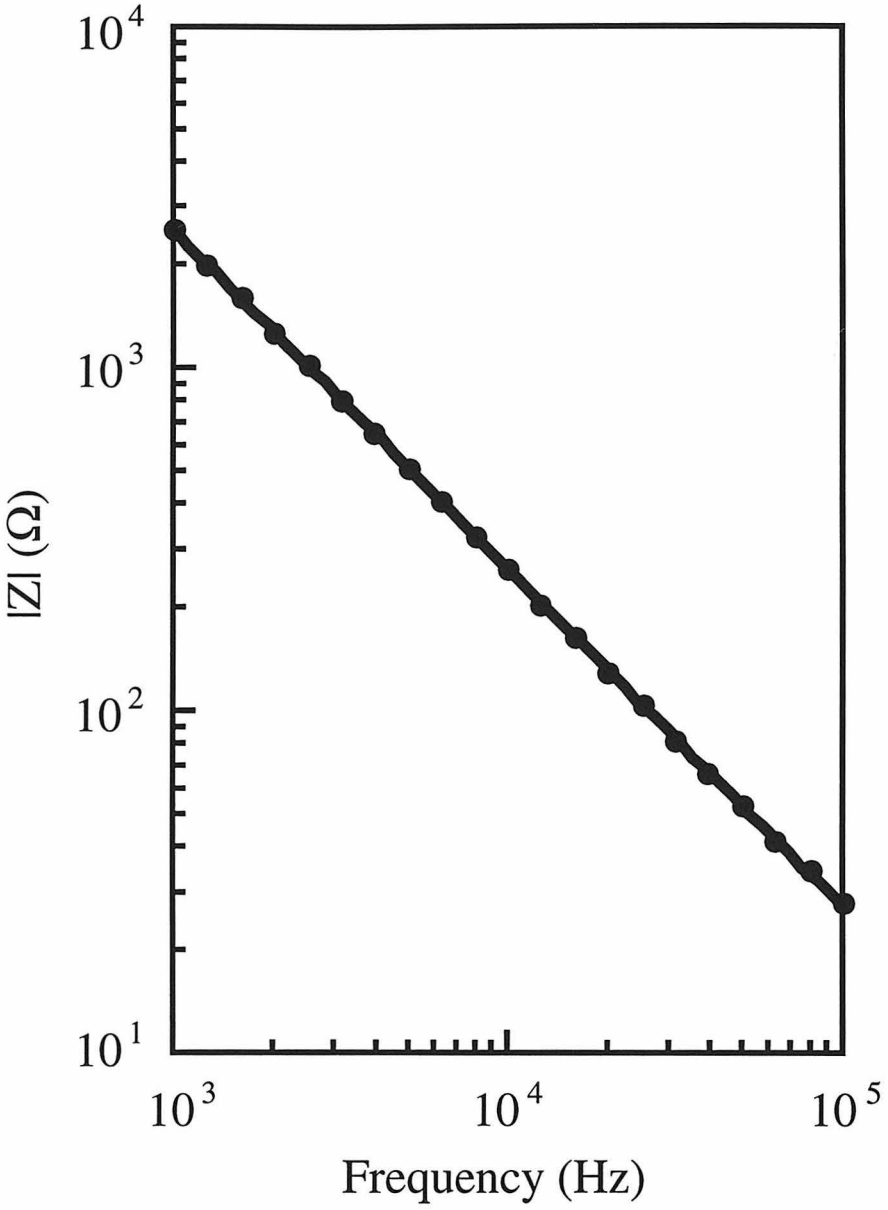
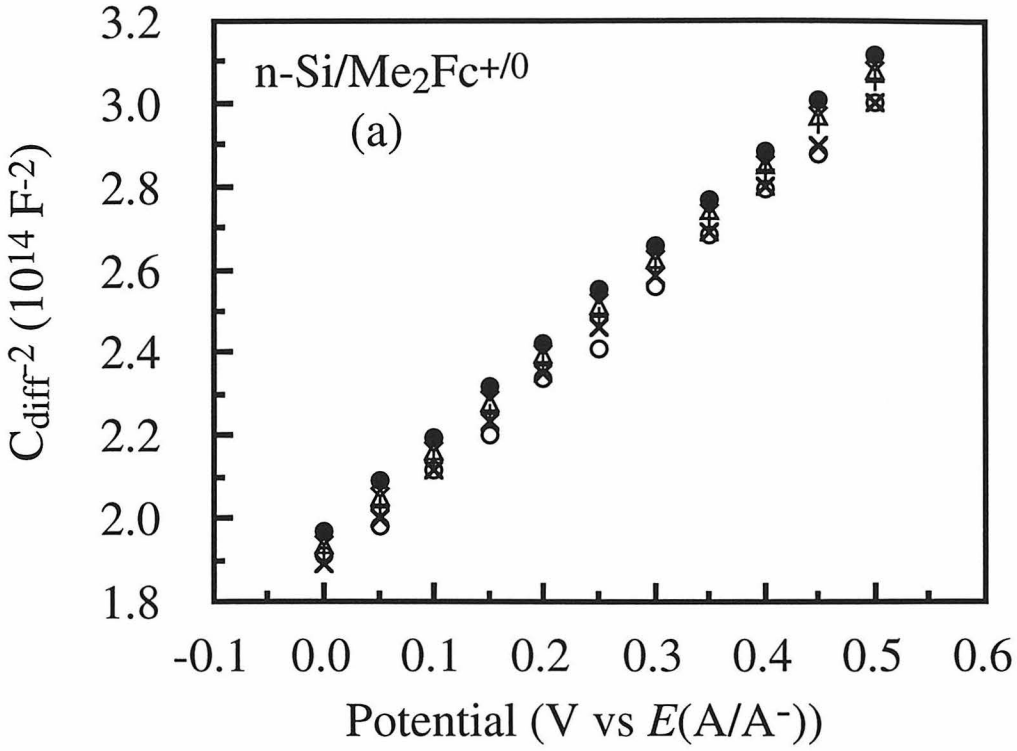
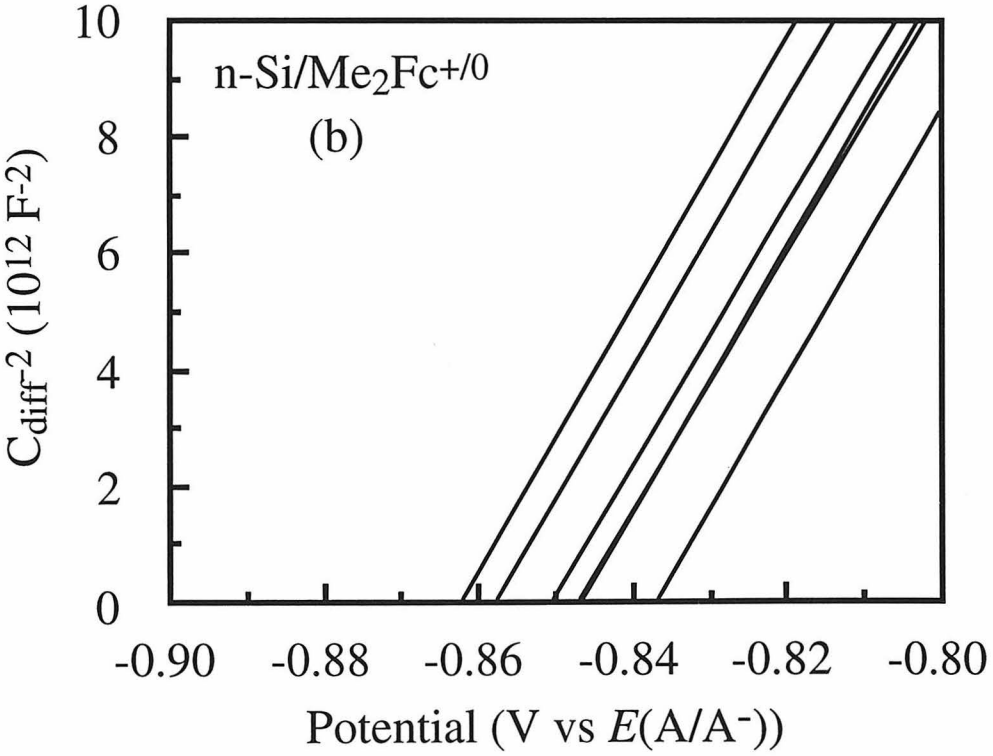

10^4
10^3
10^2
10^1
|Z| (Ω)
10^3
10^4
10^5
Frequency (Hz)

Figure 2. (a) Mott-Schottky plot of the n-Si/CH_3OH-$Me_2Fc^{+/0}$ junction described in Figure 1. The range of the six different measuring frequencies shown was 1 to 100 kHz. (b) The linear extrapolations of the data in (a). All linear fits yielded correlation coefficients of 0.999 or greater.


n-Si/Me2Fc+/0
(a)
3.2
3.0
2.8
2.6
2.4
2.2
2.0
1.8
-0.1
0.0
0.1
0.2
0.3
0.4
0.5
0.6
Cdiff-2 (1014 F-2)
Potential (V vs E(A/A-))


n-Si/Me2Fc+/0
(b)
10
8
6
4
2
0
-0.90
-0.88
-0.86
-0.84
-0.82
-0.80
Cdiff-2 (1012 F-2)
Potential (V vs E(A/A-))

average extrapolated x-intercept was 0.850±0.009 V, and thus the built-in voltage, V_{bi}, using eq 15 was 0.876±0.009 V. The value of the slope was (2.267±0.030) x 10^{14} F^{-2} V^{-1}, which was within 25% of the slope predicted from eq 15 using the independently determined values for the electrode area and dopant concentration (obtained from four-point probe measurements). The variation in V_{bi} with frequency was < 30 mV for 1 kHz < f < 100 kHz. A series of three determinations with nominally identical electrodes resulted in an average value of V_{bi} = 0.884±0.014 V for the n-Si/CH_3OH-$Me_2Fc^{+/0}$ contact.

B. Upper Bound on k_{et} for n-Si/CH_3OH-$Me_2Fc^{+/0}$ Contacts

In conjunction with eq 13, these V_{bi} values allow establishment of upper bounds on k_{et} for the n-Si/CH_3OH-$Me_2Fc^{+/0}$ interface. The barrier height of the junction is related to the built-in voltage by the equation[47]

$$\phi_b = V_{bi} + \frac{kT}{q}\ln\left(\frac{N_c}{N_d}\right) \tag{16}$$

for an n-type semiconductor. Combination of eq 16 with eq 13 yields the expression

$$V_{oc} < \left(\frac{kT}{q}\right)\left[\ln\left(\frac{J_{sc}}{qN_c k_{et}[A]}\right)\right] + \phi_b \tag{17}$$

Use of ϕ_b = 1.03 V (V_{bi} = 0.88, N_d = 9.26 x 10^{16} cm^{-3}) at [A] = 14 mM = 8.3 x 10^{18} cm^{-3} from the present differential capacitance measurements yields an upper limit of k_{et} < 10^{-15} cm^4 s^{-1}. Previous measurements of the barrier height, ϕ_b, have been made using near-surface conductance data.[46] Use of ϕ_b = 1.01 V (from the transconductance measurements[46]) at [A] = 2.7 mM = 1.7 x 10^{18} cm^{-3} in eq 17 also implies that k_{et} < 10^{-15} cm^4 s^{-1}. The ϕ_b values determined in this laboratory are in good agreement with previous measurements of ϕ_b for the n-Si/CH_3OH-$Me_2Fc^{+/0}$ interface, which have yielded values of ϕ_b = 0.98 V[57] and ϕ_b = 1.06 V.[58] Note that to the extent that reliable barrier heights are obtained, the kinetic data produces rigorous limits for k_{et}. If k_{et} were to exceed these values, the open-circuit voltage of the n-Si/CH_3OH-$Me_2Fc^{+/0}$ contact would be lower than

the value observed experimentally (eq 12), and a change in rate law to that expected for direct electron transfer (eq 9) would have been observed.[61]

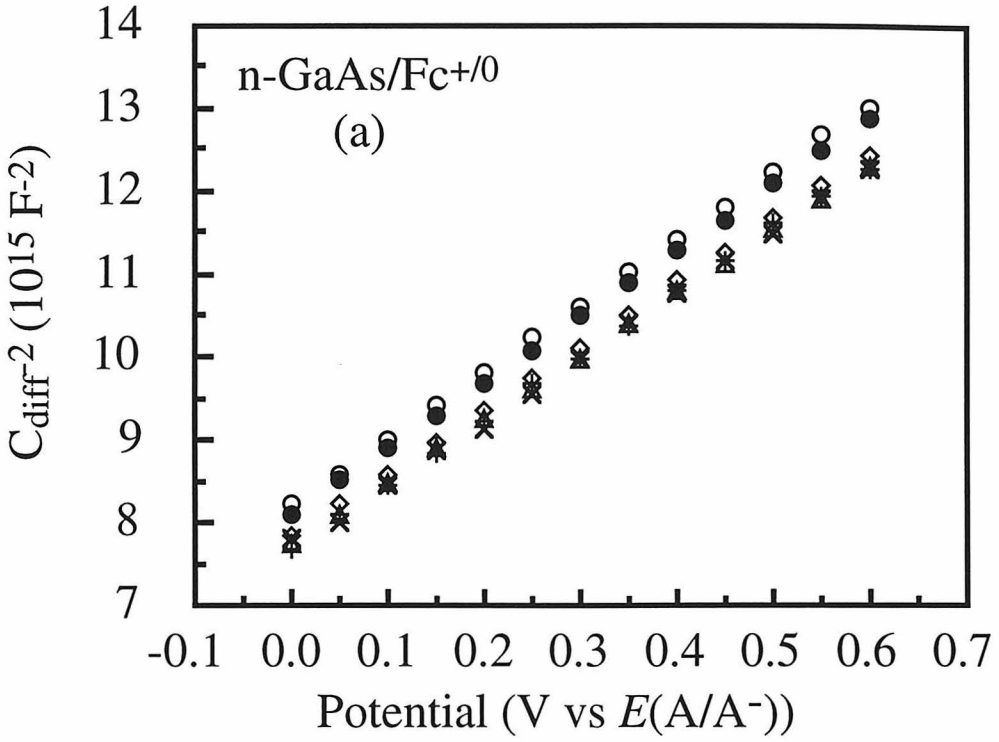
C. Barrier Height Measurements and Upper Bounds on k_{et} for n-GaAs/CH_3CN-$Fc^{+/0}$ Contacts

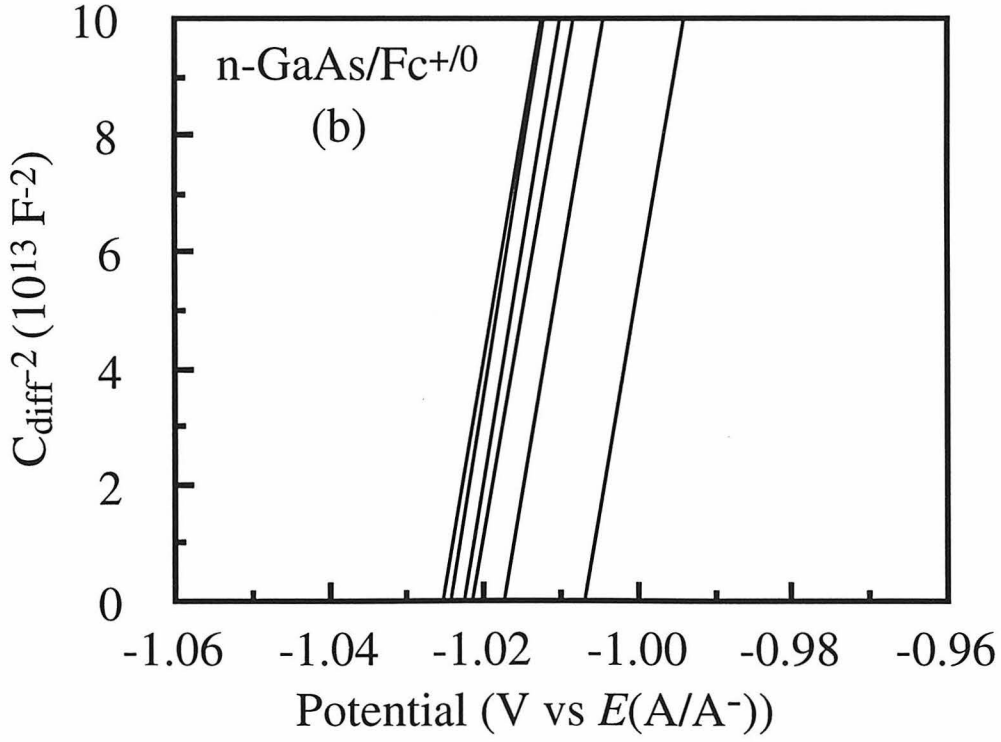
Analogous experiments have been performed for n-GaAs/CH_3CN-$Fc^{+/0}$ contacts. These interfaces also provide efficient, stable photoelectrochemical cells with an outer-sphere redox couple, so reliable determinations of ϕ_b for this system would provide an upper bound for k_{et} in this cell as well.

The n-GaAs/CH_3CN-$Fc^{+/0}$ junction yielded linear Mott-Schottky plots, and the differential capacitance of the junction was independent of frequency for $251 \leq f \leq 5012$ Hz. For example, in the specific experiment displayed in Figure 3, the average extrapolated x-intercept for six different measuring frequencies was 1.020±0.007 V. These intercepts yielded an average V_{bi} of 1.046±0.007 V. The average observed slope of (7.734±0.190) x 10^{15} F^{-2} V^{-1} yielded a value for the dopant density that was in good agreement with that specified by the manufacturer of the sample (calculated $N_d = 1.8 \times 10^{17}$ cm^{-3}; specified $N_d = (0.9\text{-}1.9) \times 10^{17}$ cm^{-3}). Three independent determinations of the Mott-Schottky behavior of n-GaAs/CH_3CN-$Fc^{+/0}$ junctions yielded an average V_{bi} of 1.053±0.023 V. This V_{bi} is lower than the value of V_{bi} = 1.27 V obtained previously for this semiconductor/liquid contact,[62] but we consider the value obtained in this work reliable in view of the internal consistency of the impedance data and its independence of frequency over the range of interest.

Previous studies have established that V_{oc} for the n-GaAs/CH_3CN-$Fc^{+/0}$ system under 1 Sun illumination at 300 K is not controlled by direct majority carrier transfer to the Fc^+ acceptor species.[54] Thus, the inequality of eq 13 applies to this system. Using the values of V_{bi} = 1.053 V, V_{oc} = 0.677 V, J_{ph} = 6.9 mA cm^{-2} and $N_d = 1.4 \times 10^{17}$ cm^{-3}

Figure 3. (a) Mott-Schottky plot of a n-GaAs/CH_3CN-$Fc^{+/0}$ junction. The cell solution contained 0.100 M Fc, 0.030 M $FcBF_4$, and 0.70 M $LiClO_4$. The electrode area was 0.0882 cm^2, and the N_d range was (0.9-1.9) x 10^{17} cm^{-3}. Six different frequencies ranging from 251 to 5012 Hz are shown. (b) The extrapolations of the data points in (a). All linear fits resulted in correlation coefficients of greater than 0.999.


n-GaAs/Fc+/0
(a)
C_{diff}^{-2} (10^{15} F^{-2})
14
13
12
11
10
9
8
7
-0.1
0.0
0.1
0.2
0.3
0.4
0.5
0.6
0.7
Potential (V vs $E(A/A^-)$)


n-GaAs/Fc+/0
(b)
C_{diff}^{-2} (10^{13} F^{-2})
10
8
6
4
2
0
-1.06
-1.04
-1.02
-1.00
-0.98
-0.96
Potential (V vs $E(A/A^-)$)

measured in this work, and the relationship between k_{et} and the photovoltage given by eq 13, yields $k_{et} < 10^{-14}$ cm^4 s^{-1}. Since the difference between V_{oc} and V_{bi} was larger for n-GaAs/CH_3CN-$Fc^{+/0}$ contacts than for n-Si/CH_3OH-$Me_2Fc^{+/0}$ contacts (vide supra), the upper bound on k_{et} obtained from the n-GaAs/CH_3CN/$Fc^{+/0}$ data is not as small as that for the n-Si/CH_3OH-$Me_2Fc^{+/0}$ system.

V. DISCUSSION

Although the data presented herein do not establish absolute values for k_{et}, they do allow definition of upper bounds on k_{et} of less than 10^{-14} cm^4 s^{-1} for the n-Si and n-GaAs semiconductor/liquid interfaces that have been investigated. This approach also extends a previously proposed protocol for establishing which interfaces are suitable for use in a comparison between the theoretical predictions and the experimental data.[55] Estimates of λ and measurements of V_{bi} for these well-behaved semiconductor/liquid junctions indicate that κ_n is on the order of 10^{-1}-10^0 for the contacts discussed herein. These data therefore serve to establish semi-quantitative upper bounds on $k_{et,max}$ for these systems. The measurements and calculations discussed above are also in agreement with recent determinations of k_{et} for p-WS_2/H_2O-$Ru(NH_3)_6^{3+/2+}$ contacts,[15] with measurements of k_{et} for n-WSe_2/CH_3CN-$Me_2Fc^{+/0}$ contacts,[63] and with upper limits on k_{et} that have been estimated previously for n-Si/liquid contacts.[14,40,46,52]

The maximum possible value of the second-order interfacial charge-transfer rate constant is pertinent to optimal efficiencies for photoelectrochemical solar energy conversion devices. Specifically, a large majority carrier charge-transfer rate constant is undesirable for the construction of efficient photoelectrochemical energy conversion devices. For example, from eq 9, with $k_{et} = 10^{-12}$ cm^4 s^{-1}, $N_d = 10^{16}$ cm^{-3} and [A] = 0.10 M, $|J_{et}(0)| = (1 \times 10^5) \exp(-qV_{bi}/kT)$. Setting $J_{rec} = J_{et}$ in eq 10, and taking $J_{ph} = 20$ mA cm^{-2} (eq 12) allow calculation of the maximum possible V_{oc} under these conditions. Such a

calculation implies that V_{oc} - V_{bi} = -0.40 V, and that the difference between ϕ_b and V_{oc} is 0.55-0.65 V. Thus, even in the optimized situation of extremely high barrier heights, with $\phi_b \approx E_g/q$, V_{oc} would be much less than (E_g/q) due to efficient majority carrier capture process. Losses in quantum yield would also be observed in the short-wavelength spectral response of such semiconductor/liquid contacts,[64] due to the efficient competition between drift-induced charge separation and concentration-gradient-driven charge recombination processes that would occur with such a large majority carrier collection velocity.[64] The construction of efficient photoelectrochemical cells, such as those reported in the literature using n-Si/CH_3OH-$Me_2Fc^{+/0}$,[51,65,66] n-GaAs/CH_3CN-$Fc^{+/0}$,[67,68] p-Si/CH_3CN-cobaltocene$^{+/0}$,[69] and other semiconductor/liquid contacts[70] would not appear to be possible with this value of the second-order rate constant for interfacial majority carrier charge transfer.[71]

Very large interfacial electron-transfer rate constants would effect unusual electrical junction properties, as underscored by comparison of the predicted recombination current density at semiconductor/liquid interfaces with various values of k_{et} to the recombination current density observed for semiconductor/metal Schottky barriers.[47] For Schottky barriers, essentially every majority carrier that reaches the semiconductor/metal junction is captured by the metal phase.[47] The thermionic emission-diffusion current density for semiconductor/metal contacts, which describes this charge-carrier capture process, is[47]

$$J_{th}(0) = -A^{*}T^{2}\exp\left(\frac{-q\phi_b}{kT}\right) \qquad (18)$$

where A^* is the effective Richardson constant for thermionic emission. Combining eqs 8 and 18 therefore yields the ratio between the charge-transfer current densities for semiconductor/metal and semiconductor/liquid contacts of identical barrier heights:

$$\frac{J_{et}(0)}{J_{th}(0)} = \left[\frac{qk_{et}[A]N_c}{A^{*}T^{2}}\right] \qquad (19)$$

With $k_{et} = 10^{-12}$ cm^4 s^{-1} and [A] = 0.10 M = 6 x 10^{19} cm^{-3} (a typical value for operating photoelectrochemical cells), eq 19 predicts that $J_{et} \approx J_{th}$. In other words, with such a large second-order electron-transfer rate constant, the steady-state majority carrier recombination losses from an interfacial electron-transfer process would be as severe as those for semiconductor/metal contacts, in which essentially every majority carrier that reaches the surface is collected in a deleterious recombination event. This efficient capture by the redox acceptors in the solution would be occurring at only [A] = 0.10 M, i.e., under conditions when > 99% of the volume of the solution, and > 99% of the geometric cross-sectional area presented to the electron, was occupied by inert, spectator species such as the electrolyte ions and the solvent molecules. Smaller values of k_{et}, such as those established in this work, therefore correspond more closely to the expected situation in which the capture cross section of the acceptor species is approximately its geometric cross section.[72] Small majority carrier interfacial rate constants are thus desirable for the construction of efficient photoelectrochemical cells.

In summary, upper limits on k_{et} have been experimentally determined for two semiconductor/liquid systems which have been previously shown to exhibit stable, nonresistive diode behavior. The limits on the second-order interfacial electron-transfer rate constants determined for these systems are consistent with theoretical expectations. Further quantitative study of these charge-transfer rate constants either requires the identification of systems in which the charge transfer over the barrier dominates the recombination current, or demands exploiting another reliable technique by which these rate constants can be measured.

VI. ACKNOWLEDGMENT

This research work was funded by the National Science Foundation, Grant CHE-9221311.

VII. REFERENCES AND NOTES

(1) Closs, G. L.; Calcaterra, L. T.; Green, N. J.; Penfield, K. W.; Miller, J. R. *J. Phys. Chem.* **1986**, *90*, 3673.

(2) McLendon, G.; Miller, J. R. *J. Am. Chem. Soc.* **1985**, *107*, 7811.

(3) Marcus, R. A.; Sutin, N. *Biochim. Biophys. Acta* **1985**, *811*, 265.

(4) Fox, L. S.; Kozik, M.; Winkler, J. R.; Gray, H. B. *Science* **1990**, *247*, 1069.

(5) Saji, T.; Yamada, T.; Aoyagui, S. *J. Electroanal. Chem.* **1975**, *61*, 147.

(6) Saji, T.; Maruyama, Y.; Aoyagui, S. *J. Electroanal. Chem.* **1978**, *86*, 219.

(7) Miller, C.; Grätzel, M. *J. Phys. Chem.* **1991**, *95*, 5225.

(8) Chidsey, C. E. D.; Bertozzi, C. R.; Putvinski, T. M.; Mujsce, A. M. *J. Am. Chem. Soc.* **1990**, *112*, 4301.

(9) Ravenscroft, M. S.; Finklea, H. O. *J. Phys. Chem.* **1994**, *98*, 3843.

(10) Morrison, S. R. *Electrochemistry at Semiconductor and Oxidized Metal Electrodes*; Plenum: New York, 1980.

(11) Koval, C. A.; Howard, J. N. *Chem. Rev.* **1992**, *92*, 411.

(12) Memming, R. *Ber. Bunsenges. Phys. Chem.* **1987**, *91*, 353.

(13) Gerischer, H. In *Physical Chemistry: An Advanced Treatise*; H. Eyring; D. Henderson and W. Yost, Ed.; Academic: New York, 1970; Vol. 9A; pp 463.

(14) Lewis, N. S. *Annu. Rev. Phys. Chem.* **1991**, *42*, 543.

(15) Horrocks, B. R.; Mirkin, M. V.; Bard, A. J. *J. Phys. Chem.* **1994**, *98*, 9106.

(16) Miller, B.; Menezes, S.; Heller, A. *J. Electrochem. Soc.* **1979**, *126*, 1483.

(17) Rosenwaks, Y.; Thacker, B. R.; Nozik, A. J.; Ellingson, R. J.; Burr, K. C.; Tang, C. L. *J. Phys. Chem.* **1994**, *98*, 2739.

(18) Marcus, R. A. *J. Phys. Chem.* **1991**, *95*, 2010.

(19) Ibach, H.; Luth, H. *Solid-State Physics*; Springer Verlag: Berlin, 1990.

(20) Miller, J. R.; Beitz, J. V.; Huddleston, R. K. *J. Am. Chem. Soc.* **1984**, *106*, 5057.

(21) Domingue, R. P.; Fayer, M. D. *J. Chem. Phys.* **1985**, *83*, 2242.

(22) Bowler, B. E.; Raphael, A. L.; Gray, H. B. *Prog. Inorg. Chem.* **1990**, *38*, 259.

(23) Axup, A. W.; Albin, M.; Mayo, S. L.; Crutchley, R. J.; Gray, H. B. *J. Am. Chem. Soc.* **1988**, *110*, 435.

(24) Elias, H.; Chou, M. H.; Winkler, J. R. *J. Am. Chem. Soc.* **1988**, *110*, 429.

(25) Mayo, S. L.; Ellis, W. R.; Crutchley, R. J.; Gray, H. B. *Science* **1986**, *233*, 948.

(26) Oevering, H.; Paddon-Row, M. N.; Heppener, M.; Oliver, A. M.; Cotsaris, E.; Verhoeven, J. W.; Hush, N. S. *J. Am. Chem. Soc.* **1987**, *109*, 3258.

(27) Paddon-Row, M. N.; Oliver, A. M.; Warman, J. M.; Smit, K. J.; de Haas, M. P.; Oevering, H.; Verhoeven, J. W. *J. Phys. Chem.* **1988**, *92*, 6958.

(28) Closs, G. L.; Miller, J. R. *Science* **1988**, *240*, 440.

(29) Penfield, K. W.; Miller, J. R.; Paddon-Row, M. N.; Cotsaris, E.; Oliver, A. M.; Hush, N. S. *J. Am. Chem. Soc.* **1987**, *109*, 5061.

(30) Isied, S. S.; Vassilian, A.; Wishart, J. F.; Creutz, C.; Schwarz, H. A.; Sutin, N. *J. Am. Chem. Soc.* **1988**, *110*, 635.

(31) Schanze, K. S.; Sauer, K. *J. Am. Chem. Soc.* **1988**, *110*, 1180.

(32) Leland, B. A.; Joran, A. D.; Felker, P. M.; Hopfield, J. J.; Zewail, A. H.; Dervan, P. B. *J. Phys. Chem.* **1985**, *89*, 5571.

(33) Geno, M. J. K.; Dawson, J. H. *Inorg. Chem.* **1984**, *23*, 1182.

(34) Finckh, P.; Heitele, H.; Volk, M.; Michelbeyerle, M. E. *J. Phys. Chem.* **1988**, *92*, 6584.

(35) Woitellier, S.; Launay, J. P.; Spangler, C. W. *Inorg. Chem.* **1989**, *28*, 758.

(36) Finklea, H. O.; Hanshew, D. D. *J. Am. Chem. Soc.* **1992**, *114*, 3173.

(37) Carter, M. T.; Rowe, G. K.; Richardson, J. N.; Tender, L. M.; Terrill, R. H.; Murray, R. W. *J. Am. Chem. Soc.* **1995**, *117*, 2896.

(38) Gerischer, H. *J. Phys. Chem.* **1991**, *95*, 1356.

(39) Morrison, S. R. *Surf. Sci.* **1969**, *15*, 363.

(40) Forbes, M. D. E.; Lewis, N. S. *J. Am. Chem. Soc.* **1990**, *112*, 3682.

(41) Fajardo, A. M.; Lewis, N. S. *Science* **1996**, *274*, 969.

(42) Pomykal, K. E.; Lewis, N. S. *J. Phys. Chem. B* **1997**, *101*, 2476.

(43) Uhlendorf, I.; Reineke-Koch, R.; Memming, R. *J. Phys. Chem.* **1996**, *100*, 4930.

(44) Smith, B. B.; Halley, J. W.; Nozik, A. J. *Chem. Phys.* **1996**, *205*, 245.

(45) Fonash, S. J. *Solar Cell Device Physics*; Academic: New York, 1981.

(46) Laibinis, P. E.; Stanton, C. E.; Lewis, N. S. *J. Phys. Chem.* **1994**, *98*, 8765.

(47) Sze, S. M. *Physics of Semiconductor Devices;* 2nd ed.; Wiley: New York, 1981.

(48) Lewis, N. S. *J. Electrochem. Soc.* **1984**, *131*, 2496.

(49) Lewis, N. S. *Acc. Chem. Res.* **1990**, *23*, 176.

(50) Rosenbluth, M. L.; Lewis, N. S. *J. Am. Chem. Soc.* **1986**, *108*, 4689.

(51) Kobayashi, H.; Chigami, A.; Takeda, N.; Tsubomura, H. *J. Electroanal. Chem.* **1990**, *287*, 239.

(52) Kumar, A.; Lewis, N. S. *J. Phys. Chem.* **1991**, *95*, 7021.

(53) Finklea, H. O. *Semiconductor Electrodes*; Elsevier: New York, 1988.

(54) Casagrande, L. G.; Lewis, N. S. *J. Am. Chem. Soc.* **1985**, *107*, 5793.

(55) Bansal, A.; Tan, M. X.; Tufts, B. J.; Lewis, N. S. *J. Phys. Chem.* **1993**, *97*, 7309.

(56) Hendrickson, D. H.; Sohn, Y. S.; Gray, H. B. *Inorg. Chem.* **1971**, *10*, 1559.

(57) Tomkiewicz, M. *Electrochim. Acta* **1990**, *35*, 1631.

(58) Kobayashi, H.; Takeda, N.; Sugahara, H.; Tsubomura, H. *J. Phys. Chem.* **1991**, *95*, 813.

(59) Nagasubramanian, G.; Wheeler, B. L.; Bard, A. J. *J. Electrochem. Soc.* **1983**, *130*, 1680.

(60) Bard, A. J.; Faulkner, L. R. *Electrochemical Methods: Fundamentals and Applications*; Wiley: New York, 1980.

(61) These upper bounds on $k_{et,max}$ are conservative because effects of band edge movement under illumination, which would tend to yield lower barrier heights and thus even smaller upper bounds on $k_{et,max}$, have not been included in computing this $k_{et,max}$ value. For the outer-sphere redox couples used in this work, band edge movement is expected to be minimal, as shown by a direct measurement on the illuminated n-Si/CH_3OH-$Me_2Fc^{+/0}$ contact, for which the quasi-Fermi level of holes was equal, within experimental error, to the Nernstian potential of the solution.[73] A differential capacitance measurement on an illuminated (J_{sc} = 2 mA cm^{-2}) n-Si/CH_3OH-$Me_2Fc^{+/0}$ contact yielded a barrier height of 0.90 V; using this value yields an upper bound on $k_{et,max}$ that is on the same order of magnitude as that determined from use of the ϕ_b value determined for this contact in the dark.

(62) Ba, B.; Cachet, H.; Fotouhi, B.; Gorochov, O. *Semiconduct. Sci. Tech.* **1994**, *9*, 1529.

(63) Howard, J. N.; Koval, C. A. *Anal. Chem.* **1994**, *66*, 4525.

(64) Kumar, A.; Lewis, N. S. *J. Phys. Chem.* **1990**, *94*, 6002.

(65) Rosenbluth, M. L.; Lieber, C. M.; Lewis, N. S. *Appl. Phys. Lett.* **1984**, *45*, 423.

(66) Gibbons, J. F.; Cogan, G. W.; Gronet, C. M.; Lewis, N. S. *Appl. Phys. Lett.* **1984**, *45*, 1095.

(67) Kohl, P. A.; Bard, A. J. *J. Electrochem. Soc.* **1979**, *126*, 603.

(68) Gronet, C. M.; Lewis, N. S. *Appl. Phys. Lett.* **1983**, *43*, 115.

(69) Lieber, C. M.; Gronet, C. M.; Lewis, N. S. *Nature* **1984**, *307*, 533.

(70) Heben, M. J.; Kumar, A.; Zheng, C.; Lewis, N. S. *Nature* **1989**, *340*, 621.

(71) It is possible to speculate that effects of an extremely strong interfacial electric field could increase k_{et} for minority carriers above those described herein while not affecting the interfacial rate constant for minority carriers. As yet there appears to be neither theoretical nor experimental support for a process in which interfacial electric fields would accelerate the electron into a liquid sufficiently rapidly to produce a significant increase in the capture cross section for ions that are generally at distances in excess of the electron mean free path in the liquid phase.

(72) A semiclassical collision theory approach to estimate k_{et} yields

$$k_{et} = \sigma v \delta \qquad (20)$$

where σ is the cross section for reaction, v is the relative velocity of the reactants, and δ is the effective zone of reaction. For a typical molecular dimension of 3×10^{-8} cm, with a relative velocity of 10^7 cm s^{-1} (dominated by the thermal velocity of the charge carrier in the solid) and an effective distance for electron transfer of 10^{-7} cm, $k_{et} = 10^{-12}$ cm^4 s^{-1} implies a value for the cross section of $\sigma = 10^{-12}$ cm^2. Thus, $k_{et} = 10^{-12}$ cm^4 s^{-1} implies that ions which participate in the charge transfer process (presumably proceeding off-resonance) would exhibit the curious behavior of possessing capture cross sections that far exceeded their geometric cross sections. "Giant" cross sections for carrier capture of this magnitude have been reported for the solid state, but such processes are dominated by Coulombic attraction effects.[74] Coulombic attractions will be minimized in interfacial charge transfer processes by the presence of the electrolyte and the correspondingly small Debye screening lengths in the liquid phase.

(73) Tan, M. X.; Kenyon, C. N.; Lewis, N. S. *J. Phys. Chem.* **1994**, *98*, 4959.

(74) Fahrenbruch, A. L.; Bube, R. H. *Fundamentals of Solar Cells: Photovoltaic Solar Energy Conversion*; Academic: New York, 1983.

Chapter Three

Free-Energy Dependence of Electron-Transfer Rate Constants at Silicon/Liquid Interfaces

ABSTRACT

Differential capacitance vs potential and current density vs potential measurements have been used to characterize the interfacial energetics and kinetics, respectively, of n-type Si electrodes in contact with a series of one-electron, outer-sphere redox couples. The differential capacitance data yielded values for the electron concentration at the surface of the semiconductor as well as values for the driving force of the interfacial electron-transfer event at Si/CH_3OH-bipyridinium$^{2+/+}$ junctions. The differential capacitance vs potential measurements were essentially independent of the ac frequency imposed on the interface, with linear Bode plots (log |impedance| vs log frequency, at a fixed potential) between $\approx 10^3$ and $\approx 10^5$ Hz, with slopes typically between -0.99 and -1.00. The slopes of C^{-2}-E (Mott-Schottky) plots were in excellent agreement with theory, and little frequency dispersion was observed in the x-intercepts of such plots. The conduction band edge of the n-type Si anodes was invariant to within $\pm$ 40 mV in response to a variation in the redox potential of the solution of greater than 400 mV, indicating "ideal" interfacial energetic behavior of this system with no evidence for Fermi level pinning. From these measurements, the surface state density of the Si/CH_3OH contact can be estimated as $< 6 \times 10^{10}$ cm^2, *i.e.*, less than 1 defect for 10^4 surface atoms. The current density vs potential plots exhibited a first-order kinetic dependence on the concentration of electrons at the semiconductor surface and a first-order kinetic dependence on the concentration of acceptors in the solution. Rate constants for transfer of charge from the semiconductor to the acceptor were determined as a function of the driving force for the interfacial charge-transfer event. The rate constants

varied from 4 x 10^{-18} cm^4 s^{-1} to 6 x 10^{-17} cm^4 s^{-1} and were well fit to Marcus-type behavior, with a reorganization energy of 0.7 eV and a maximum rate constant at optimal exoergicity of 6 x 10^{-17} cm^4 s^{-1}. This maximum rate constant value is in excellent agreement with theoretical expectations for transfer of charge from a delocalized carrier in a semiconductor to a one-electron, outer-sphere redox acceptor dissolved in the electrolyte solution.

I. INTRODUCTION

An investigation of the upper limits on the charge-transfer rate constants across the semiconductor/liquid junction serves as a convenient starting point for the understanding of interfacial kinetic behavior. The upper limits on the electron-transfer rate constants at the n-Si/CH_3OH and n-GaAs/CH_3CN junctions, discussed in Chapter 2, provide valuable experimental results that corroborate the theoretical treatments.[1] These two junctions have previously been established as stable cells that exhibit predictable electrical behavior,[2,3] and while the currents through these systems are not limited by interfacial electron transfer, the facility of the necessary experiments somewhat compensates for the reduced scientific utility of an upper limit relative to a true rate constant. A more daunting enterprise would be to identify these same qualities of stability and well-behaved electrical properties in a semiconductor/liquid junction, the current of which is dominated by interfacial electron transfer, although such a system is precisely what is required for robust, steady-state measurements of the electron-transfer rate constant.

It is notable that despite the obvious pertinence of interfacial charge-transfer kinetics, not only to the performance of semiconductor-based electrochemical devices but also to the basic theories of heterogeneous charge transfer, only a handful of investigations have yielded conclusive evidence characterizing the movement of charge across the semiconductor/liquid junction.[4-8] Measurements of rate constants for the transfer of a delocalized charge carrier in a semiconductor phase to a localized, outer-sphere molecular species in a liquid phase have been thwarted by the poorly understood, nonideal behavior of most semiconductor/liquid contacts,[9,10] by the instability of semiconductor electrodes in aqueous electrolytes,[11,12] and by the inability to perform a systematic study of the interfacial kinetic processes for a homologous series of one-electron, outer-sphere redox systems having similar reorganization energies.

Recent work from our laboratory has shown that these drawbacks can be largely overcome through use of n-type Si electrodes in CH_3OH with a series of bipyridinium dications as the soluble one-electron acceptors.[7] Si electrodes are stable towards passivation or corrosion reactions in dry methanol,[13,14] and the driving force for interfacial charge transfer can be varied in this solvent system through the use of a homologous series of bipyridinium$^{2+/+}$ redox species.[2] Furthermore, such interfaces appear to exhibit simple and nearly ideal energetic and kinetic behavior.[7] The ability to vary the energetics for the interfacial charge-transfer event makes it possible to investigate the predictions of Marcus theory with regard to the variation in rate constant as function of driving force at the semiconductor/liquid contact.[15-17] In addition, such measurements allow experimental determination of the maximum charge-transfer rate constant at optimal exoergicity for such contacts, thereby allowing an estimate of the electronic coupling between the delocalized charge carriers in the semiconductor electrode and the localized electron acceptors in the solution phase. In the present work, we provide full details of these kinetic measurements and report new results on the kinetic and energetic behavior of this set of semiconductor/liquid junctions.

As explained in Chapter 1, the second-order reaction between delocalized electrons in the conduction band of the semiconductor and localized acceptors in the solution phase defines the current density J across a semiconducting electrode:[15,17]

$$J(E) = - q\, k_{et}\, n_s\, [A] \qquad (1)$$

where q is the electronic charge, k_{et} is the second-order rate constant, n_s is the electron concentration at the surface of the semiconductor, and [A] is the acceptor concentration. Measurement of J at a given potential E is straightforward, as is the measurement of [A]. The value of n_s can be also determined experimentally, as it is related to the electron concentration in the bulk, n_b, through a Boltzmann relation:[18]

$$n_s = n_b \exp\{q(E_{fb} - E)/kT\} \qquad (2)$$

where k is Boltzmann's constant, T is temperature and E_{fb} is the flat-band potential of the semiconductor. The value of the potential drop in the semiconductor electrode can be determined through a variety of methods,[18-21] and n_b can be measured from knowledge of the resistivity and mobility of carriers in the solid.[18,22,23]

In this chapter, we have determined n_s, [A], and J experimentally for a series of Si/methanol contacts using redox species that have a relatively constant reorganization energy but which produce varying values of $\mathbf{E}_{cb} - qE^{\circ\prime}(A/A^-)$, where $\mathbf{E}_{cb}$ is the conduction band edge energy at the interface and $E^{\circ\prime}(A/A^-)$ is the formal electrochemical potential of the redox couple A/A^-. In each system, the rate law of eq 1 was obeyed experimentally, so that k_{et} could be computed. The data thus yielded values of k_{et} for transfer of delocalized electrons from a narrowly defined region of energy in the semiconductor to the redox acceptors in the solution. The observed dependence of k_{et} on $\mathbf{E}_{cb} - qE^{\circ\prime}(A/A^-)$ permits evaluation of the predicted dependence of the rate constant on the driving force for the interfacial charge-transfer event. Since the measurements have been performed for a redox species that is dissolved in homogeneous solution, these data necessarily involve an integration over distance between the acceptor and the interface, in contrast to the fixed-distance rate constant data that have been obtained recently by Chidsey and collaborators for charge transfer at metal/liquid interfaces.[24,25] The maximum value of k_{et} determined experimentally for the n-Si/CH_3OH contact also allows estimation of the electronic coupling between the delocalized electron in the solid and the electron acceptor in the solution phase, and provides a basis for comparison of the experimental data to the predictions of theoretical models[16,17] for this charge-transfer process.

II. EXPERIMENTAL

A. Electrodes and Solutions

The n-type Si wafers (phosphorus-doped, <100> orientation) were purchased from Silicon Sense, Inc. (Nashua, NH) and had resistivities of either 0.74 or 5.9 cm. Resistivities were measured with a four-point probe and were converted into dopant densities via empirical relationships that have been published previously.[23] A Ga:In eutectic provided an ohmic contact to the n-Si, which was then attached to a Sn:Cu wire using conductive Ag print (GC Electronics). The n-Si wafer and Sn:Cu wire were sealed in a glass tube through use of white epoxy (Dexter Corp.). Photographs of the exposed Si areas alongside a microruler were digitized to determine the electrode areas, which were typically 0.75 to 0.85 cm^2.[26]

Before each electrochemical measurement, n-Si electrodes were etched in 48% HF(aq) (Mallinckrodt, Inc.), rinsed with 18 MΩ cm resistivity H_2O (from a Barnstead NANOPure filter), and dried with $N_2(g)$. In addition, the Pt wire reference electrode and the Pt gauze counter electrode (Aldrich; 52 mesh, 5 cm^2) were cleaned in a 3:1 (v/v) solution of HCl(aq) (37% w/w, EM Science) and HNO_3(aq) (70% w/w, EM Science). The electrodes were then rinsed with 18 MΩ cm resistivity H_2O and dried under flowing $N_2(g)$. All electrical measurements were conducted in a $N_2(g)$-purged Plexiglas box, which had less than 10 ppm of O_2 as monitored by the lack of fuming of $(CH_3CH_2)_2Zn$.

Methanol was obtained from EM Science and was distilled over Mg prior to use. Lithium chloride (EM Science) was dried under active vacuum for at least 6 h at 240°C and was stored under $N_2(g)$ until use. The electrolyte and redox compounds were maintained under $N_2(g)$ while they were loaded into the cell vessel and dissolved into the solvent. All electrochemical cell solutions contained 1.0 M LiCl. The cation radicals of the bipyridinium compounds were created *in situ* via bulk electrolysis with a Pt gauze counter electrode separated from the main cell solution by a Vycor™ frit. Formal reduction potentials were taken to be the cyclic voltammetric half-wave potentials that were measured at a Pt wire in a CH_3OH-1.0 M LiCl solution containing 20 mM of the bipyridinium

dication of interest. Nernstian solution potentials were monitored before and after each set of electrical measurements through use of a CH_3OH-LiCl saturated calomel reference electrode (SCE). The potential of this electrode was -0.050 V vs a standard aqueous SCE.

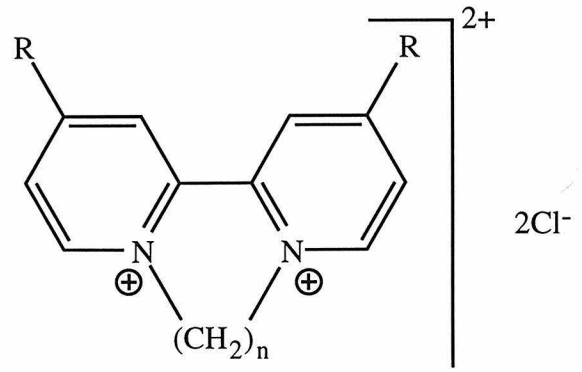
B. Redox Compounds

The structures of the seven redox compounds used in this work are given in Figure 1. For brevity, these compounds have been assigned numeric symbols that generally increase with more positive formal reduction potentials (Table I). Methyl viologen dichloride (**IV**) hydrate and benzyl viologen dichloride (**V**) were purchased from Aldrich, Inc., and were dried under active vacuum for 6 h at 60°C before use. The other bipyridinium compounds were synthesized according to the general Menschutkin reaction, in which an amine is quaternized with an alkyl halide.[27] In this procedure, the dibromide salts were formed initially and (except for compound **VII**) were converted to the dichloride products by anion-exchange with a Sephadex DEAE A-50 resin. The preparative routes were obtained from literature.[28,29] Acetone, diethyl ether, and Na_2CO_3 were obtained from EM Science, and all other reagents were purchased from Aldrich, Inc. All materials were used as received.

7,8-Dihydro-6H-dipyrido[1,2-a:2',1'-c]-[1,4]-diazepinium dichloride (I). 2,2'-dipyridyl (2 g) was dissolved in 1,3-dibromopropane (10 mL). The solution was stirred under reflux at 165°C for 20 h. The resultant pale yellow dibromide precipitate was washed with acetone and converted to the dichloride salt in a CH_3OH solution. This solution was concentrated to 20 mL via rotary evaporation, and the product was recrystallized by addition of acetone. The crystals were rinsed with acetone and diethyl ether and were then dried under active vacuum for 2 h. ^1H NMR (D_2O) δ: CH_2 3.4 (quintet); CH_2N^+ 5.1 (triplet); aromatic 8.5 (multiplet), 8.6, 9.4 (doublet), 9.6 (doublet).

Figure 1. The structures of the seven bipyridinium compounds used in this work. Compounds **I**, **II**, and **III** had the structure illustrated in (a), whereas compounds **IV**, **V**, **VI**, and **VII** had the structure shown in (b). Values of R and n for each reagent are given in Table I, and specific preparative procedures are described in the text.

(a)



(b)

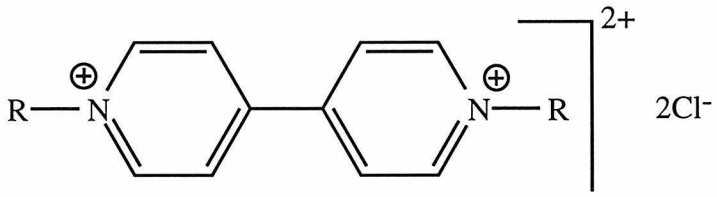


Table I. Formal reduction potentials of bipyridinium$^{2+/+}$ compounds

Redox compound	n	R	$E^{\circ\prime}$(A/A$^-$), V vs SCE
I	3	H	-0.572
II	2	CH_3	-0.518
III	2	H	-0.399
IV	---	CH_3	-0.453
V	---	$CH_2C_6H_5$	-0.382
VI	---	$CH_2COOC_2H_5$	-0.296
VII	---	$CH(COOC_2H_5)_2$	-0.195

The standard reduction potentials were obtained from the cyclic voltammetric half-wave potential at a Pt wire. Each solution for cyclic voltammetry consisted of 20 mM bipyridinium dication and 1.0 M LiCl in CH_3OH.

6,7-Dihydro-2,11-dimethyldipyrido[1,2-a:2',1'-c]pyrazinium dichloride (II). 1,2-dibromoethane (3 mL) was added to a solution of 4,4'-dimethyl-2,2'-dipyridyl (3 g) in nitrobenzene (19 mL). The mixture was stirred at 170°C for 10 h. The dull purple solid was collected and rinsed with acetone and diethyl ether. The dichloride salt was obtained as a CH_3OH solution, and the final product was recrystallized by addition of acetone. The crystals were washed with acetone and diethyl ether and were dried at 70°C under active vacuum for 6 h. ^1H NMR (D_2O) δ: CH_3 2.8; CH_2N^+ 5.2; aromatic 8.2 (doublet), 8.8, 9.0 (doublet).

6,7-Dihydrodipyrido[1,2-a:2',1'-c]pyrazinium dichloride (III). 2,2'-dipyridyl (2.83 g) was dissolved in 1,2-dibromoethane (14.2 mL). The solution was stirred under reflux at 130°C for 17 h. The green-yellow precipitate was collected and rinsed with acetone and diethyl ether. The CH_3OH solution of the dichloride salt was reduced in volume via rotary evaporation, and addition of acetone induced recrystallization. The crystals were rinsed with acetone and were dried at 60°C under active vacuum for 6 h. ^1H NMR (D_2O) δ: CH_2N^+ 5.4; aromatic 8.4-9.0 (multiplet), 9.2 (doublet).

1,1'-Bis(ethoxycarbonylmethyl)-4,4'-bipyridinium dichloride (VI). Ethyl bromoacetate (5 g) was added to a solution of 4,4'-dipyridyl (2 g) in acetonitrile (50 mL). The mixture was stirred under reflux at 90°C for 48 h, and the resultant yellow dibromide salt was collected and rinsed with acetonitrile and diethyl ether. After the conversion to the dichloride compound, the final product was recrystallized from CH_3OH by addition of diethyl ether. After several rinses with diethyl ether, the collected crystals were dried for 3 h under active vacuum. ^1H NMR (D_2O) δ: CH_3 1.3 (triplet); CH_2O 4.3 (quartet); CH_2N^+ 5.7; aromatic 8.6, 9.1 (both doublets).

1,1'-Bis(diethoxycarbonylmethyl)-4,4'-bipyridinium dichloride (VII). Diethyl bromomalonate (5 mL) was added to a solution of 4,4'-dipyridyl (2 g) in absolute ethanol (10 mL). The reaction mixture was stirred at room temperature for 48 h,

stirred under reflux for 4 h, and then allowed to return to room temperature. A saturated aqueous solution of Na_2CO_3 (10 mL) was added to the deep red solution. The red precipitate was collected and rinsed with H_2O. This solid was dissolved in boiling N,N'-dimethylformamide, and insoluble material was removed by hot gravity filtration. Once the mixture had cooled to room temperature, the recrystallized solid was collected (2.0 g) and rinsed with diethyl ether. This intermediate product was suspended in CH_3OH and made soluble by addition of concentrated HCl(aq) (0.5 mL). Recrystallization of the final dichloride compound was induced by diethyl ether. The brown crystals were washed with diethyl ether and dried under active vacuum for 3 h. ^1H NMR (D_2O) δ: CH_3 1.3 (triplet); CH_2 4.4 (quartet); aromatic 8.7, 9.3 (both doublets).

C. Electrical Measurements

After an HF-etched n-Si electrode was transferred into the N_2 atmosphere, the electrode was immersed for 2 min in a 0.2 M solution of ferrocenium tetrafluoroborate (available from previous work in this laboratory[1]) in CH_3OH, rinsed with CH_3OH, and dried in flowing N_2(g). This chemical treatment induced a reproducible flat-band shift, as reported in prior work,[2] and was found to result in stable and reproducible current density-potential (J-*E*) behavior at the n-Si/CH_3OH-bipyridinium$^{2+/+}$ interface. To ensure electrode stability, the semiconductor working electrode was cycled between +0.500 and -0.100 V vs the Nernstian solution potential $E(A/A^-)$ for 30 min under ambient room illumination before use. Any unstable electrodes were then discarded. J-*E* properties were recorded before and after the differential capacitance measurements. Both the steady-state J-*E* behavior and the differential capacitance vs potential (C^{-2}-*E*) behavior were performed in the dark. $E(A/A^-)$ was measured before and after collection of the J-*E* and C^{-2}-*E* data.

J-*E* data were obtained with an EG&G Princeton Applied Research Model 273 Potentiostat and a Houston Instruments Omnigraphic 2000 X-Y recorder. The scan rate

was 50 mV s^{-1} in all experiments. The dark J-*E* curves were digitized and were corrected for concentration overpotential and cell resistance losses by measuring the mass-transport-limited currents at a one-sided Pt foil electrode. For a given redox solution, the limiting anodic current density, $J_{l,a}$, and the limiting cathodic current density, $J_{l,c}$, at this Pt foil electrode were used with the current densities J at an n-Si electrode to correct the Si J-*E* data for any concentration overpotential η_{conc}:[30]

$$\eta_{conc} = \left(\frac{RT}{nF}\right)\left\{\ln\left(\frac{J_{l,a}}{-J_{l,c}}\right) - \ln\left(\frac{J_{l,a} - J}{J - J_{l,c}}\right)\right\} \qquad (3)$$

where R is the gas constant, n is the number of electrons transferrred (1 in this case) and F is the Faraday constant. The cell resistance R_{cell} was extracted from the high-frequency limits of the Bode plots of the n-Si/CH_3OH-bipyridinium$^{2+/+}$ junctions. The final corrected potential, E_{corr}, was calculated from *E*, η_{conc}, R_{cell}, and the current *i* using the equation

$$E_{corr} = E - \eta_{conc} - iR_{cell} \qquad (4)$$

The reference point of the potentials was then changed to SCE by accounting for the difference between $E(A/A^-)$ and SCE.

As observed previously, n-Si electrodes in contact with these bipyridinium solutions exhibited stable J-*E* characteristics within the typical measurement timescale of several hours.[2,7] For an individual cell, the cathodic currents at a given forward bias changed by less than 10% over the course of the differential capacitance experiments. For an entire series of Si/liquid contacts with each individual redox couple, the current density at a given potential was likewise constant to within ±10%. Cell stability was further verified by monitoring $E(A/A^-)$, which changed by no more than 3 mV from the beginning to the end of the J-*E* and C^{-2}-*E* measurements performed using a given electrode.

The differential capacitance experiments were performed on a Schlumberger Instruments Model 1260 Impedance/Gain-Phase Analyzer that was linked to a Model 1286 Electrochemical Interface. Both instruments were driven by computer control. A 10 mV ac

signal was superimposed on the dc bias, and the sample integration time was 10 s. Every capacitance measurement consisted of 13 frequency sweeps (each from 100 kHz to 1 kHz, at evenly spaced logarithmic intervals) at positive dc biases that were stepped over the desired potential range in 50 mV increments.

The equivalent circuit assumed in this work was a resistor R_{cell} (the resistance of the solution and the bulk semiconductor) in series with two parallel components, a resistor R_{sc} (the resistance to Faradaic charge transfer) and a capacitor C_{sc} (the semiconductor space-charge capacitance). The value of R_{cell} was typically 20 Ω. The value of R_{sc} at each dc potential was derived from the diameter of the circular fit of the Nyquist curve, which plots the imaginary component of the impedance, Z_{im}, vs the real component of the impedance, Z_{re}. In these differential capacitance measurements, the angular frequency of the excitation voltage, ω, obeyed the condition $\omega >> (C_{sc}R_{sc})^{-1}$, and R_s was therefore not included in the extraction of the C_{sc} values. The appropriate formula relating the impedance to the capacitance is then

$$C_{sc} = \frac{1+\sqrt{1-4\frac{Z_{im}^2}{R_{sc}^2}}}{2\omega Z_{im}} \qquad (5)$$

Since C_{sc} is much less than the differential capacitance of either the Helmholtz layer or the double layer, the measured differential capacitance C_{diff} was, to an excellent approximation, equal to the desired quantity, C_{sc}. The C_{diff} vs E data were thus interpreted through use of the Mott-Schottky equation:[15]

$$C_{diff}^{-2} = \frac{2}{q\varepsilon\varepsilon_o N_d A_s^2}\left(E - E_{fb} - \frac{kT}{q}\right) \qquad (6)$$

where ε is the dielectric constant of the semiconductor (11.7 for Si), ε_o is the permittivity of free space, N_d is the dopant density of the semiconductor, A_s is the area of the semiconductor electrode, and E_{fb} is the flat-band potential. Each linear regression of a C_{diff}^{-2} vs E ("Mott-Schottky" or "M-S") plot was extrapolated to $C_{diff}^{-2} = 0$ and adjusted by

kT/q to yield the value of E_{fb} for that measurement frequency. E_{fb} is related to the barrier height of the junction, ϕ_b, by the equation[18]

$$\phi_b = E(A/A^-) - \frac{E_{cb}}{q} = E(A/A^-) - E_{fb} + \frac{kT}{q}\ln\left(\frac{N_c}{N_d}\right) \qquad (7)$$

The values of $N_c = 2.8 \times 10^{19}$ cm^{-3} (ref. 18) and either $N_d = 6.95 \times 10^{15}$ cm^{-3} (for the 0.74 Ω cm n-Si) or $N_d = 7.84 \times 10^{14}$ cm^{-3} (5.9 Ω cm) were used in the calculations that related ϕ_b to E_{fb}.

It should be noted that the experimental conditions described above yielded reproducible barrier height results that varied only slightly with the ac frequency, and that other conditions resulted in irreproducibility or frequency dispersion in the M-S plots. Electrode areas of 0.1-0.2 cm^2 displayed more frequency dispersion than did electrode areas of 0.75-0.85 cm^2. Acceptor ion concentrations of 5 mM or less led to irreproducible barrier height results and produced C^{-2}-E behavior whose slopes deviated from the predictions of eq 6.[1] Similarly, if the measuring resistor of the impedance analyzer was too low, the M-S plots were dependent on the ac signal frequency. Careful attention to all of these instrumental and cell-dependent factors was required in order to obtain the experimental behavior reported herein.

III. RESULTS

Two separate criteria are required for a reliable rate constant evaluation in response to a changing driving force at the semiconductor/liquid junction. The interface must display ideal energetic behavior as well as ideal kinetic behavior. The junction energetics are discussed in the following section, and the results of the kinetic measurements are then presented in section **III.B**.

A. C^{-2}-E Data for n-Si/CH_3OH-Bipyridinium$^{2+/+}$ Contacts

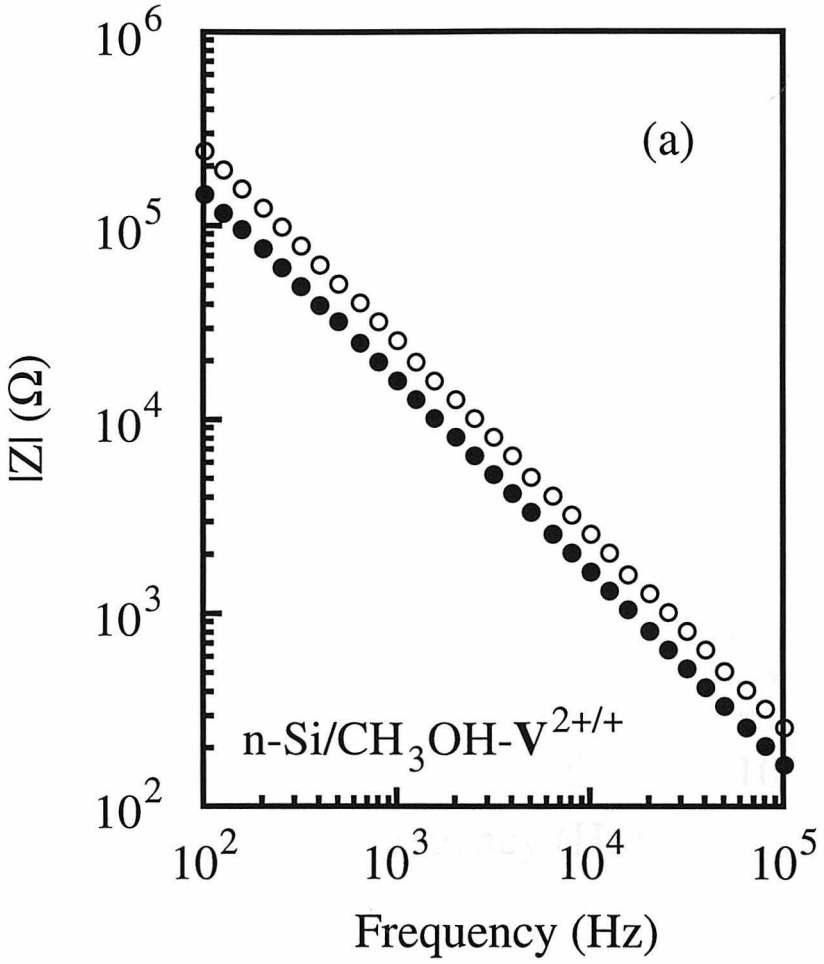
Figure 2 presents typical Bode plots for two of the n-Si/CH_3OH junctions studied in this work. Figure 2a shows Bode plots obtained at two different potentials of an n-Si/CH_3OH-$\mathbf{V}^{2+/+}$ junction, while Figure 2b shows analogous data for an n-Si/CH_3OH-$\mathbf{II}^{2+/+}$ contact. For all junctions, the Bode plots were linear over at least one order of magnitude variation in frequency, and such behavior was observed at a variety of potentials in reverse bias. For example, in Figure 2a, the slopes of the impedance magnitude |Z| vs the ac signal frequency were -0.998 at +0.200 V vs $E(A/A^-)$ and -1.000 at +0.800 V vs $E(A/A^-)$. The linearity and unity slopes of these plots indicated that the system behaved as a simple capacitive circuit element from $\approx 10^3$ to 10^5 Hz, verifying that the imaginary component $Z_{im} \approx (\omega C_{diff})^{-1}$ dominated the total impedance of the cell under such conditions.

Since the Bode plots were linear over a significant range of frequencies and potentials (Table II), the simple equivalent circuit described in section **II.C.**, in which $C_{diff} = C_{sc}$, was assumed to be adequate to describe the impedance behavior. If this model is correct, plots of C_{sc}^{-2} vs E should be linear and should have a slope that can be calculated from the area and dopant density of the semiconductor (eq 6). From the E_{fb} results, the position of the conduction band edge can then be calculated according to eq 7.

Figure 3 displays some representative Mott-Schottky (C^{-2}-E) plots for n-Si/CH_3OH-bipyridinium$^{2+/+}$ contacts under conditions that yielded linear Bode plots. Regression of the C^{-2}-E data yielded slopes that were in good agreement with those expected from the known dopant density and area of the electrodes. Moreover, the C^{-2}-E slopes displayed minimal frequency dispersion. This behavior was expected, because the linear Bode plots indicated that the measured differential capacitance was essentially independent of the measurement frequency.

The intercepts on the x-axis of C^{-2}-E plots yielded the desired energetic data for the junctions of concern. For a given solid/liquid contact, the extrapolated intercepts of the

Figure 2. Representative Bode plots (impedance |Z| vs frequency) for the n-Si/CH_3OH junction. (a) Bode plots for the n-Si/CH_3OH-$\mathbf{V}^{2+/+}$ interface are shown for an applied potential of +0.200 V vs $E(A/A^-)$ (filled circles) and for an applied potential of +0.800 V vs $E(A/A^-)$ (open circles). In both cases, the concentrations of the redox couple were [A] = [A^-] = 10 mM. $E(A/A^-)$ was -0.382 V vs SCE. The n-Si electrode had a measured dopant density of 7.84 x 10^{14} cm^{-3} and a photographic area of 0.75 cm^2. (b) Bode plots for the n-Si/CH_3OH-$\mathbf{II}^{2+/+}$ interface, for an applied potential of +0.300 V vs $E(A/A^-)$ (filled circles) and for an applied potential of +0.800 V vs $E(A/A^-)$ (open circles). The concentrations of the redox couple were [A] = [A^-] = 10 mM. $E(A/A^-)$ was -0.518 V vs SCE. The n-Si electrode had a measured dopant density of 7.84 x 10^{14} cm^{-3} and a photographic area of 0.75 cm^2.


10^6
10^5
10^4
10^3
10^2
|Z| (Ω)
(a)
n-Si/CH_3OH-$V^{2+/+}$
10^2
10^3
10^4
10^5
Frequency (Hz)

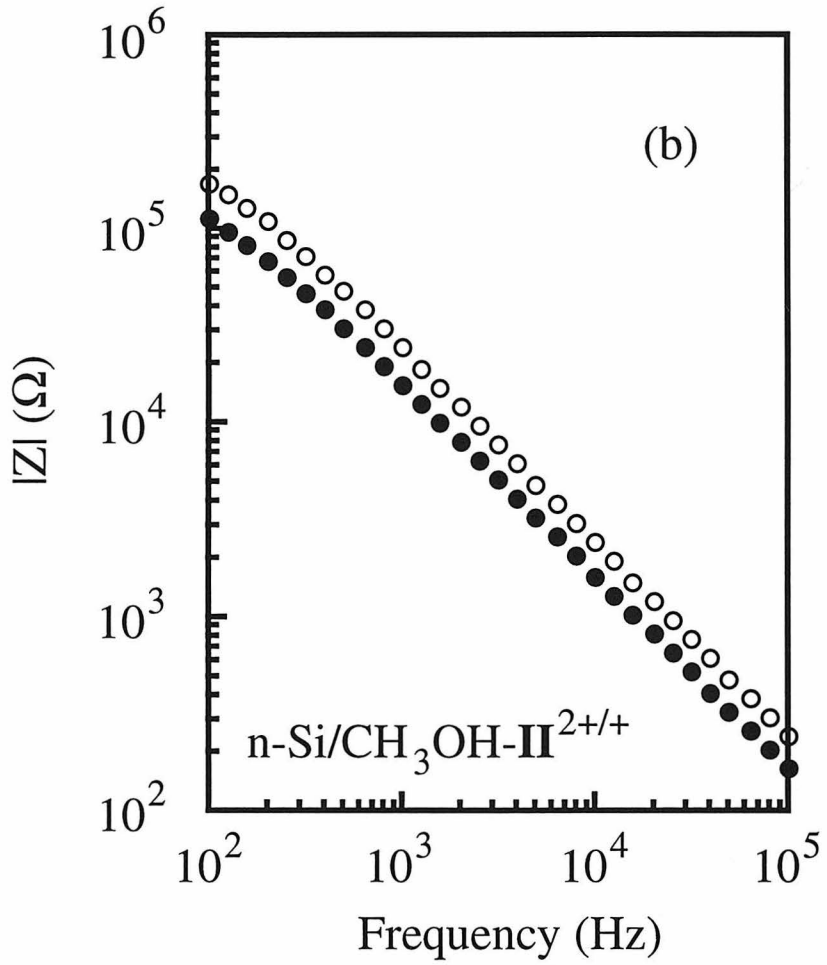

(b)
n-Si/CH3OH-II2+/+
|Z| (Ω)
Frequency (Hz)
10^6
10^5
10^4
10^3
10^2
10^2
10^3
10^4
10^5

Figure 3. Mott-Schottky plots for compounds **II-VII**, each illustrating the shift in electric field at different [A] and constant [A^-]. The donor concentration [A^-] was always 10 mM. The filled circles in all plots represent data for [A] = 10 mM , while the open circles represent data for [A] = 100 mM in plots (a)-(e) and [A] = 85 mM in plot (f). In plots (a), (b), (d), (e), and (f), the N_d measured from four-point probe techniques was 7.84 x 10^{14} cm^{-3}, whereas in (c), the measured N_d was 6.95 x 10^{15} cm^{-3}. Areas of the n-Si electrodes were 0.75-0.85 cm^2. The M-S results used the average of six frequencies equally spaced logarithmically; for clarity, only the data of the upper and lower limits of each frequency range are displayed. The relevant frequency ranges are given in Tables II and III. (a) The average shift in ϕ_b was 54 mV. (b) $\Delta\phi_b$ = 71 mV. (c) $\Delta\phi_b$ = 58 mV. (d) $\Delta\phi_b$ = 63 mV. (e) $\Delta\phi_b$ = 80 mV. (f) $\Delta\phi_b$ = 40 mV.

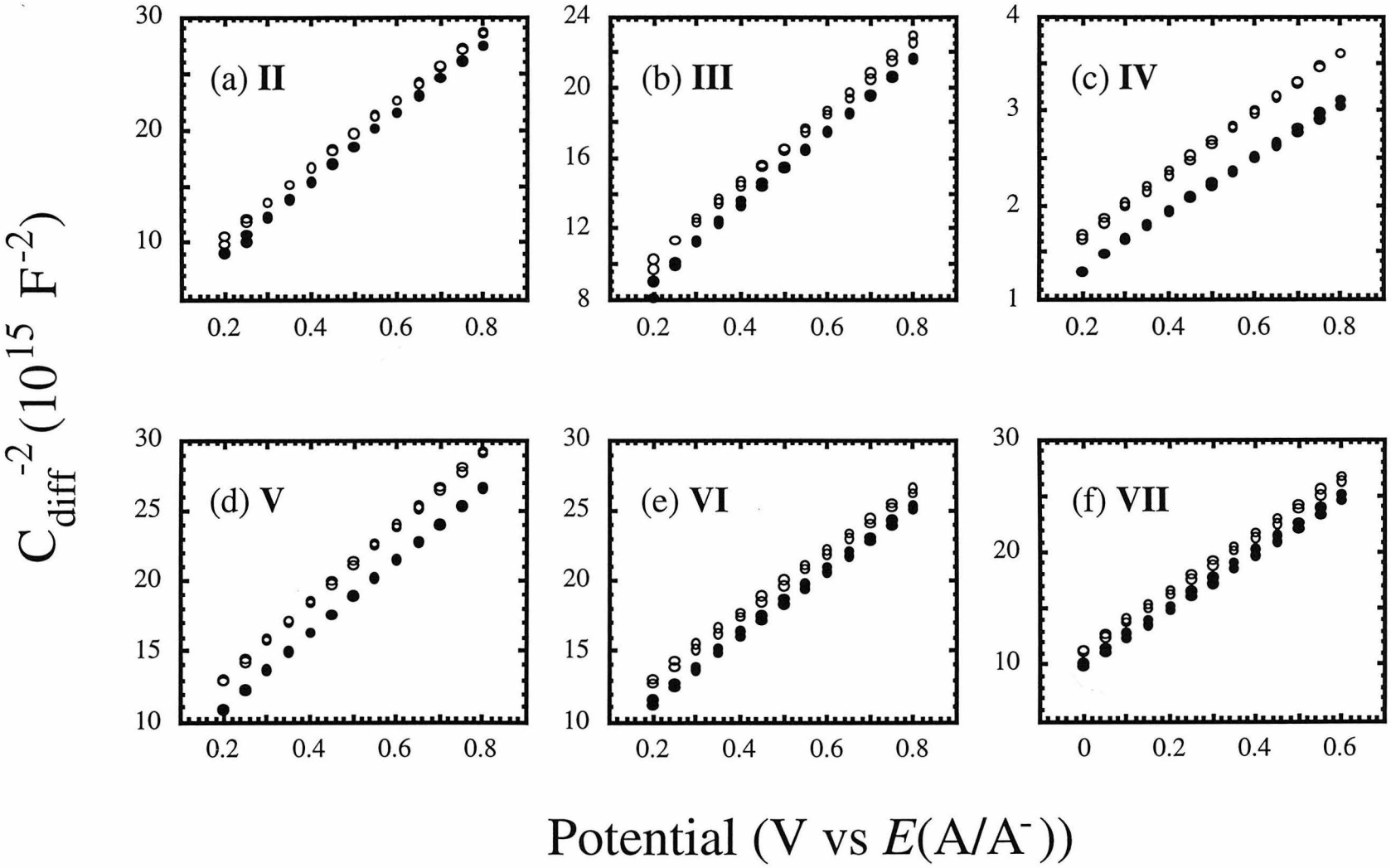

(a) II
(b) III
(c) IV
(d) V
(e) VI
(f) VII
C_{diff}^{-2} (10^{15} F^{-2})
Potential (V vs $E(A/A^-)$)

Table II. Impedance data for n-Si/CH_3OH interfaces

$I^{2+/+}$

Potential (V vs $E(A/A^-)$)	slope of Bode plot	average C (10^{-9} F) [a]
+0.400	-0.987	8.47 ± 0.09
+0.450	-0.992	8.00 ± 0.04
+0.500	-0.994	7.61 ± 0.03
+0.550	-0.994	7.29 ± 0.03
+0.600	-0.994	7.00 ± 0.03
+0.650	-0.994	6.75 ± 0.02
+0.700	-0.994	6.52 ± 0.02
+0.750	-0.994	6.32 ± 0.02
+0.800	-0.994	6.14 ± 0.02
+0.850	-0.994	5.97 ± 0.02
+0.900	-0.994	5.82 ± 0.02
+0.950	-0.994	5.67 ± 0.02
+1.000	-0.994	5.54 ± 0.02

$III^{2+/+}$

Potential (V vs $E(A/A^-)$)	slope of Bode plot	average C (10^{-9} F)
+0.300	-1.002	9.46 ± 0.09
+0.350	-1.003	9.03 ± 0.09
+0.400	-1.003	8.67 ± 0.09
+0.450	-1.003	8.35 ± 0.08
+0.500	-1.002	8.07 ± 0.08
+0.550	-1.002	7.81 ± 0.07
+0.600	-1.001	7.58 ± 0.07
+0.650	-1.001	7.37 ± 0.06
+0.700	-1.001	7.17 ± 0.06
+0.750	-1.001	6.99 ± 0.06
+0.800	-1.000	6.82 ± 0.06

$V^{2+/+}$

Potential (V vs $E(A/A^-)$)	slope of Bode plot	average C (10^{-9} F)
+0.200	-0.998	9.55 ± 0.03
+0.250	-0.999	9.01 ± 0.02
+0.300	-0.999	8.55 ± 0.01
+0.350	-0.999	8.16 ± 0.01
+0.400	-0.999	7.82 ± 0.01
+0.450	-0.999	7.52 ± 0.01
+0.500	-0.999	7.26 ± 0.01
+0.550	-0.999	7.02 ± 0.01
+0.600	-0.999	6.81 ± 0.01
+0.650	-1.000	6.62 ± 0.01
+0.700	-0.999	6.45 ± 0.01
+0.750	-1.000	6.27 ± 0.01
+0.800	-1.000	6.12 ± 0.01

$II^{2+/+}$

Potential (V vs $E(A/A^-)$)	slope of Bode plot	average C (10^{-9} F)
+0.300	-0.996	9.01 ± 0.03
+0.350	-0.998	8.46 ± 0.01
+0.400	-0.999	8.02 ± 0.01
+0.450	-0.999	7.65 ± 0.01
+0.500	-0.999	7.33 ± 0.01
+0.550	-0.999	7.04 ± 0.01
+0.600	-0.999	6.79 ± 0.01
+0.650	-0.999	6.57 ± 0.01
+0.700	-0.999	6.37 ± 0.01
+0.750	-0.999	6.19 ± 0.01
+0.800	-0.999	6.02 ± 0.01

$IV^{2+/+}$

Potential (V vs $E(A/A^-)$)	slope of Bode plot	average C (10^{-8} F)
+0.200	-0.992	2.48 ± 0.01
+0.250	-0.994	2.35 ± 0.01
+0.300	-0.994	2.23 ± 0.01
+0.350	-0.994	2.14 ± 0.01
+0.400	-0.993	2.05 ± 0.01
+0.450	-0.993	1.97 ± 0.01
+0.500	-0.993	1.91 ± 0.01
+0.550	-0.993	1.85 ± 0.01
+0.600	-0.992	1.79 ± 0.01
+0.650	-0.992	1.75 ± 0.01
+0.700	-0.991	1.70 ± 0.01
+0.750	-0.991	1.66 ± 0.01
+0.800	-0.991	1.62 ± 0.01

$VI^{2+/+}$

Potential (V vs $E(A/A^-)$)	slope of Bode plot	average C (10^{-9} F)
+0.200	-1.004	9.31 ± 0.08
+0.250	-1.004	8.85 ± 0.07
+0.300	-1.004	8.45 ± 0.07
+0.350	-1.004	8.11 ± 0.07
+0.400	-1.004	7.81 ± 0.06
+0.450	-1.004	7.55 ± 0.06
+0.500	-1.004	7.31 ± 0.06
+0.550	-1.004	7.09 ± 0.06
+0.600	-1.004	6.90 ± 0.05
+0.650	-1.004	6.72 ± 0.05
+0.700	-1.004	6.56 ± 0.05
+0.750	-1.003	6.41 ± 0.05
+0.800	-1.003	6.27 ± 0.05

VII$^{2+/+}$

Potential (V vs $E(A/A^-)$)	slope of Bode plot	average C (10^{-9} F)
+0.000	-1.006	9.87 ± 0.12
+0.050	-1.006	9.30 ± 0.11
+0.100	-1.006	8.83 ± 0.11
+0.150	-1.006	8.42 ± 0.10
+0.200	-1.006	8.07 ± 0.09
+0.250	-1.006	7.75 ± 0.09
+0.300	-1.006	7.47 ± 0.08
+0.350	-1.006	7.22 ± 0.08
+0.400	-1.006	7.00 ± 0.08
+0.450	-1.006	6.79 ± 0.07
+0.500	-1.005	6.61 ± 0.07
+0.550	-1.005	6.43 ± 0.07
+0.600	-1.005	6.28 ± 0.06

For all data, [A] = [A^-] = 10 mM. The upper limit of the ac frequency range for each n-Si/CH_3OH interface was 100.0 kHz. Various lower limits of the frequency range were used: **I**, 6.3 kHz; **II** - **IV**, 4.0 kHz; **V** - **VII**, 2.5 kHz. In each decade of ac frequency, ten individual frequencies, which were equally spaced on a logarithmic scale, comprised the data set. In no case was the correlation coefficient for the slope of the Bode plot less than 1.0000.

For these impedance measurements, the areas of the relevant n-Si electrodes were as follows: **I**, 0.75 cm^2; **II**, 0.75 cm^2; **III**, 0.81 cm^2; **IV**, 0.78 cm^2; **V**, 0.83 cm^2; **VI**, 0.86 cm^2; **VII**, 0.83 cm^2. The data for the n-Si/CH_3OH-**IV**$^{2+/+}$ interface were obtained using a semiconductor electrode of $N_d = 6.95 \times 10^{15}$ cm^{-3}, and the data for all other n-Si/CH_3OH contacts were obtained using semiconductor electrodes of $N_d = 7.84 \times 10^{14}$ cm^{-3}.

[a] Standard deviations are reported.

data collected at various measurement frequencies were generally within 10-20 mV of each other (Table III). Because errors in the value of the conduction band edge energy translate exponentially into errors in the calculated rate constant (eqs 3 and 8), significant effort was devoted to obtaining reliable statistical measures of the mean and standard deviation of the value of $\mathbf{E}_{cb}$ for each system. Each value was obtained by first averaging, for each junction, the barrier height values that were computed from C^{-2}-E plots obtained at six different measurement frequencies. These frequencies were chosen to represent the extent of ϕ_b variation over the relevant Bode plot range. The ϕ_b averages of six to eight junctions of nominally identical solution compositions and Si electrodes were further combined to yield an average and a standard deviation for the interface of concern. These data are also summarized in Table III. We believe that the reported standard deviations for determination of $\mathbf{E}_{cb}$, which are generally < 20 meV, represent reliable estimates of the random errors involved in our C^{-2}-E analysis of $\mathbf{E}_{cb}$ for each contact.

Since validation of the rate law of eq 1 generally involved changing the concentration of redox acceptor while holding the concentration of the redox donor constant, it was important to ensure that the band edge positions were fixed as $E(A/A^-)$ varied. Otherwise, different rate constants would be calculated at different acceptor concentrations, and interpretation of the kinetic data would be problematic. One method to evaluate whether $\mathbf{E}_{cb}/q$ was fixed vs a standard reference potential was to investigate whether the observed barrier height for a given redox system changed in response to changes in $E(A/A^-)$. For a fixed value of $\mathbf{E}_{cb}$, ϕ_b should respond to the variation in $E(A/A^-)$ induced by changing the concentration of donors or of acceptors in the solution phase. As outlined in Table III, such behavior was generally observed, within experimental error, for each n-Si/CH_3OH-bipyridinium$^{2+/+}$ contact studied in this work.

An alternate, and arguably more statistically meaningful, approach to validating that $\mathbf{E}_{cb}/q$ was fixed vs an absolute reference potential is to combine the entire collection of ϕ_b

Table III. Barrier height results for n-Si/CH_3OH interfaces

	$I^{2+/+}$		$II^{2+/+}$		$III^{2+/+}$		$IV^{2+/+}$		$V^{2+/+}$		$VI^{2+/+}$		$VII^{2+/+}$	
Frequency, kHz	ϕ_b, [a] V	pred. N_d, [b] 10^{14} cm^{-3}	ϕ_b, V	pred. N_d, 10^{14} cm^{-3}	ϕ_b, V	pred. N_d, 10^{15} cm^{-3}	ϕ_b, V	pred. N_d, 10^{15} cm^{-3}	ϕ_b, V	pred. N_d, 10^{14} cm^{-3}	ϕ_b, V	pred. N_d, 10^{14} cm^{-3}	ϕ_b, V	pred. N_d, 10^{14} cm^{-3}
100.00	0.353	6.75	0.406	6.96	0.529	1.00	0.472	5.67	0.518	8.08	0.588	9.14	0.699	8.60
79.433	0.357	6.77	0.406	6.97	0.533	1.00	0.483	5.72	0.519	8.10	0.590	9.17	0.697	8.61
63.096	0.357	6.80	0.407	6.95	0.535	1.00	0.491	5.73	0.519	8.09	0.592	9.14	0.698	8.57
50.119	0.356	6.79	0.407	6.94	0.537	1.01	0.494	5.75	0.520	8.09	0.594	9.16	0.700	8.54
39.811	0.357	6.82	0.407	6.94	0.540	1.04	0.490	5.72	0.520	8.07	0.599	9.25	0.701	8.42
31.623	0.355	6.82	0.407	6.93	0.539	1.07	0.486	5.69	0.520	8.05	0.605	9.33	0.704	8.29
25.119	0.355	6.84	0.406	6.91	0.537	1.05	0.485	5.70	0.519	8.04	0.604	9.23	0.706	8.28
19.953	0.355	6.85	0.406	6.90	0.537	1.03	0.486	5.72	0.520	8.04	0.602	9.12	0.707	8.30
15.849	0.354	6.86	0.405	6.90	0.539	1.02	0.491	5.77	0.520	8.04	0.600	9.04	0.707	8.28
12.589	0.351	6.85	0.404	6.89	0.543	1.02	0.496	5.83	0.520	8.05	0.601	8.98	0.707	8.25
10.000	0.349	6.85	0.404	6.89	0.544	1.02	0.501	5.89	0.520	8.06	0.599	8.92	0.707	8.21
7.9433	0.345	6.83	0.403	6.89	0.548	1.02	0.505	5.94	0.519	8.05	0.599	8.90	0.707	8.20
6.3906	0.342	6.81	0.401	6.88	0.554	1.02	0.508	6.00	0.518	8.05	0.602	8.93	0.706	8.20
5.0019			0.400	6.88	0.557	1.03	0.510	6.04	0.518	8.05	0.602	8.95	0.706	8.22
3.9811			0.398	6.88	0.561	1.04	0.510	6.07	0.518	8.06	0.602	9.01	0.706	8.29
3.1623									0.515	8.04	0.601	9.07	0.707	8.38
2.5119									0.513	8.03	0.601	9.14	0.705	8.44
avg. ϕ_b, V *one electrode*[c] *[A]=10 mM*	0.353 ± 0.005		0.404 ± 0.003		0.542 ± 0.009		0.494 ± 0.011		0.519 ± 0.002		0.599 ± 0.005		0.704 ± 0.004	
avg. ϕ_b, V *all electrodes*[d] *[A]=10 mM*	0.331 ± 0.015		0.396 ± 0.014		0.508 ± 0.021		0.491 ± 0.012		0.509 ± 0.015		0.613 ± 0.020		0.695 ± 0.018	
avg. ϕ_b, V *all electrodes* *[A]=100 mM*	------- [e]		0.434 ± 0.018		0.608 ± 0.018		0.541 ± 0.021		0.567 ± 0.012		0.690 ± 0.008		0.758 ± 0.012 [f]	

$[A^-]$ = 10 mM for all data shown here. The potential limits for the C^{-2}-*E* measurements for each redox compound are given in Table II, and in no case was the correlation coefficient for the slope of the C^{-2}-*E* plot less than 0.9996. [a] Data from one representative contact between a single n-Si electrode and the specified redox couple; the average ϕ_b from these data is listed in the row labeled "*one electrode.*" The n-Si electrode areas and dopant densities (N_d = 6.95 x 10^{15} cm^{-3} for the $\mathbf{IV}^{2+/+}$ interface, 7.84 x 10^{14} cm^{-3} for all other interfaces) are identical to those specified in Table II. [b] Predicted N_d values are derived from the slopes of the C^{-2}-*E* plots. [c] Standard deviations are reported with the average values. [d] Average values of ϕ_b over all electrodes, representing the results from six to eight separate n-Si/CH_3OH contacts. Each individual result was itself an average of ϕ_b values obtained at six different ac measurement frequencies, selected to indicate the extent of ϕ_b variation over the pertinent frequency range. [e] The second-order kinetic mechanism was tested by increasing the concentrations to [A] = $[A^-]$ = 30 mM. [f] [A] = 85 mM.

vs $E(A/A^-)$ data for all redox systems investigated in this work, and to plot the entire data set on a single graph. If the band edge position were fixed and no Fermi level pinning[15] were to occur over the potential range of interest, then ϕ_b should increase linearly with $E(A/A^-)$ with a slope of unity, and this plot should yield a single, fixed value for the conduction band edge energy for the entire range of measurements. These data have been compiled in Figure 4. The plot clearly shows a linear dependence of ϕ_b on $E(A/A^-)$ for the entire set of n-Si/CH_3OH-bipyridinium$^{2+/+}$ contacts. A linear-regression analysis of ϕ_b against $E(A/A^-)$ yielded a slope of 0.984 ± 0.044 and a correlation coefficient of 0.988. The x-intercept produced a value for $\mathbf{E}_{cb}/q$ of -0.920 ± 0.044 V vs SCE for these sets of Si/CH_3OH contacts, which was taken to be a reliable mean determination of $\mathbf{E}_{cb}/q$ for the junctions studied in this work.

B. J-*E* Behavior for n-Si/CH_3OH-Bipyridinium$^{2+/+}$ Contacts

All of the n-Si/CH_3OH-bipyridinium$^{2+/+}$ contacts exhibited rectifying J-*E* behavior, producing a limiting value for the anodic current density and an approximately exponential increase in the cathodic current density as *E* was made more negative. Figure 5 displays the as-collected J-*E* data for an n-Si/CH_3OH junction in contact with three typical redox systems, $\mathbf{III}^{2+/+}$, $\mathbf{V}^{2+/+}$, and $\mathbf{VII}^{2+/+}$. For each system, the figure also displays the J-*E* behavior that was measured at a Pt electrode of similar area and in nominally the same cell configuration as the Si electrode. Clearly, the current density at the Si electrode was limited by kinetics and not by mass transport, because the current density at each potential of the Pt electrode was significantly larger than that observed at the Si electrode surface.

Figure 6 displays the J-*E* data, in the form of ln |J| vs E_{corr}, following correction for concentration and series resistance overpotentials. The protocols used to perform these corrections are described in the Experimental section and are in accord with conventional electrochemical treatments of these effects.[30] These corrections were required because the

Figure 4. A plot of the barrier height vs the Nernstian solution potential. Each of the compounds **I**-**VII** contributed two ϕ_b points, one at [A] = [A^-] = 10 mM and one at either [A] = [A^-] = 30 mM (**I**) or [A] > [A^-] = 10 mM (**II**-**VII**). Each compound is represented by the following symbols: **I**, filled circles; **II**, open circles; **III**, filled squares; **IV**, open squares; **V**, filled diamonds; **VI**, open diamonds; **VII**, X. The linear regression slope was 0.984 ± 0.044, and the correlation coefficient was 0.988.

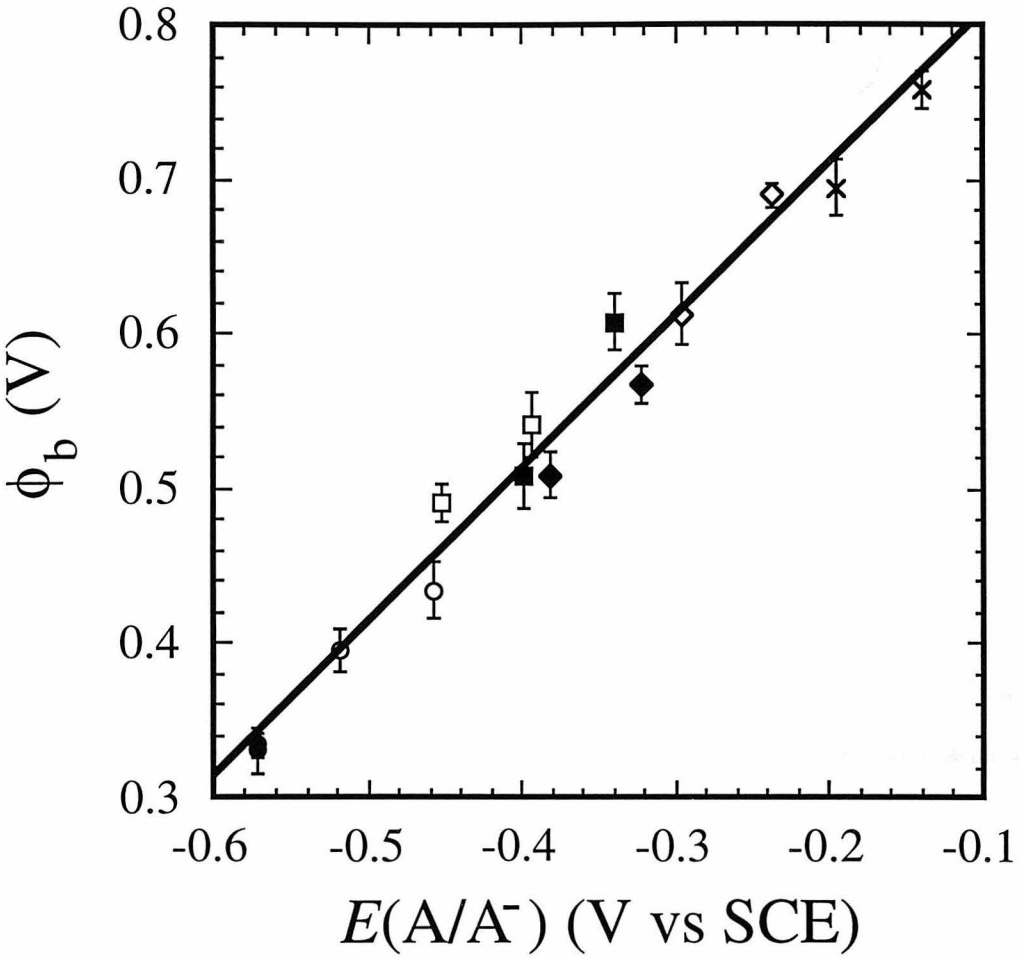
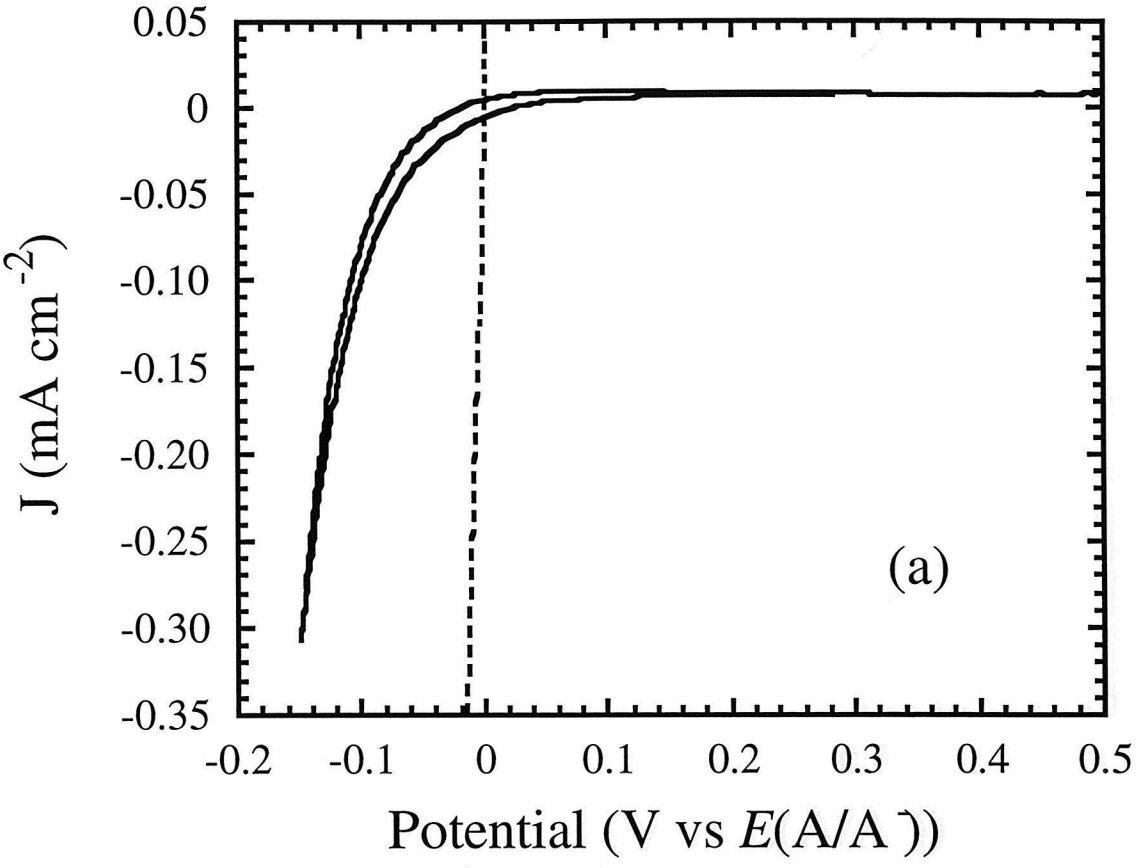
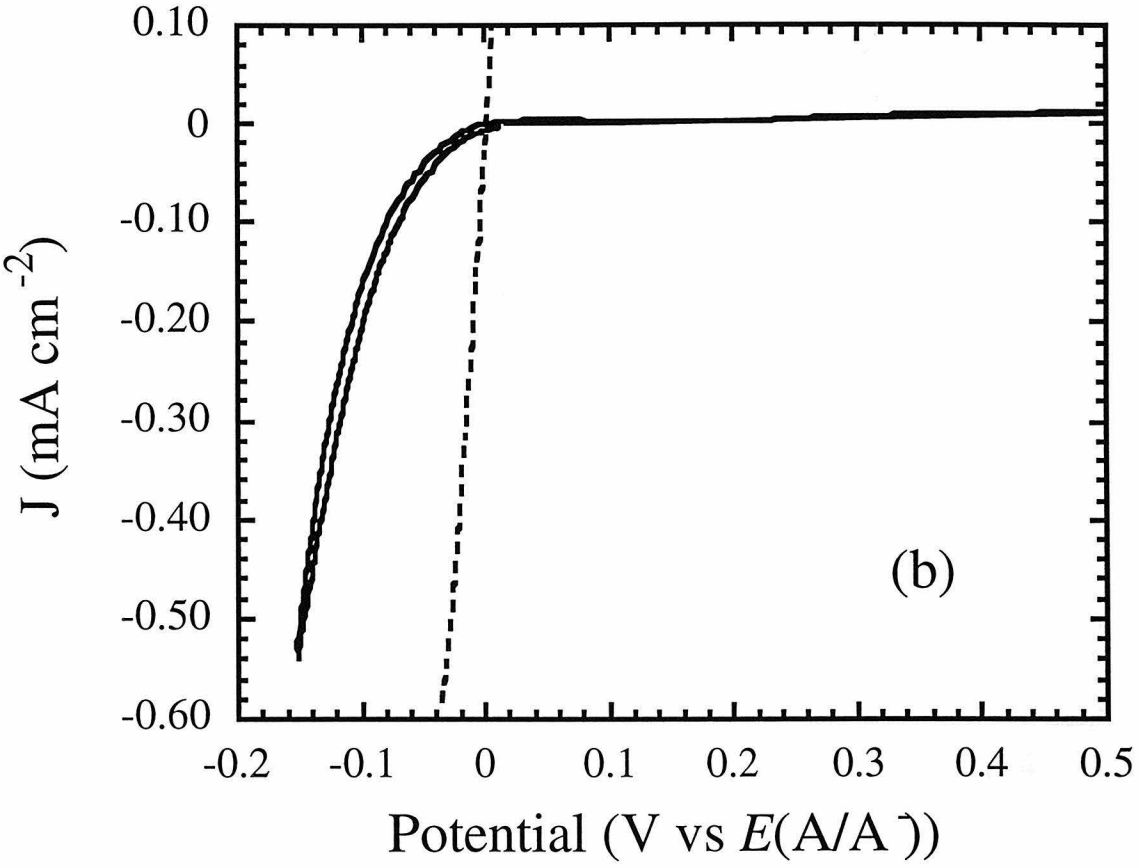

0.8
0.7
0.6
0.5
0.4
0.3
ϕ_b (V)
-0.6
-0.5
-0.4
-0.3
-0.2
-0.1
$E(A/A^-)$ (V vs SCE)

Figure 5. Representative current density-potential (J-*E*) behavior for electrodes in contact with CH_3OH-bipyridinium$^{2+/+}$ solutions. The solid line represents the J at an n-Si working electrode, while the dashed line depicts the J at a Pt working electrode of similar geometry (1.31 cm^2). The data have not been corrected for concentration overpotentials nor for cell resistance. For each set of J-*E* data shown, the redox solution consisted of [A] = [A^-] = 10 mM. The dopant density of the n-Si was 7.84 x 10^{14} cm^{-3} for all three J-*E* curves. (a) The redox couple was **III**$^{2+/+}$, and the n-Si electrode area was 0.81 cm^2. The solution potential *E*(A/A^-) was -0.399 V vs SCE. (b) **V**$^{2+/+}$; the n-Si electrode area was 0.83 cm^2. *E*(A/A^-) was -0.382 V vs SCE. (c) **VII**$^{2+/+}$; the n-Si electrode area was 0.83 cm^2. *E*(A/A^-) was -0.195 V vs SCE.


0.05
0
-0.05
-0.10
-0.15
-0.20
-0.25
-0.30
-0.35
J (mA cm-2)
-0.2
-0.1
0
0.1
0.2
0.3
0.4
0.5
Potential (V vs E(A/A-))
(a)


0.10
0
-0.10
-0.20
-0.30
-0.40
-0.50
-0.60
J (mA cm-2)
-0.2
-0.1
0
0.1
0.2
0.3
0.4
0.5
Potential (V vs E(A/A))
(b)

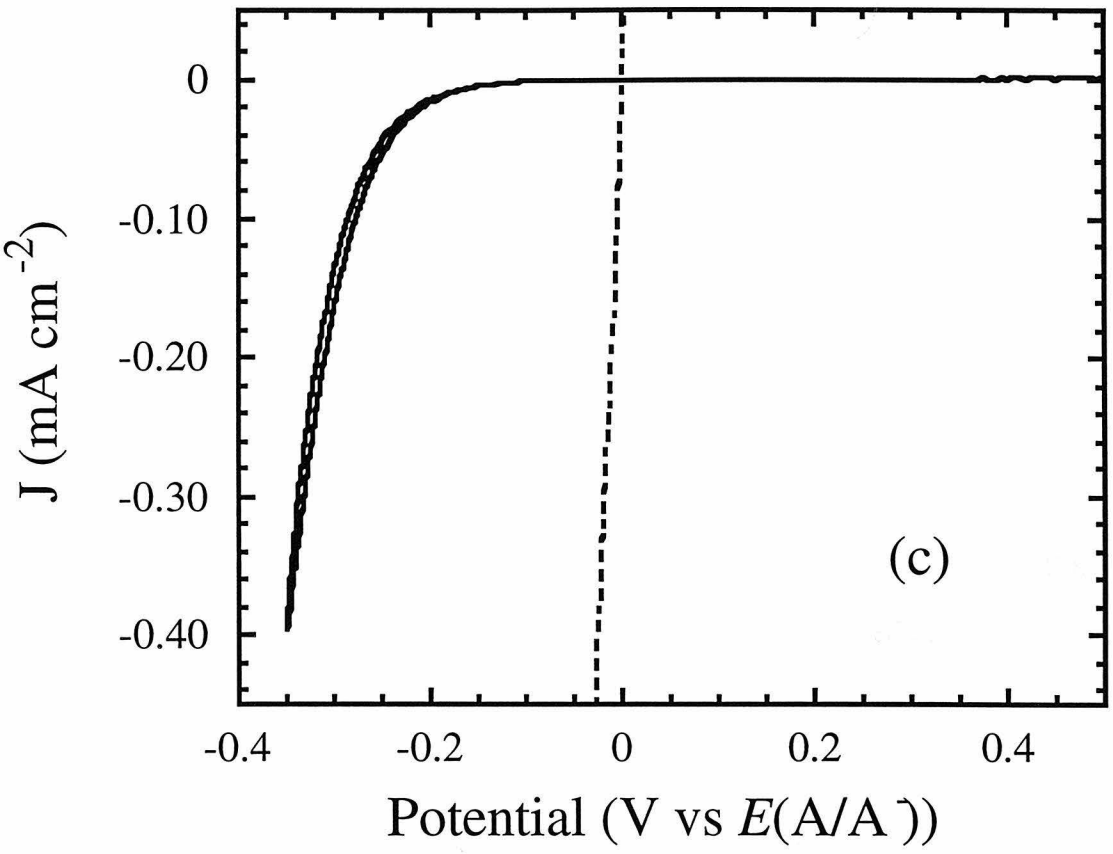
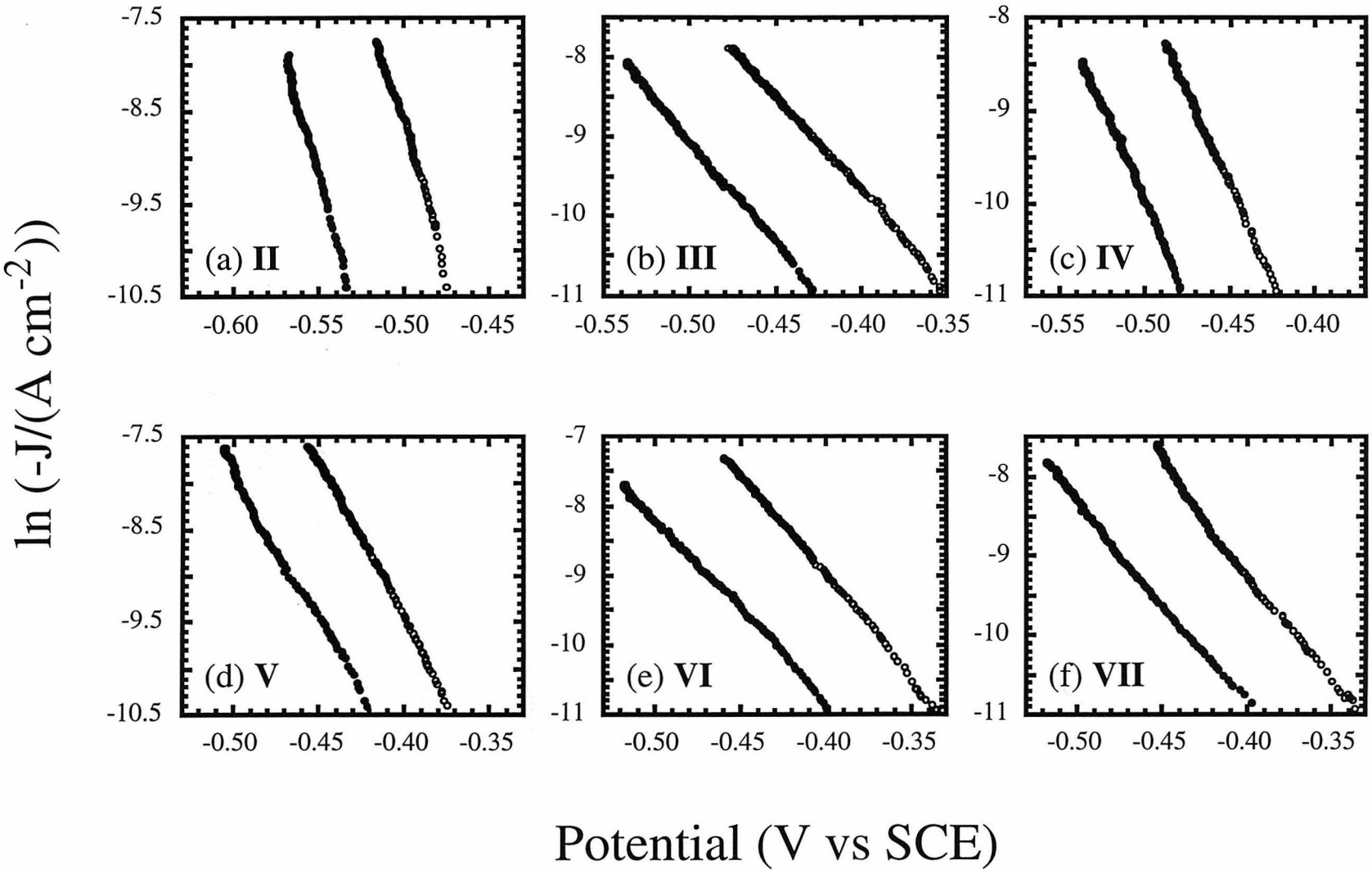

0
-0.10
-0.20
-0.30
-0.40
J (mA cm-2)
(c)
-0.4
-0.2
0
0.2
0.4
Potential (V vs E(A/A))

Figure 6. Dark J-E_{corr} characteristics for compounds **II-VII**, each showing the shift as [A] was increased and [A^-] held constant. In each plot, the curve on the left is the J-E response at [A] = [A^-] = 10 mM, while the curve to the right is that at [A] = 100 mM (85 mM for part (f)) and [A^-] = 10 mM. For clarity, the potential is referenced to SCE. As detailed in the text, a tenfold higher [A] with fixed [A^-] should shift the Nernstian potential by +59 mV, increase the barrier height by 59 mV, and decrease the potential vs SCE by 59 mV that is needed to obtain a given current density. The cells described in (a)-(f) correspond to the cells shown in Figure 3, (a)-(f).


ln (-J/(A cm^{-2}))
(a) II
(b) III
(c) IV
(d) V
(e) VI
(f) VII
-7.5
-8.5
-9.5
-10.5
-8
-9
-10
-11
-7
-0.60
-0.55
-0.50
-0.45
-0.40
-0.35
Potential (V vs SCE)

nonaqueous solvent had a significantly higher cell resistance than the aqueous solutions used in previous kinetic studies.[4,6] In addition, limitations on the concentration of redox species due to solubility considerations imposed nonnegligible mass-transport overpotential corrections at the highest current densities of interest. The corrected J-*E* data yielded excellent linearity in ln |J| vs E_{corr} plots, indicating adherence to the diode-like behavior expected for a semiconductor/liquid contact. The diode quality factors, γ, were not precisely unity, but were generally close to the predicted value of 1.0; mean values of γ ranged from 1.1 to 1.4 for the various junctions of interest (Table IV). The diode quality factor can be interpreted as the reaction order of the interfacial kinetics in the surface electron concentration, with a quality factor of 1.0 indicating a strict first-order kinetic dependence on n_s, as predicted by eq 1.

Figure 6 also depicts the change in ln |J|-E_{corr} data for six bipyridinium redox systems in response to variation in the concentration of the acceptor species A. If the rate law of eq 1 were obeyed, increasing the acceptor concentration by a factor of 10 should decrease the value of E_{corr} vs a fixed reference, such as SCE, by (kT/q)(ln 10) = 59 mV needed to obtain a given current density. This behavior was generally observed for all of the junctions investigated in this work, with the data for all systems summarized in Table IV.

Rate constant data were computed by dividing the current density by the quantity {q n_s [A]}. The value of [A] was taken to be the same as its value in the bulk of the solution, because the Frumkin-like double-layer corrections that relate the concentration of redox species at the edge of the outer Helmholtz plane to the concentration of redox species in the bulk of the solution are negligible for a semiconductor electrode under depletion conditions.[31] The value of n_s was computed according to eqs 3 and 8 using the value of ϕ_b obtained from analysis of the C^{-2}-*E* data for the specific junction of concern. For example, for one particular n-Si/CH_3OH-$\mathbf{IV}^{2+/+}$ cell, J = -2.88 x 10^{-4} A cm^{-2} at E_{corr} = -0.087 V vs

Table IV. Current density-potential data for n-Si/CH_3OH interfaces

Redox compound	Diode quality factor	Current density [a] ($mA\ cm^{-2}$)	E shift with [A] [b] (mV vs SCE)
II	1.37	-0.373	52
III	1.44	-0.305	68
IV	1.04	-0.209	52
V	1.16	-0.489	51
VI	1.34	-0.453	73
VII	1.49	-0.397	69 [c]

The diode quality factors represent the mean of the two (ln J)-E_{corr} curves illustrated in Figure 6. [a] The maximum cathodic J for which data were analyzed for each n-Si/CH_3OH junction, in cells with [A] = [A^-] = 10 mM. This current density is also the value at which the dependence of J on acceptor concentration was assessed. [b] For each specified current density, the shift in potential (vs SCE) as [A] was changed from 10 mM to 100 mM, while [A^-] was constant at 10 mM. In the case of fixed band edges, the expected shift for a tenfold increase in [A] is 59 mV. [c] Since [A] was increased from 10 mM to 85 mM in this particular experiment, the expected shift in potential vs SCE is 55 mV.

$E(A/A^-)$ with [A] = 10 mM. The value of ϕ_b was determined as 0.477 V, so eqs 3 and 8 yielded $n_s = 7.19 \times 10^{12}$ cm^{-3} at E_{corr} = -0.087 V vs $E(A/A^-)$. Substitution of these values into the rate law of eq 1 produces $k_{et} = 4.2 \times 10^{-17}$ cm^4 s^{-1} for this specific measurement. For a given n-Si/CH_3OH interface with compounds **II-VII**, 12 to 16 individual rate constant determinations, each using the J and ϕ_b measurements from one particular electrode-solution combination, resulted in an average k_{et} and an associated standard deviation for that system.

The diode quality factors of 1.1 to 1.4 introduced two ambiguities into the data analysis. The γ values greater than unity might suggest a recombination mechanism other than electron transfer from the semiconductor conduction band to the solution acceptor, since J changed with E_{corr} to a smaller extent than described by eqs 2 and 3. However, the possibility of surface-state mediation is contradicted by the dependence of J on both redox concentration and applied potential. The corrections of E for overpotential and resistance effects may have introduced a residual systematic error into the J-E_{corr} curves. The second issue concerns the choice of J-E_{corr} points used in each k_{et} calculation. If $\gamma > 1$, the k_{et} calculated from eqs 2 and 3 would decrease with larger J and E_{corr} values. In this work, any artificial variations in k_{et} were minimized by choosing similar current densities (-(2-5) x 10^{-4} A cm^{-2}) for the rate constant calculations for compounds **II-VII**. In addition, the maximum J and E_{corr} of each interface were used because at higher forward bias, the cathodic recombination pathways that have $\gamma = 1$ prevail over those that have $\gamma > 1$.

For the redox couple with the most negative redox potential, $\mathbf{I}^{2+/+}$, a different approach was required to evaluate the interfacial charge-transfer kinetics. The low barrier height of this system produced a relatively high exchange current density and therefore resulted in significant interfacial currents at relatively small forward bias potentials relative to $E(A/A^-)$. In fact, the cathodic current densities for n-Si/CH_3OH-$\mathbf{I}^{2+/+}$ contacts were sufficiently large that mass-transport limits constrained the potential range available for

study. For these systems, the interfacial kinetics were instead evaluated through measurement of the anodic saturation current density, J_o. The anodic saturation current density reflects the rate of electron movement from the donor species in solution into the conduction band of the semiconductor. Because the full diode equation is[18]

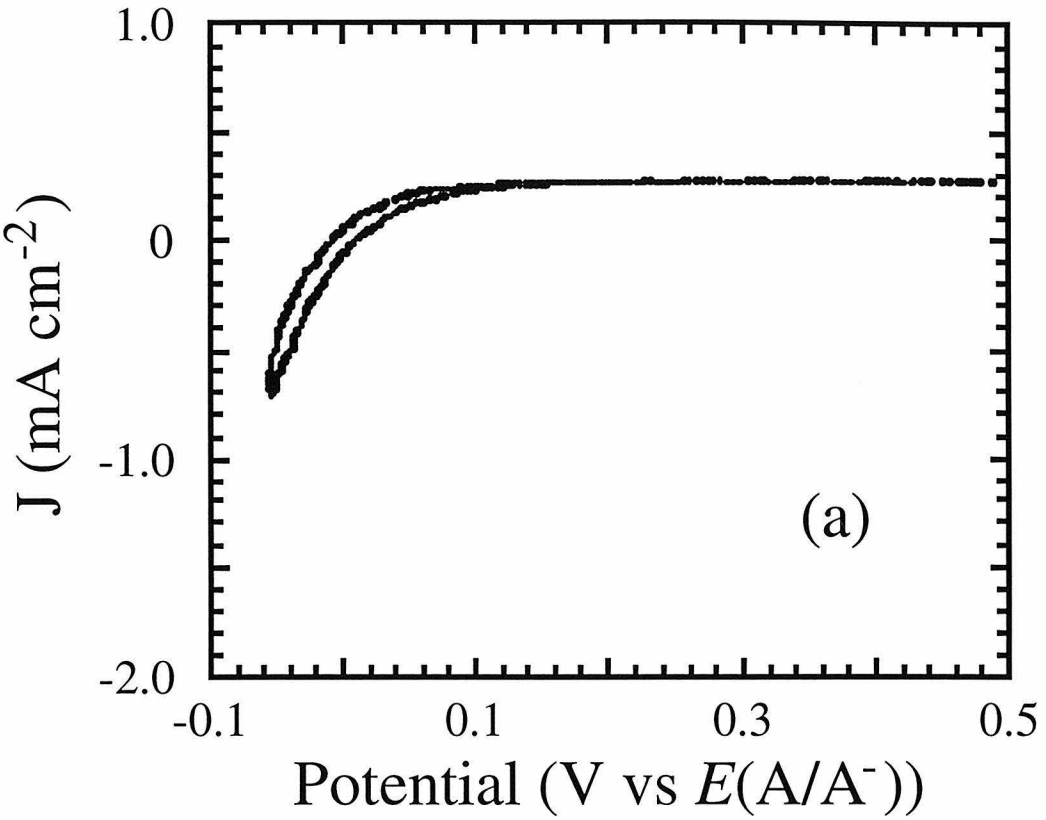
$$J = -J_o\left[\exp\left(-qE_{corr}/kT\right) - 1\right] \quad (8)$$

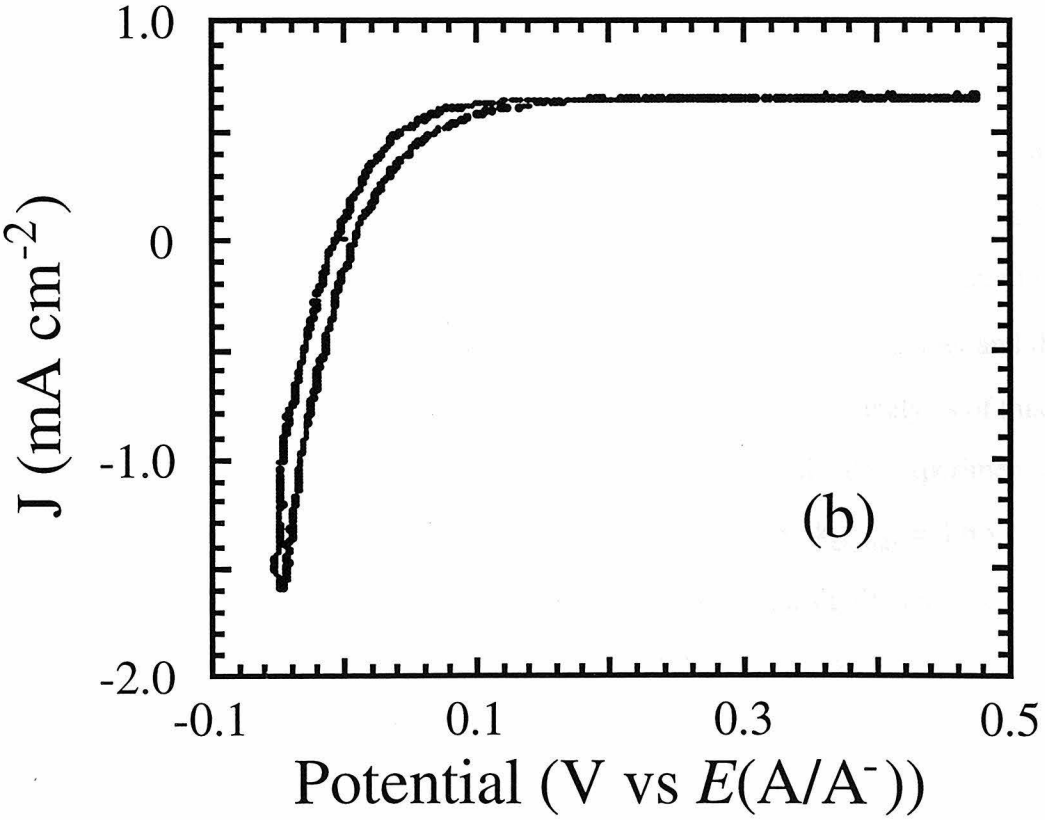
the value of J_o at positive potentials can be directly related to the desired interfacial rate constant without evaluating a plot of ln |J| vs E_{corr} at negative potentials.

Although the saturation current density for high-barrier-height systems is notoriously sensitive to the presence of surface defects,[15] the low barrier height of n-Si/CH_3OH junctions with the redox species **I** and **II** produced a sufficiently large saturation current density that leakage currents were insignificant. This behavior allowed estimation of the rate constant from an analysis of the anodic portion of the J-*E* data. To verify this approach, the rate constant for compound **II** was determined from both the anodic and cathodic portions of J-*E* plots. A k_{et} of 2.7 x 10^{-17} cm^4 s^{-1} was computed for an n-Si/CH_3OH-$\mathbf{II}^{2+/+}$ contact from the cathodic J-*E* data and a k_{et} of 1.7 x 10^{-17} cm^4 s^{-1} was obtained from the anodic J_o value.

For n-Si/CH_3OH-$\mathbf{I}^{2+/+}$ contacts, the kinetics scaled with acceptor concentration. For example, the exchange current density of an n-Si/CH_3OH contact was 2.67 x 10^{-4} A cm^{-2} in a solution of $[\mathbf{I}^{2+}] = [\mathbf{I}^{+}] = 10$ mM but was 6.61 x 10^{-4} A cm^{-2} in a more concentrated solution of $[\mathbf{I}^{2+}] = [\mathbf{I}^{+}] = 30$ mM (Figure 7). With the measured barrier heights of 0.331 V for the 10 mM solution and 0.334 V for the 30 mM solution, these J_o data produced rate constants of 3.9 x 10^{-18} cm^4 s^{-1} and 3.6 x 10^{-18} cm^4 s^{-1}, respectively. To ensure that the J_o values were not limited by mass transport of donors to the electrode, the anodic current density was measured for a Pt electrode in nominally the same configuration as the Si working electrode. The limiting current densities at a Pt foil of 1.3 x 10^{-3} A cm^{-2} in the dilute solution and 3.0 x 10^{-3} A cm^{-2} in the concentrated solution were

Figure 7. Dark J-*E* properties for compound **I** at different total concentrations of redox species in solution. $E(A/A^-)$ was -0.572 V vs SCE in both cases. The n-Si electrode had a measured N_d of 7.84 x 10^{14} cm^{-3} and an area of 0.75 cm^2. (a) At [A] = [A^-] = 10 mM, the J_o observed at +0.450 V vs $E(A/A^-)$ was 2.67 x 10^{-4} A cm^{-2}. (b) At [A] = [A^-] = 30 mM, the J_o at +0.450 V vs $E(A/A^-)$ was 6.61 x 10^{-4} A cm^{-2}.


1.0
0
-1.0
-2.0
J (mA cm-2)
(a)
-0.1
0.1
0.3
0.5
Potential (V vs E(A/A-))


1.0
0
-1.0
-2.0
J (mA cm-2)
(b)
-0.1
0.1
0.3
0.5
Potential (V vs E(A/A-))

significantly in excess of the anodic saturation current densities at the n-Si contacts, so no mass-transport corrections were required in the analysis of the Si electrode data obtained under these conditions.

C. Trend in k_{et} for n-Si/CH_3OH-Bipyridinium$^{2+/+}$ Contacts

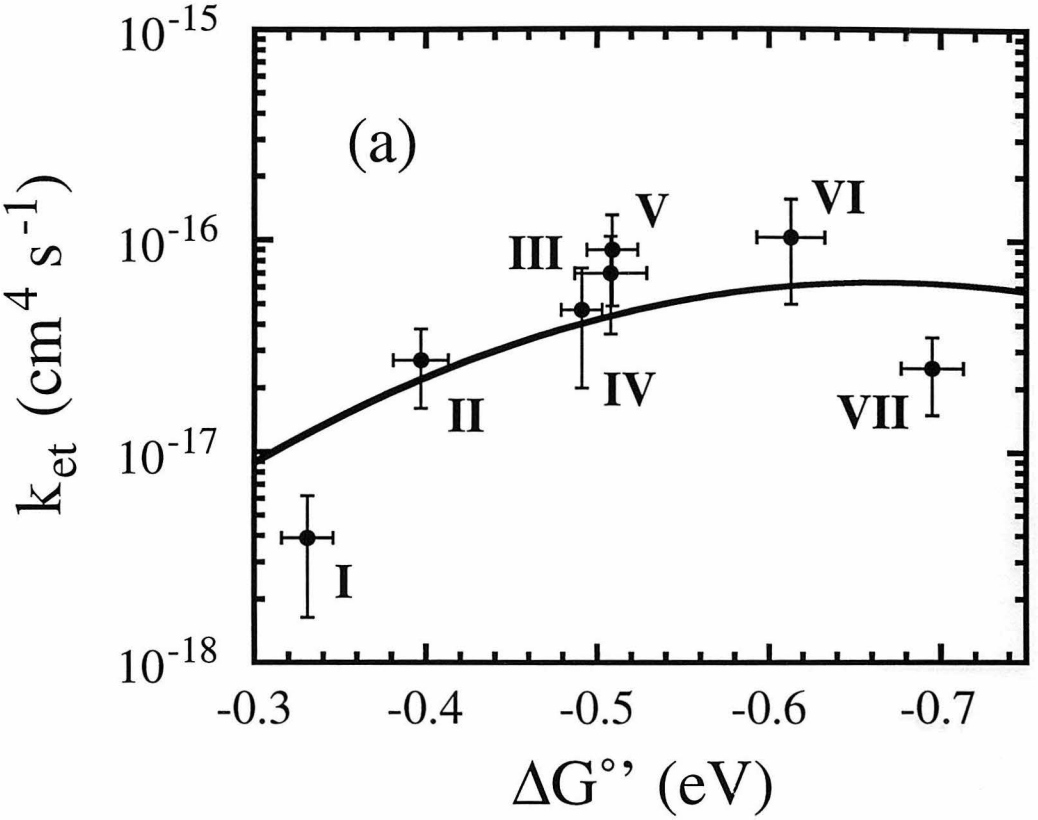
Figure 8a presents a semilogarithmic plot of k_{et} vs the standard driving force for interfacial electron transfer, $\Delta G^{\circ\prime}$. This latter quantity is the driving force for an electron at the surface transferring to an acceptor under standard conditions, and is thus given as $\mathbf{E}_{cb} - qE^{\circ\prime}(A/A^-)$. The driving force for each n-Si/CH_3OH-bipyridinium$^{2+/+}$ contact was determined from measurements of the barrier height when $E(A/A^-) = E^{\circ\prime}(A/A^-)$, *i.e.*, specifically in this work when [A] = [A^-] = 10 mM.

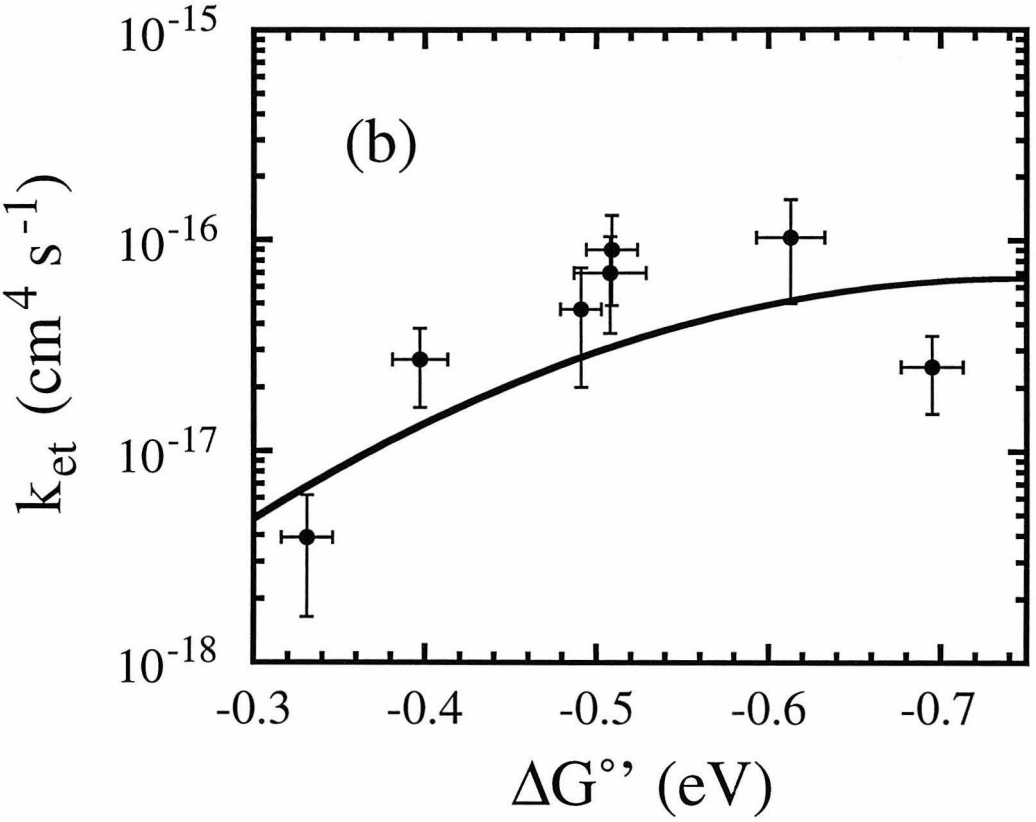
The data were fit to a classical version of the Marcus theory, which has the form

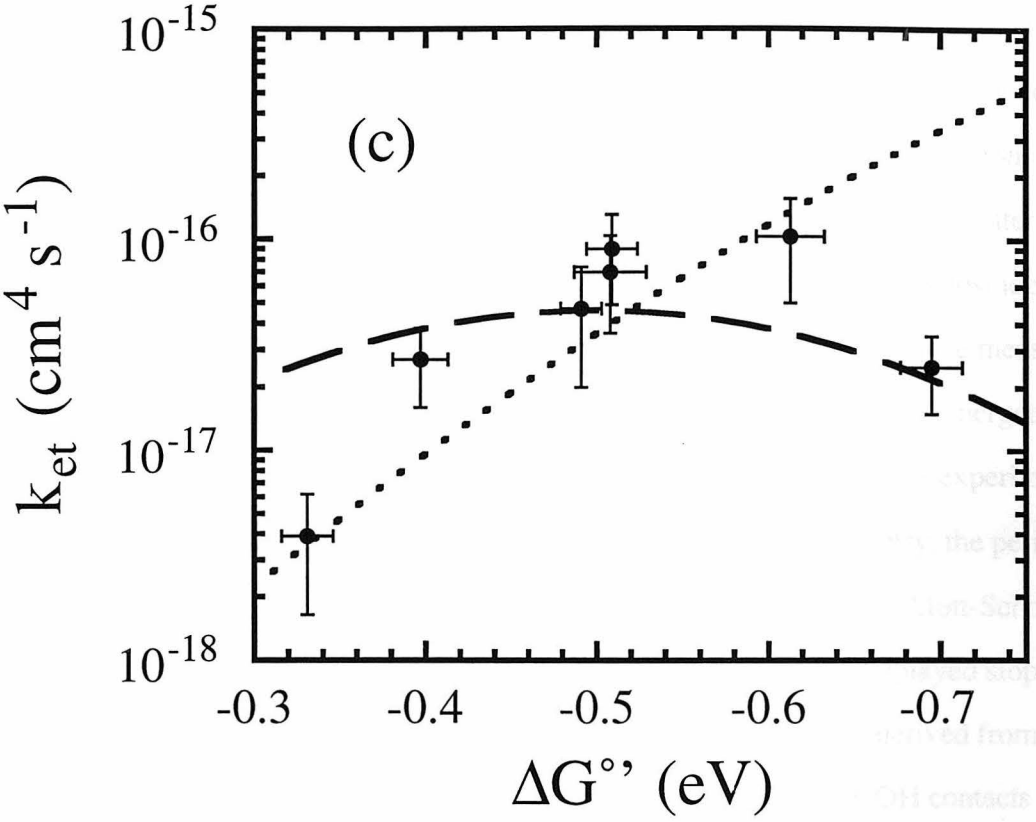
$$k_{et} = k_{et,max} \exp\left\{\frac{-(\Delta G^{\circ\prime} + \lambda)^2}{4\lambda kT}\right\} \qquad (9)$$

where λ is the solvent reorganization energy at the interface. In this analysis, $k_{et,max}$ and λ were both floating parameters. The ensuing fit, with all experimental data points weighted equally, yielded $k_{et,max} = (6.4 \pm 1.7) \times 10^{-17}$ cm^4 s^{-1} and $\lambda = 0.67 \pm 0.12$ eV. A slightly more visually satisfying fit to the available data, shown in Figure 8b, was obtained by increasing λ to 0.75 eV, resulting in $k_{et,max} = 6.6 \times 10^{-17}$ cm^4 s^{-1}. This fit agreed more closely with the data points at lower driving force, which are fewer in number and thus weighted less than those at higher driving force in a purely statistical analysis of this specific data set. Other λ and $k_{et,max}$ combinations did not describe the experimental data as satisfactorily (Figure 8c). When λ was constrained at 0.5 eV, $k_{et,max} = 4.6 \times 10^{-17}$ cm^4 s^{-1} was obtained as the best-fit to the data, but this fit produced a significant discrepancy in the value of k_{et} for the n-Si/CH_3OH-$\mathbf{I}^{2+/+}$ junction. When $k_{et,max}$ was constrained to 1×10^{-14} cm^4 s^{-1}, the fit deviated considerably from the k_{et} data of the n-Si/CH_3OH-$\mathbf{II}^{2+/+}$ and the n-Si/CH_3OH-$\mathbf{VII}^{2+/+}$ contacts. Furthermore, the constraint of $k_{et,max}$ to 1×10^{-14} cm^4

Figure 8. Plots of the electron-transfer rate constant as a function of the driving force for charge transfer. The $G^{\circ\prime}$ values were taken to be the barrier heights measured at [A] = [A^-] = 10 mM. The error in $\Delta G^{\circ\prime}$ was the standard deviation of ϕ_b measured at these concentrations, while the error in k_{et} was the standard deviation of 12 to 16 rate constant determinations for each interface. (a) When both the maximum electron-transfer rate constant and the reorganization energy were floated, the fitted parabolic curve had parameters of $k_{et,max} = (6.4 \pm 1.7) \times 10^{-17}$ cm^4 s^{-1} and $\lambda = 0.67 \pm 0.12$ eV. (b) A slightly more visually satisfying fit was obtained by using parameters of $k_{et,max} = 6.6 \times 10^{-17}$ cm^4 s^{-1} and $\lambda = 0.75$ eV. (c) When λ was fixed at 0.50 eV, the best-fit $k_{et,max}$ was 4.6×10^{-17} cm^4 s^{-1} (dashed line). When $k_{et,max}$ was fixed at 1×10^{-14} cm^4 s^{-1}, the best-fit λ was 1.4 eV (dotted line).


(a)
I
II
III
IV
V
VI
VII
10^{-15}
10^{-16}
10^{-17}
10^{-18}
k_{et} (cm^4 s^{-1})
-0.3
-0.4
-0.5
-0.6
-0.7
ΔG°' (eV)


(b)
10^{-15}
10^{-16}
10^{-17}
10^{-18}
k_{et} (cm^4 s^{-1})
-0.3
-0.4
-0.5
-0.6
-0.7
ΔG°' (eV)


(c)
10^{-15}
10^{-16}
10^{-17}
10^{-18}
k_{et} (cm^4 s^{-1})
-0.3
-0.4
-0.5
-0.6
-0.7
$\Delta G^{\circ\prime}$ (eV)

s^{-1} forced λ to be 1.4 eV, which is an unrealistically large value for the reorganization energy for this system (*vide infra*).

IV. DISCUSSION

A. Energetic Behavior of n-Si/CH_3OH-Bipyridinium$^{2+/+}$ Contacts

A striking feature of the results presented above is the nearly ideal energetic behavior of n-Si/CH_3OH-bipyridinium$^{2+/+}$ contacts. Prior studies on small-band-gap semiconductors in general, and on Si electrodes in particular, have reported nonideal energetic behavior in contact with nonaqueous solvents,[10,11,32,33] although later work demonstrated that the photovoltage of Si/liquid contacts could respond almost ideally to $E(A/A^-)$.[2,34] Moreover, frequency dispersion in the differential capacitance measurements of some semiconductor/liquid interfaces has hindered the straightforward energetic characterization of these systems.[35-39] In our work, careful control over experimental variables (*e.g.*, etching procedures, counter electrode size, cell geometry, the perimeter/area ratio of the semiconductor electrode, *etc.*) led to behavior in which the Mott-Schottky plots of n-Si/CH_3OH contacts showed small frequency dispersions and displayed slopes that agreed well with theoretical expectations. The energetic parameters derived from these M-S measurements revealed that the band edge positions of the n-Si/CH_3OH contacts remained fixed to within $\approx$ 40 mV while the Nernstian potential of the solution was changed by over 400 mV (Figure 4), underscoring the lack of surface-state charging that is displayed by this system.

An upper limit on the surface state capacity for this system can be estimated from the ϕ_b vs $E(A/A^-)$ behavior of Figure 4. Assuming a differential capacitance of the Helmholtz layer of 10 $\mu F\ cm^{-2}$ and a double layer thickness of 3 Å, 10^{12} surface states cm^{-2} (N_{ss}) would be sufficient to pin the Fermi level completely if such states were charged or discharged over the potential range of interest.[10] Within this framework, the linearity of

the data of Figure 4 implies an upper bound on N_{ss} of $< 10^{11}$ cm^{-2} for these systems. This low electrical defect density, which corresponds to less than 1 electrical defect per 10^4 surface atoms, attests to the high degree of electrical perfection that can be attained from small-band-gap semiconductors in carefully controlled solid/liquid junctions.

B. Kinetic Behavior of n-Si/CH_3OH-Bipyridinium$^{2+/+}$ Contacts

A second striking feature of the n-Si/CH_3OH-bipyridinium$^{2+/+}$ contacts is their J-*E* behavior. Prior studies of semiconductor/liquid contacts have not observed kinetic behavior in accord with the rate law of eq 1, but have instead observed no dependence of the interfacial current density on the concentration of acceptor species in the solution phase.[2,9,17] This lack of adherence to the expected rate law of eq 1 has thwarted routine investigation of charge-transfer kinetics at semiconductor/liquid contacts, although a linear dependence of J on [A] has been observed in a few systems.[4,6,40] The n-Si/CH_3OH-bipyridinium$^{2+/+}$ interfaces described in this paper display kinetics that are first-order in the acceptor concentration and first-order in the concentration of electrons at the semiconductor surface, thereby allowing k_{et} to be extracted from a simple arithmetic analysis of the current density-potential data of such systems.

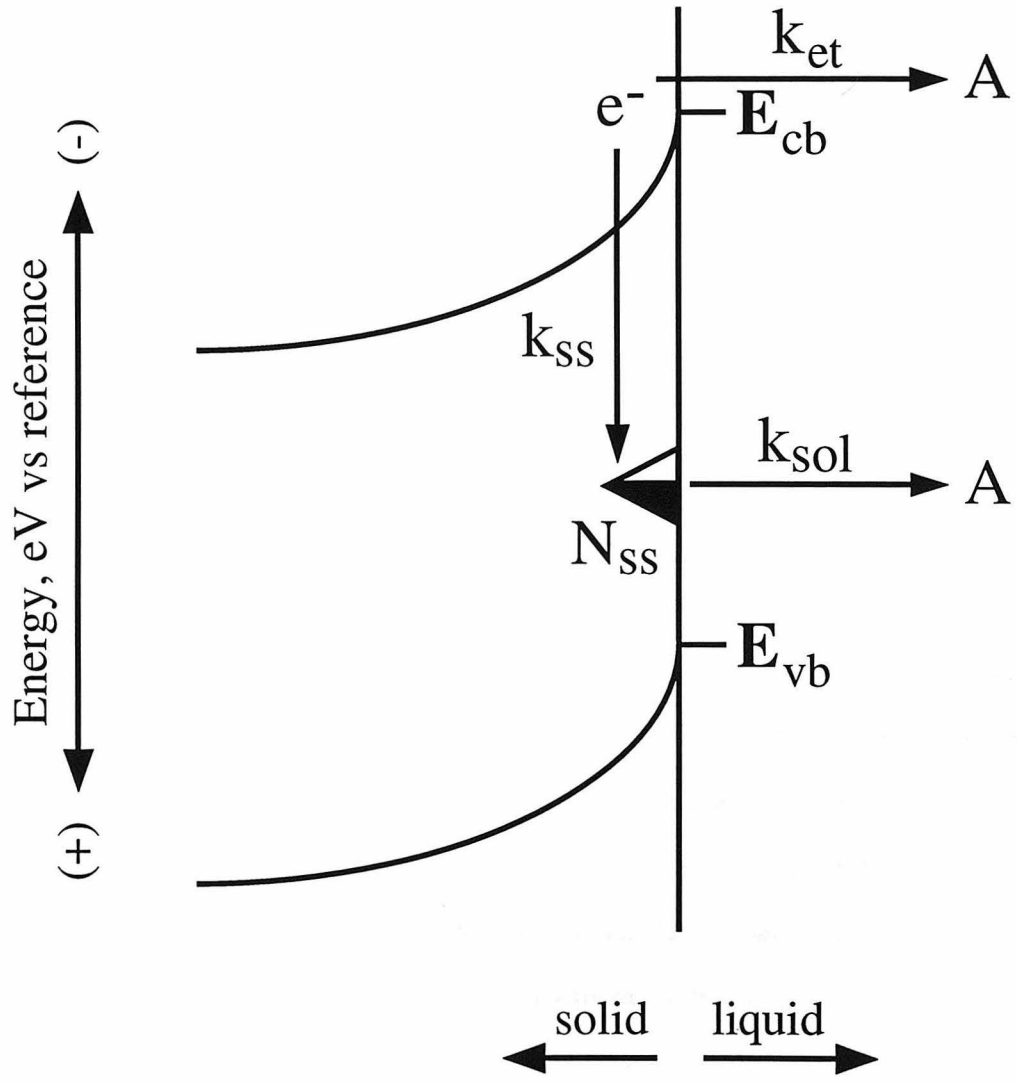
The J-*E* behavior establishes an even more strict upper limit on N_{ss} than does the C^{-2}-*E* behavior. Including surface-state capture as an intermediate pathway for electron transfer from the semiconductor to the acceptor in solution (Scheme 1) produces the following rate law:

$$\text{rate} = k_{et}[A]n_s + k_{sol}[A]N_{ss}f_{ss} \tag{10}$$

In eq 10, N_{ss} is the density of surface states, f_{ss} is the fraction of surface states that are filled with electrons, and k_{sol} is the electron-transfer rate constant from a surface trap to a solution acceptor. At steady state, $df_{ss}/dt = 0$, producing the following rate expression:

$$\text{rate} = k_{et}[A]n_s + k_{sol}[A]N_{ss}\left[\frac{k_{ss}n_s}{k_{ss}n_s + k_{sol}[A]}\right] \tag{11}$$

Scheme 1. Two possible mechanisms for interfacial electron transfer. The upper pathway shows the direct transfer of electrons from the conduction band edge of the semiconductor to the acceptor in solution, with the rate constant k_{et}. The lower pathway depicts the surface-state mediation of interfacial electron transfer. N_{ss} is the density of surface states, k_{ss} is the rate constant for electron capture from the conduction band into surface states, and k_{sol} is the rate constant for electron injection from the surface states into solution.


k_{et}
A
e^-
E_{cb}
k_{ss}
k_{sol}
A
N_{ss}
E_{vb}
Energy, eV vs reference
(-)
(+)
solid
liquid

where k_{ss} is the rate constant for transfer of an electron from the conduction band into a surface state. If an electron slowly fills a surface trap and proceeds quickly to the solution, such that $k_{sol}[A] >> k_{ss}n_s$, and k_{ss} is interpreted as a collisional event, eq 11 becomes

$$\text{rate} = k_{et}[A]n_s + (\sigma\upsilon)N_{ss}n_s \qquad (12)$$

where the parenthetical term is k_{ss}, σ is the cross section of a trap for charge capture, and υ is the thermal velocity of the charge carriers. The thermal velocity of electrons is well-known for n-Si to be 10^7 cm s^{-1}.[18] Eq 12 indicates that, in the scenario of slow electron trapping by surface states and fast electron ejection into solution, a large N_{ss} will eliminate the dependence of J on $[A]_s$. In the converse case of fast electron trapping and a rate-determining step of electron ejection into solution, such that $k_{ss}n_s >> k_{sol}[A]_s$, eq 11 reduces to

$$\text{rate} = k_{et}[A]n_s + k_{sol}[A]N_{ss} \qquad (13)$$

For the rate in eq 13, a large N_{ss} will eliminate the dependence of J on n_s. Regardless of which surface-state mediation step dictates the rate, a significant density of electrical traps will at best hamper and at worst prevent steady-state measurements of k_{et}. Gerischer has suggested that redox species couple more strongly to surface states than to conduction band states, and hence even a small N_{ss} would generally overwhelm the steady-state, electron-transfer current flow under practical experimental conditions.[16] It is thus readily possible, through improper etching, scratching the electrode surface, using substrates with a large density of electrical traps, or using electrodes such as GaAs that have an inherently unstable surface termination chemistry,[41] to prepare highly defective semiconductor/liquid contacts which exhibit surface electron capture velocities that are limited only by thermionic emission of majority carriers from the bulk to the surface of the semiconductor. Obtaining direct, robust information on the rate constants of outer-sphere, interfacial charge-transfer events using steady-state J-*E* methods requires careful control over the electrode surface condition, so that the resultant surface is nearly defect-free.

In our kinetic experiments, the n-Si/CH_3OH interface displayed a negligible density of surface states. Because J varied linearly with [A], the rate given in eq 12 favors the k_{et} pathway by at least one order of magnitude. The condition that $N_{ss} \leq (k_{et}[A]_s)/(10\sigma\upsilon)$ and the representative values of $k_{et} = 10^{-16}$ cm^4 s^{-1}, $[A]_s$ = 10 mM = 6 x 10^{18} cm^{-3}, $\sigma = 10^{-15}$ cm^2, and $\upsilon = 10^7$ cm s^{-1} yield $N_{ss} \leq 6 \times 10^9$ cm^{-2}, or in other words, less than 1 electrical defect in every 10^5 surface atoms. In contrast, the lack of dependence of J on [A] observed for the n-WSe_2/CH_3CN interface was attributed to surface state densities of $N_{ss} \geq 10^{12}$ cm^{-2}, and only an upper limit on the rate constant for the direct charge-transfer pathway could be obtained from that semiconductor/liquid contact.[9]

C. Heterogeneous Charge-Transfer Rate Constants: Comparison Between Theory and Experiment

1. Semiclassical Approach

The rate constant data produced a value of the maximum charge-transfer rate constant, $k_{et,max}$, of 6 x 10^{-17} cm^4 s^{-1}. This value is consistent with expectations from a semiclassical approach to predicting such $k_{et,max}$ values.[17] An electron-ion collisional event can be described in terms of the cross section for electron capture, σ, the relative velocity of the reactants, υ, and the effective zone over which this electron transfer will take place, δ. Taking δ = 10 Å, $\upsilon = 10^7$ cm s^{-1} (because the thermal velocity of electrons in the semiconductor will closely approximate the relative velocity of the reactants), and a geometric cross section for the ion that is appropriate for an off-resonance event such as electron transfer, $\sigma = 10^{-15}$ cm^2, yields $k_{et,max} = 10^{-15}$ cm^4 s^{-1}. However, in the absence of solvent relaxation, the collision will be elastic and the electron will not reduce the ion. Therefore, this estimate of $k_{et,max}$, which has been described earlier,[17] should be reduced by approximately the ratio of the electronic relaxation frequency compared to the frequency factor for the solvent relaxation, *i.e.*, by a factor of $(10^{15}$ $s^{-1})/(10^{13}$ $s^{-1}) = 10^2$. This yields

a semiclassical estimate for $k_{et,max}$ of 10^{-17} cm^4 s^{-1}, in good agreement with the experimental observations reported herein.

2. Electronic Coupling Estimate

An alternate expression for k_{et}, adapted from a Marcus liquid-liquid relation with the donors and acceptors separated into immiscible phases,[42] is[17]

$$k_{et} = \nu_n \kappa_{el} \kappa_n \tag{14a}$$

where ν_n is the attempt frequency of the process, κ_{el} is the electronic coupling between the donor and acceptor, and κ_n is the nuclear term that contains the Franck-Condon factor for the electron-transfer event. The latter two parameters are further described by

$$\kappa_{el} = \pi\left[\frac{2(r_e + r_A)}{\beta^3} + \frac{6}{\beta^4}\right] \tag{14b}$$

and

$$\kappa_n = \exp\left\{\frac{-(\lambda + \Delta G^{\circ\prime})^2}{4\lambda kT}\right\} \tag{14c}$$

where r_e is the effective radius of the delocalized donor in the semiconductor, r_A is the radius of the acceptor ion in solution, and β is the attenuation factor for the electronic overlap between the donor and acceptor in the nonadiabatic electron-transfer regime.

Since the effective Bohr radius in Si is known,[22,43] and since β is roughly 1 $Å^{-1}$ for most electron-transfer systems studied to date,[25,44-53] using $\nu_n = 10^{13}$ s^{-1}, $r_e = 1 \times 10^{-7}$ cm, $r_A = 3 \times 10^{-8}$ cm, $\beta = 1 \times 10^8$ cm^{-1}, and $\kappa_n = 1$ yields $k_{et,max} = 10^{-17}$ cm^4 s^{-1}. This prediction is clearly in excellent agreement with the experimental data reported herein on n-Si/CH_3OH-bipyridinium$^{2+/+}$ contacts.

A recent paper has questioned whether the electron transfer indeed occurs nonadiabatically from a semiconductor to an acceptor in solution and has also questioned other aspects of the theory summarized above.[54] We note, however, that in fact adiabaticity has already been included in the above treatments. In the electronic coupling

model, the representation of the electron as a delocalized particle having a radius greater than an atomic radius implicitly incorporates the adiabaticity of the reaction into the estimate of $k_{et,max}$.[1] Similarly, the distance of the effective reaction zone, δ, incorporates adiabaticity into the semiclassical model.[1] Addition of another separate correction to the two-sphere model, which already uses a Bohr radius to describe the electronic delocalization, seems to require careful consideration and justification.

A more refined procedure, which involves laminae instead of simple spheres and which more explicitly includes the electrons within a Bohr radius of the interface into the charge-transfer event, has been proposed recently.[55] We note, however, that any electrons which are located at distances of less than a Bohr radius from the interface will no longer experience the periodic potential of the semiconductor crystal but will instead be more localized and thus higher in energy. These localized electrons will require a more complete formulation of their effective radius, their solvation and nuclear reorganization energies, their electronic coupling parameters, *etc.*, than is available from any theoretical description available to date. In fact, these charges more closely resemble surface states than delocalized electronic carriers in the semiconducting solid. Therefore, it is not clear that a full description of the population, kinetics and electronic coupling parameters of this subspecies of carriers in the solid will affect significantly the order-of-magnitude estimate of $k_{et,max}$ that is produced by the two-sphere model presented above. The experimental data described above clearly are incompatible with hypotheses that $k_{et,max} > 10^{-14}$ cm^4 s^{-1},[55] but are in excellent agreement with predictions that $k_{et,max} = 10^{-17}$-10^{-16} cm^4 s^{-1} according to eqs 14a-c.

3. Electronic Coupling Estimates of Semiconducting Electrodes Based on Coupling Values of Metal/Electrolyte Contacts

It is also possible to confirm the $k_{et,max}$ values of 10^{-17} cm^4 s^{-1} discussed above through reference to kinetic measurements at metal electrodes. An expression for the potential dependence of the charge-transfer rate at a metal electrode to a solution of randomly dissolved, outer-sphere redox acceptors may be written as[24,25,56,57]

$$\text{rate}(E) = \rho_{\text{eff}}\,[\text{A}]\left\{\frac{4\pi^2}{\text{h}}(4\pi\text{kT}\lambda)^{-1/2}\right\}\left\{\frac{\overline{H}^{\circ 2}_{\text{AB}}}{\beta}\right\}\int_{-\infty}^{\infty}\frac{\exp\left\{-(\mathbf{E}-\mathbf{E}^{\circ\prime}+\lambda)^2/4\lambda\text{kT}\right\}}{1+\exp\left\{(qE+\mathbf{E}^{\circ\prime}-\mathbf{E})/\text{kT}\right\}}\,d\mathbf{E} \tag{15}$$

where ρ_{eff} is the effective number of states in the electrode (in units of states eV^{-1}) that participate in the charge-transfer event, h is Planck's constant, $\mathbf{E}^{\circ\prime}$ is the formal electrochemical potential for the redox couple A/A^-, and $\overline{H}^{\circ 2}_{\text{AB}}$ is the square of the electronic coupling matrix element, averaged over all degenerate states at each energy **E**, at closest approach of the acceptor to the electrode surface.

At each distance r, the electronic coupling, $\overline{H}^{2}_{\text{AB}}(\text{r})$, represents the average electronic coupling matrix element over all degenerate states at energy **E**. This quantity is assumed to be independent of energy over the experimental range of concern, and thus can be taken out of the integral. Because the electronic coupling generally decays exponentially with β, the term $\{\overline{H}^{\circ 2}_{\text{AB}}/\beta\}$ represents the result of integrating $\overline{H}^{2}_{\text{AB}}(\text{r})$ with respect to r. Similarly, the effective number of states is expected to be essentially constant over the energy range of concern, and its value also can be removed from the integral of eq 15. For the terms remaining in the integral, the numerator of the rational term describes the nuclear activation energy, and the denominator describes the Fermi function occupancy of electronic states, at each energy **E**.

Eq 15 also describes rigorously the theoretical expectations for interfacial charge-transfer kinetic processes at a semiconductor electrode. In this case, evaluation of the integral is somewhat different than for a metal, due to the limited energy range over which

electronic states are occupied in the conduction band of the semiconducting electrode. Evaluating this integral and extracting the rate constant $k_{et,max}$ from the resulting expression produces the following ratio between $k_{et,max}$ and $k_m(E)$:[58]

$$\frac{k_{et,max}}{k_m(E)} = D_m^{-1}\left\{\frac{\overline{H}^{\circ 2}_{AB,sc}}{\overline{H}^{\circ 2}_{AB,m}}\right\}\left\{\frac{\beta_m}{\beta_{sc}}\right\}\left\{\frac{l_{sc}}{l_m}\right\}\left\{\frac{d_m}{d_{sc}}\right\}^{2/3}\left\{\frac{\lambda_m}{\lambda_{sc}}\right\}^{1/2} I^{-1}(\lambda_m, E) \qquad (16)$$

where the subscripts sc and m refer respectively to a semiconductor electrode and a metal electrode, and $I(\lambda_m, E)$ represents the integral in eq 15. The density of states, D (in units of states cm^{-3} eV^{-1}), the effective coupling length, l, and the atomic density of the electrode material, d, quantify the number of states per eV that participate in the coupling event.

Assuming that the total electronic coupling to a state in the metal is similar to that of a state in the semiconductor, *i.e.*, that $\overline{H}^{\circ 2}_{AB}$ is similar for a metal and for a semiconductor, and assuming that the ratios of the coupling lengths, decay lengths through the solvent, and reorganization energies in the two systems are on the order of unity, one can then estimate $k_{et,max}$ from experimental measurements of $k_m(E)$ vs E. Voltammetric data of Terrettaz *et al.*[59] for the reaction of freely diffusing Fe(2,2'-bipyridine)$_2$(CN)$_2^+$ on insulated Au electrodes have yielded excellent agreement with the predicted dependence of $k_m(E)$ on E (eq 15). Specifically, a value of $k_m(E) = 0.0078$ cm s^{-1} was determined at $E = -0.73$ V vs $E^{\circ\prime}(A/A^-)$, and a fit of the entire $k_m(E)$ vs E data set yielded $\lambda = 0.79$ eV for this redox couple at a Au electrode.[59] With these values for E and λ, the definite integral in eq 15 can be established numerically to be 0.195 eV for this metal/electrode interface. Extrapolation of $k_m(E)$ to zero thickness of the blocking layer can be performed using the experimentally observed exponential attenuation of the rate constant, assuming a 16-methylene-unit barrier layer and a decay constant of 1.08 per methylene unit. This yields an expected value of 2.5 x 10^5 cm s^{-1} for the reaction of Fe(2,2'-bipyridine)$_2$(CN)$_2^+$ at an unmodified Au electrode. Use of eq 16, with $D_m = 1.6 \times 10^{22}$ states cm^{-3} eV^{-1} for Au,[22] therefore predicts that if similar electronic coupling occurs at the metal and semiconductor surfaces, then $k_{et,max} = 9$

x 10^{-17} cm^4 s^{-1}. This estimate, although it involves a significant extrapolation of the experimental data from a 20 Å blocking layer thickness, provides an experimentally based, independent estimate of the $k_{et,max}$ values expected from the semiclassical and electronic coupling models discussed above. Notably, this quantum mechanically-based estimate for $k_{et,max}$ is in excellent agreement with the experimental $k_{et,max}$ result obtained for the Si/liquid contacts described in this work, further validating the theory and experimental data discussed above.

D. Comparison to Other Rate Constants For Charge Transfer Across Semiconductor/Liquid Interfaces

The theoretical estimates and experimental data presented in this work appear to be remarkably consistent with other kinetic data for charge-transfer processes at semiconductor/liquid junctions. For instance, scanning electrochemical microscopy techniques have been used to measure a k_{et} of 5.7 x 10^{-17} cm^4 s^{-1} at the p-WSe_2/H_2O-$Ru(NH_3)_6^{3+/2+}$ interface.[5] Substituting reasonable estimates of $\Delta G^{\circ\prime}$ = -1.09 eV and λ = 1.5 eV[60] into eq 9 results in a $k_{et,max}$ at optimal exoergicity of 2 x 10^{-16} cm^4 s^{-1}. A recent study of the n-InP/CH_3OH junction estimated that $k_{et,max}$ = 10^{-16} cm^4 s^{-1} for redox couples such as dimethylferrocene$^{+/0}$ ($Me_2Fc^{+/0}$) and 1,1'-diphenyl-4,4'-bipyridinium$^{2+/+}$.[8] Differential capacitance measurements have yielded a k_{et} of 10^{-18} cm^4 s^{-1} for the p-GaAs/HCl(aq)-$Cu^{2+/+}$ interface,[6] which when corrected for the nuclear terms, also resulted in an estimate of $k_{et,max}$ = 10^{-16} cm^4 s^{-1}. It is not clear that this interface consists of an outer-sphere, nonadsorbing redox system, so the agreement in this case between theory and experiment might be fortuitous. Earlier measurements of heterogeneous electron- transfer rates at the n-ZnO/H_2O-$Fe(CN)_6^{3-/4-}$ junction yielded a k_{et} of 10^{-18} cm^4 s^{-1}.[4] This value also agrees qualitatively with theory, but like $Cu^{2+/+}$ in HCl(aq), it is not clear that $Fe(CN)_6^{3-/4-}$ is an outer-sphere, nonadsorbing redox couple.

In several other systems, alternate pathways dominate the interfacial flux, and only upper limits on k_{et} can be established.[1,9] However, the upper bounds on k_{et} in these measurements are also consistent with a $k_{et,max}$ of 10^{-16} cm^4 s^{-1}. For example, an upper limit on k_{et} of 2 x 10^{-17} cm^4 s^{-1} has been established for the n-WSe_2/CH_3CN-$Me_2Fc^{+/0}$ interface through use of differential capacitance methods.[9] Assuming that $\Delta G^{\circ\prime}$ = -0.65 eV and that λ = 1 eV, eq 9 yields $k_{et,max} < 7 \times 10^{-17}$ cm^4 s^{-1}. Additionally, upper bounds on k_{et} of 10^{-14} cm^4 s^{-1}, 10^{-15} cm^4 s^{-1}, and 10^{-20} cm^4 s^{-1} have been observed at n-GaAs/CH_3CN-ferrocene$^{+/0}$, n-Si/CH_3OH-$Me_2Fc^{+/0}$, and oxidized n-InP/$HCl_{(aq)}$-$Fe(CN)_6^{3-/4-}$ junctions respectively.[1] A $k_{et,max}$ of 10^{-12} cm^4 s^{-1} has been reported from an analysis of p-InP/H_2O-$Fe(CN)_6^{3-/4-}$contacts,[61] and this observation was used to suggest that the theory discussed above needed major revision or correction. However, this InP rate constant has now been assigned to experimental artifacts, including corrosion of the electrode, a passivation process related to light intensity, a time dependence of the electrode decay dynamics, *etc.*, and the rate constant measurement has been withdrawn.[62] Similarly, recent work has shown that a measurement of $k_{et} = 10^{-12}$ cm^4 s^{-1} for a p-GaAs/CH_3CN interface[63] also suffers from the experimental artifacts of adsorption, electrode passivation, *etc.*, that prohibit the use of this system to test reliably the predictions of a theory developed to describe electron-transfer events with nonadsorbing, outer-sphere redox species.[64] Thus, it appears that to date there are no published reports, to our knowledge, of robust rate constant values for semiconductor/liquid contacts using nonadsorbing, randomly distributed, outer-sphere redox couples that contradict the theoretical estimates of $k_{et,max}$ described above.

E. Free-Energy Dependence of the Electron-Transfer Rate Constants at n-Si/CH_3OH-Bipyridinium$^{2+/+}$ Contacts

The n-Si/CH_3OH-bipyridinium$^{2+/+}$ contact is, to our knowledge, the first interface that has allowed a systematic study of the free-energy dependence of charge transfer from a semiconductor to a homologous series of nonadsorbing, outer-sphere redox couples. The k_{et} vs $G^{\circ\prime}$ data fit satisfactorily to a Marcus-type expression and yielded a reorganization energy of 0.7 eV with a $k_{et,max}$ of 6×10^{-17} cm^4 s^{-1}. Other fits to the data were less satisfactory, because a higher $k_{et,max}$ (10^{-12} cm^4 s^{-1} or even 10^{-14} cm^4 s^{-1}) implied an unreasonably large value of λ.

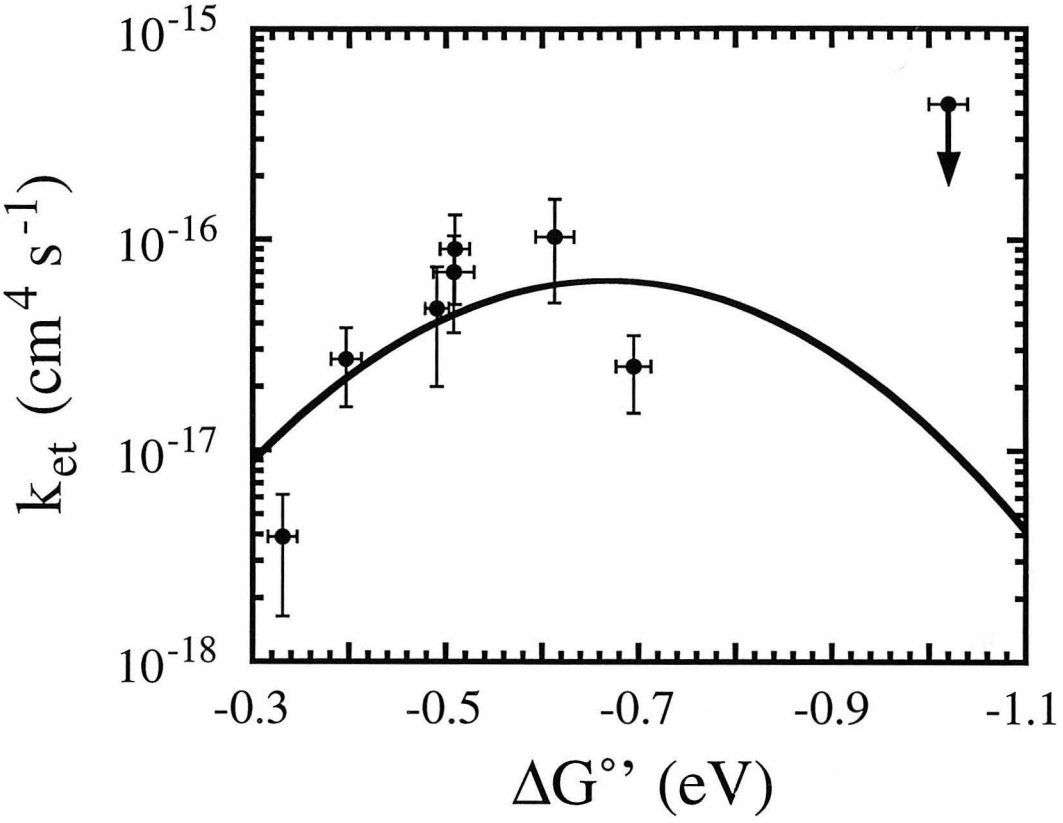
Additional information on the free-energy dependence of k_{et} can be obtained by including an upper limit on k_{et} that has been established for a system with an even larger interfacial charge-transfer driving force, the n-Si/CH_3OH-$Me_2Fc^{+/0}$ contact. In this system, minority-carrier injection dominates majority-carrier transfer,[2] so only an upper limit on k_{et} can be established.[1] This upper limit on k_{et} is, however, 4×10^{-16} cm^4 s^{-1}, and the driving force of this process is 1.03 to 1.01 eV, as determined by C^{-2}-E plots[1] and transconductance measurements.[65] Placing this data point onto an expanded graph, Figure 9, clearly constrains even further the maximum value of k_{et} for the n-Si/CH_3OH system at optimal exoergicity for an outer-sphere redox reagent.

For the n-Si/CH_3OH-bipyridinium$^{2+/+}$ contacts, the λ of 0.7 eV from the parabolic fit to the data of Figure 8a is somewhat larger than the solution reorganization energy for the bipyridinium redox reagents. The self-exchange rate constant, k_{se}, of methyl viologen dication with its cation radical has been measured via electron spin resonance methods to be 2.0×10^8 M^{-1} s^{-1} in methanol.[66,67] The ionic-strength dependence of the self-exchange rate may be included to obtain a corrected rate constant, k_{corr}, using[68]

$$\ln k_{corr} = \ln k_{se} + \frac{2Z_1Z_2\alpha\sqrt{\mu}}{1+\kappa r_r} \qquad (17)$$

where Z_1 and Z_2 are the charges on reactants 1 and 2, α is a constant with the value 1.17, μ is the ionic strength, κ equals $0.5099(\mu)^{0.5}$ $Å^{-1}$ for CH_3OH at 25°C, and r_r is the

Figure 9. Experimental results of k_{et} for the n-Si/CH_3OH-bipyridinium$^{2+/+}$ systems, in conjunction with the upper limit on k_{et} for the n-Si/CH_3OH-dimethylferrocene$^{+/0}$ interface (indicated by the arrow). The driving force for the k_{et} upper limit data was derived from the average barrier height for this system measured using C^{-2}-*E* (ϕ_b = 1.03 V[1]) and transconductance (ϕ_b = 1.01 V[65]) techniques.


10^{-15}
10^{-16}
10^{-17}
10^{-18}
k_{et} (cm^4 s^{-1})
-0.3
-0.5
-0.7
-0.9
-1.1
ΔG°' (eV)

reactant radius, which is assumed to be identical for reactants 1 and 2. The value of λ may then be calculated from k_{corr} as follows:[69]

$$\lambda = -4kT \ln\left(\frac{k_{corr}}{Z_{bi}}\right) \qquad (18)$$

where Z_{bi} is the normal collisional vibration frequency for bimolecular reactions at room temperature. Substitution of $k_{se} = 2.0 \times 10^8$ M^{-1} s^{-1}, $\mu = 1.0$ M, and $r_r = 5$ Å into eq 17 and $Z_{bi} = 1 \times 10^{11}$ M^{-1} s^{-1} into eq 18 yields $\lambda = 0.50$ eV. Since most of the inner-sphere reorganization involves electrons delocalized over the bipyridine rings, it was assumed that the different functionalities did not significantly perturb this reorganization energy for the redox systems employed in this work. Moreover, the analogous geometry of the other six compounds to that of methyl viologen implies that these other compounds should have comparable outer-sphere reorganization energies. Therefore, λ for all seven compounds was estimated as ≈ 0.5 eV. This assumption of constant λ for the redox reagents studied in this work is implicit in the use of a single Marcus curve to compare the seven k_{et} vs $\Delta G^{\circ\prime}$ data points reported herein.

The 0.7 eV reorganization energy derived from the fit to the k_{et} vs $\Delta G^{\circ\prime}$ plot may originate from a larger reorganization energy for an acceptor in the vicinity of a semiconductor electrode than in the bulk solution, as has been postulated previously.[70,71] However, the role of both the static and high-frequency dielectric constants must be explored before this explanation can be considered rigorously.[72] In addition, the electrons in the solid may have appreciable reorganization energy due to solvation near the semiconductor/liquid interface. The results reported herein on n-Si/CH_3OH junctions cannot distinguish between these possibilities, and analogous studies on other interfaces are required to assess the generality of this observation for outer-sphere redox couples and semiconducting electrodes.

It would also be interesting to extend these kinetic measurements into the higher driving force regime in an attempt to observe the Marcus inverted region experimentally at

the Si/liquid interface. Efforts to extend the 0.4 eV free energy range towards more negative $\Delta G^{\circ\prime}$ values using n-Si/CH_3OH contacts have so far been unsuccessful. Within the family of substituted bipyridinium compounds, there appears to be no reagent that has a reduction potential 0.1-0.2 V positive of the $E^{\circ\prime}(A/A^-)$ for $\mathbf{VII}^{2+/+}$ and that is also highly soluble in CH_3OH.[27] More importantly, as $E(A/A^-)$ approaches the energy of the valence band edge of Si, minority-carrier processes such as bulk recombination become rate-limiting and preclude mesurement of the desired majority-carrier transfer step.[17] It is possible, however, that the use of a wider-band-gap semiconductor would eliminate this problem, and such measurements are being pursued at present in our laboratory.

V. SUMMARY

In this work, n-Si/CH_3OH-bipyridinium$^{2+/+}$ contacts displayed nearly ideal energetic and kinetic behavior and allowed experimental determination of the rate constant for charge transfer between a stable, small-band-gap semiconductor electrode and a series of homologous, one-electron, outer-sphere redox couples. Differential capacitance measurements indicated that the conduction band edge of Si was fixed, to within 40 mV, as the electrochemical potential of the solution was changed by over 400 mV, indicating a lack of Fermi level pinning for this Si/liquid system. Charge-transfer rate constants for electrons reducing bipyridinium acceptors were determined to be between 10^{-18} cm^4 s^{-1} and 10^{-16} cm^4 s^{-1}, and the dependence of k_{et} on driving force was described satisfactorily by a Marcus-type expression with a $k_{et,max}$ of 6 x 10^{-17} cm^4 s^{-1} and a reorganization energy of 0.7 eV. The value for $k_{et,max}$ is in accord with theoretical predictions for charge-transfer rate constants at semiconductor/liquid contacts, and this value provides insight into the factors that control back reactions and other processes involved in charge separation at illuminated semiconductor/liquid interfaces.

VI. ACKNOWLEDGMENTS

I thank M. C. Lonergan for obtaining the ^{1}H NMR spectra of compounds **I**, **II**, **III**, **VI**, and **VII**. This research was supported by the National Science Foundation, Grant CHE-9634152. I would also like to acknowledge a generous gift from the Eastman Kodak Company in support of photoelectrochemistry research at Caltech.

VII. REFERENCES AND NOTES

(1) Pomykal, K. E.; Fajardo, A. M.; Lewis, N. S. *J. Phys. Chem.* **1996**, *100*, 3652.

(2) Rosenbluth, M. L.; Lewis, N. S. *J. Am. Chem. Soc.* **1986**, *108*, 4689.

(3) Casagrande, L. G.; Lewis, N. S. *J. Am. Chem. Soc.* **1985**, *107*, 5793.

(4) Morrison, S. R. *Surf. Sci.* **1969**, *15*, 363.

(5) Horrocks, B. R.; Mirkin, M. V.; Bard, A. J. *J. Phys. Chem.* **1994**, *98*, 9106.

(6) Uhlendorf, I.; Reineke-Koch, R.; Memming, R. *J. Phys. Chem.* **1996**, *100*, 4930.

(7) Fajardo, A. M.; Lewis, N. S. *Science* **1996**, *274*, 969.

(8) Pomykal, K. E.; Lewis, N. S. *J. Phys. Chem. B* **1997**, *101*, 2476.

(9) Howard, J. N.; Koval, C. A. *Anal. Chem.* **1994**, *66*, 4525.

(10) Bard, A. J.; Bocarsly, A. B.; Fan, F.-R. F.; Walton, E. G.; Wrighton, M. S. *J. Am. Chem. Soc.* **1980**, *102*, 3671.

(11) Wrighton, M. S. *Acc. Chem. Res.* **1979**, *12*, 303.

(12) Bard, A. J.; Wrighton, M. S. *J. Electrochem. Soc.* **1977**, *124*, 1706.

(13) Gronet, C. M.; Lewis, N. S.; Cogan, G.; Gibbons, J. *Proc. Natl. Acad. Sci. USA* **1983**, *80*, 1152.

(14) Shreve, G. A.; Karp, C. D.; Pomykal, K. E.; Lewis, N. S. *J. Phys. Chem.* **1995**, *99*, 5575.

(15) Morrison, S. R. *Electrochemistry at Semiconductor and Oxidized Metal Electrodes*; Plenum: New York, 1980.

(16) Gerischer, H. *J. Phys. Chem.* **1991**, *95*, 1356.

(17) Lewis, N. S. *Annu. Rev. Phys. Chem.* **1991**, *42*, 543.

(18) Sze, S. M. *Physics of Semiconductor Devices;* 2nd ed.; Wiley: New York, 1981.

(19) Chazalviel, J.-N. *Electrochim. Acta* **1988**, *33*, 461.

(20) Fonash, S. J. *Solar Cell Device Physics*; Academic: New York, 1981.

(21) Fahrenbruch, A. L.; Bube, R. H. *Fundamentals of Solar Cells: Photovoltaic Solar Energy Conversion*; Academic: New York, 1983.

(22) Kittel, C. *Introduction to Solid State Physics;* 6^{th} ed.; Wiley: New York, 1986.

(23) Thurber, W. R.; Mattis, R. L.; Liu, Y. M.; Filliben, J. J. *J. Electrochem. Soc.* **1980**, *127*, 1807.

(24) Chidsey, C. E. D. *Science* **1991**, *251*, 919.

(25) Smalley, J. F.; Feldberg, S. W.; Chidsey, C. E. D.; Linford, M. R.; Newton, M. D.; Liu, Y. P. *J. Phys. Chem.* **1995**, *99*, 13141.

(26) Atomic force microscopy of the HF-etched n-Si showed that, over an area of 500 nm x 500 nm, the surface was flat to within 1 nm. The area calculated from the three-dimensional topography of the surface was thus equal to the area determined from the two-dimensional projection to within $< 0.1\%$ accuracy.

(27) Bird, C. L.; Kuhn, A. T. *Chem. Soc. Rev.* **1981**, *10*, 49.

(28) Homer, R. F.; Tomlinson, T. E. *J. Chem. Soc.* **1960**, 2498.

(29) Hünig, S.; Schenk, W. *Liebigs Ann. Chem.* **1979**, 727.

(30) Bard, A. J.; Faulkner, L. R. *Electrochemical Methods: Fundamentals and Applications*; Wiley: New York, 1980.

(31) Royea, W. J.; Krüger, O.; Lewis, N. S. *J. Electroanal. Chem.* **1997**, *438*, 191.

(32) Bocarsly, A. B.; Bookbinder, D. C.; Dominey, R. N.; Lewis, N. S.; Wrighton, M. S. *J. Am. Chem. Soc.* **1980**, *102*, 3683.

(33) Laser, D.; Bard, A. J. *J. Phys. Chem.* **1976**, *80*, 459.

(34) Lieber, C. M.; Gronet, C. M.; Lewis, N. S. *Nature* **1984**, *307*, 533.

(35) Tomkiewicz, M. *Electrochim. Acta* **1990**, *35*, 1631.

(36) Nagasubramanian, G.; Wheeler, B. L.; Fan, F.-R. F.; Bard, A. J. *J. Electrochem. Soc.* **1982**, *129*, 1742.

(37) Nagasubramanian, G.; Wheeler, B. L.; Bard, A. J. *J. Electrochem. Soc.* **1983**, *130*, 1680.

(38) Nagasubramanian, G.; Wheeler, B. L.; Hope, G. A.; Bard, A. J. *J. Electrochem. Soc.* **1983**, *130*, 385.

(39) Kobayashi, H.; Takeda, N.; Sugahara, H.; Tsubomura, H. *J. Phys. Chem.* **1991**, *95*, 813.

(40) Rosenwaks, Y.; Thacker, B. R.; Bertness, K.; Nozik, A. J. *J. Phys. Chem.* **1995**, *99*, 7871.

(41) Heller, A. In *Photoeffects at Semiconductor-Electrolyte Interfaces*; Nozik, A. J., Ed.; ACS Symposium Series 146; American Chemical Society: Washington, DC, 1981; pp 57-77.

(42) Marcus, R. A. *J. Phys. Chem.* **1990**, *94*, 4152.

(43) Ibach, H.; Luth, H. *Solid-State Physics*; Springer Verlag: Berlin, 1990.

(44) Miller, J. R.; Beitz, J. V.; Huddleston, R. K. *J. Am. Chem. Soc.* **1984**, *106*, 5057.

(45) Domingue, R. P.; Fayer, M. D. *J. Chem. Phys.* **1985**, *83*, 2242.

(46) Oevering, H.; Paddon-Row, M. N.; Heppener, M.; Oliver, A. M.; Cotsaris, E.; Verhoeven, J. W.; Hush, N. S. *J. Am. Chem. Soc.* **1987**, *109*, 3258.

(47) Penfield, K. W.; Miller, J. R.; Paddon-Row, M. N.; Cotsaris, E.; Oliver, A. M.; Hush, N. S. *J. Am. Chem. Soc.* **1987**, *109*, 5061.

(48) Closs, G. L.; Miller, J. R. *Science* **1988**, *240*, 440.

(49) Elias, H.; Chou, M. H.; Winkler, J. R. *J. Am. Chem. Soc.* **1988**, *110*, 429.

(50) Isied, S. S.; Vassilian, A.; Wishart, J. F.; Creutz, C.; Schwarz, H. A.; Sutin, N. *J. Am. Chem. Soc.* **1988**, *110*, 635.

(51) Schanze, K. S.; Sauer, K. *J. Am. Chem. Soc.* **1988**, *110*, 1180.

(52) Bowler, B. E.; Raphael, A. L.; Gray, H. B. *Prog. Inorg. Chem.* **1990**, *38*, 259.

(53) Finklea, H. O.; Hanshew, D. D. *J. Am. Chem. Soc.* **1992**, *114*, 3173.

(54) Smith, B. B.; Halley, J. W.; Nozik, A. J. *Chem. Phys.* **1996**, *205*, 245.

(55) Smith, B. B.; Nozik, A. J. *Chem. Phys.* **1996**, *205*, 47.

(56) Levich, V. G. In *Adv. Electrochem. Electrochem. Eng.*; P. Delahay, Ed.; Wiley Interscience: New York, 1966; Vol. 4; pp 249-371.

(57) Marcus, R. A. *Annu. Rev. Phys. Chem.* **1964**, *15*, 155.

(58) Royea, W. J.; Fajardo, A. M.; Lewis, N. S. *J. Phys. Chem. B* **1997**, *101*, 11152.

(59) Terrettaz, S.; Becka, A. M.; Traub, M. J.; Fettinger, J. C.; Miller, C. J. *J. Phys. Chem.* **1995**, *99*, 11216.

(60) In these experiments, the valence band edge potential was observed to be +0.86 V vs SCE, while the formal potential of $Ru(NH_3)_6^{3+/2+}$ was -0.23 V vs SCE. The driving force for hole transfer is therefore $qE^{\circ\prime}(A/A^-) - \mathbf{E}_{vb} = -1.09$ eV. The self-exchange rate constant, corrected for the ionic-strength dependence, has been reported as $k_{corr} = 5 \times 10^4$ M^{-1} s^{-1} (Weaver, M. J.; Yee, E. L. *Inorg. Chem.* **1980**, *19*, 1936). Substitution of this value for k_{corr} with $Z_{bi} = 1 \times 10^{11}$ M^{-1} s^{-1} into eq 18 yields $\lambda = 1.5$ eV.

(61) Rosenwaks, Y.; Thacker, B. R.; Nozik, A. J.; Ellingson, R. J.; Burr, K. C.; Tang, C. L. *J. Phys. Chem.* **1994**, *98*, 2739.

(62) Nozik, A. J. Presented at the 211th National Meeting of the American Chemical Society, New Orleans, LA, March 1996; paper PHYS 11.

(63) Rosenwaks, Y.; Thacker, B. R.; Ahrenkiel, R. K.; Nozik, A. J. *J. Phys. Chem.* **1992**, *96*, 10096.

(64) Bansal, A.; Tan, M. X.; Tufts, B. J.; Lewis, N. S. *J. Phys. Chem.* **1993**, *97*, 7309.

(65) Laibinis, P. E.; Stanton, C. E.; Lewis, N. S. *J. Phys. Chem.* **1994**, *98*, 8765.

(66) Dai, S. Ph.D. Thesis, University of Tennessee, Knoxville, 1990.

(67) Williams, F. "Electron Spin Resonance Spectroscopic Studies of Radical Cation Reactions"; Report 91015008, U. S. Dept. of Energy, 1991.

(68) Wherland, S.; Gray, H. B. *Proc. Natl. Acad. Sci. USA* **1976**, *73*, 2950.

(69) Marcus, R. A. *J. Phys. Chem.* **1963**, *67*, 853.

(70) Smith, B. B.; Koval, C. A. *J. Electroanal. Chem.* **1990**, *277*, 43.

(71) Marcus, R. A. *J. Phys. Chem.* **1990**, *94*, 1050.

(72) Tan, M. X.; Lewis, N. S. *Inorg. Chim. Acta* **1996**, *242*, 311.

Chapter Four

Bohr Radius Effects on the Majority-Carrier Charge-Transfer Rate Constants at InP/CH_3OH Interfaces

ABSTRACT

The p-InP/CH_3OH interface was characterized by differential capacitance-potential and current density-potential techniques in an endeavor to measure the rate constants for hole transfer across this junction. Previously developed theoretical models speculate that the extent of charge delocalization, possibly exemplified by the Bohr radius of a charge carrier in a solid, influences the magnitude of the charge-transfer rate constant. Prior work in this laboratory has successfully measured the electron-transfer rate constants at various n-InP/CH_3OH contacts, and a determination of the hole-transfer rate constants at the p-InP/CH_3OH contact would provide an experimental test of this hypothesis. Differential capacitance measurements provided linear, well-behaved Mott-Schottky plots. The energetics of the p-InP/CH_3OH junction with four different outer-sphere redox couples were quantified, but they responded nonideally to variations in the Nernstian solution potential. Current density-potential measurements indicated diode-like, exponential behavior and a first-order dependence of the interfacial charge flux on the surface hole concentration. However, the current density did not respond to variations in the donor concentration as expected for a system dominated by hole transfer from the valence band of the semiconductor to the redox donor in solution. Surface electrical traps likely prevent a straightforward analysis of the kinetics across this interface.

I. INTRODUCTION

Chapter 3 outlines the work in this laboratory on the determination of the electron-transfer rate constant, k_{et}, at various n-Si/CH_3OH-bipyridinium$^{2+/+}$ junctions. The excellent agreement between the observed electrochemical data and the predicted "ideal" behavior appears to establish differential capacitance and steady-state current density-potential measurements as a reliable route to obtain the heretofore elusive experimental measure of k_{et} at a semiconductor in contact with a nonadsorbing, outer-sphere redox couple.[1] In this regard the results summarized in Chapter 3 are significant, as they represent the opportunity to compare the experimental interfacial charge-transfer rate constants with those postulated by theory.

However, what distinguishes the present n-Si/CH_3OH-bipyridinium$^{2+/+}$ results from previous investigations of kinetics at the semiconductor/liquid junction is the experimental dependence of k_{et} on the free-energy change of the electron-transfer reaction, $\Delta G^{\circ\prime}$.[1] Although earlier research on the n-ZnO/H_2O interface endeavored to relate k_{et} to $\Delta G^{\circ\prime}$, this work not only employed a nonhomologous set of inner-sphere redox couples having widely varying reorganization energies but also yielded inconclusive results.[2,3] Since the bipyridinium$^{2+/+}$ redox couples described in Chapter 3 possess a common skeleton and therefore similar reorganization energies, the experiments can isolate $\Delta G^{\circ\prime}$ as the sole variable and quantify its effect on the observed rate constant.[1] The quality of these k_{et} results implies that we can now explore how other factors affect the rate constant.

In particular, material characteristics of the semiconductor solid may also influence the magnitude of the charge-transfer rate constant. One model for charge transfer across the semiconductor/liquid interface specifies that the effective radius of the charge carrier in the solid participates in determining the electronic coupling.[4,5] While this model does not precisely locate "effective radius" within the context of an observable parameter, the experiments on n-Si/CH_3OH junctions demonstrate that this quantity corresponds

adequately with the Bohr radius.[1] The Bohr radius accounts for the electrostatic interaction between an ionized dopant atom and the associated free charge carrier.[6] Due to the small ionization energy of the nonbonding charge on the dopant atom, as well as screening by the low-dielectric medium, the free charge is weakly bound to the fixed, ionized dopant. The resulting charge delocalization over the neighboring lattice atoms may be treated by assuming the free charge orbits the ionized dopant according to the Bohr model of atomic structure. The extent of delocalization is illustrated by the example of an electron in the conduction band of Si, as its Bohr radius of 21 Å indicates that the negative charge is "spread out" over 10^3 lattice atoms in the vicinity of the ionized dopant.[6]

Unfortunately, the role of the Bohr radius in interfacial charge transfer remains unknown, presumably because of the traditional difficulty of measuring rate constants at the semiconductor/liquid interface.[4,7] An understanding of the empirical relationship between the Bohr radius and the rate constant is required in order to evaluate more critically the prevailing theories of interfacial charge transfer. To this end, an approach may be outlined. The ideal experimental procedure would vary the Bohr radius while maintaining invariant all other parameters. Given the number of variables related to the nature of the solid (e.g., surface structure, carrier mobility, dielectric constant), the most efficient method of accomplishing this goal is to change only the type of doping while using the same semiconductor lattice. Since electrons and holes in most semiconductors differ in their Bohr radii, they should cross the interface with different rate constants, all other variables being equal. In both cases, the experiments would observe the rate constants for majority-carrier charge transfer: electron transfer in the case of n-type doping, and hole transfer in the case of p-type.

This chapter reports the attempts made in this laboratory to measure the hole-transfer rate constants at the p-InP/CH_3OH junction. Because a prior study in this research group has successfully measured the electron-transfer rate constants at the n-InP/CH_3OH

junction,[8] these values may be readily compared with the values from the present work to determine if rate constant differences correlate as predicted with Bohr radius variations. As with the work described in Chapters 2 and 3, differental capacitance vs potential and current density vs potential techniques were used, the former for measuring the energetics of the interface and the latter for measuring the kinetics.

II. THEORY

For the theory of interfacial charge transfer, we return to the electronic-coupling treatment discussed in Chapters 2 and 3, except that the expression for k_{et} is generalized to a charge-transfer rate constant, k_{ct}:[4]

$$k_{ct} = \nu_n \kappa_{el} \kappa_n \tag{1}$$

where ν_n is the attempt frequency of the microscopic reaction, κ_{el} is the electronic term, and κ_n is the nuclear term. Because the identities of the donor and acceptor depend on the type of doping of the semiconductor, the definition of κ_{el} likewise varies. For electron transfer from an n-type semiconducting electrode,

$$k_{et} = \nu_n \kappa_{el,n} \kappa_n \tag{2}$$

where

$$\kappa_{el,n} = \pi \left[\frac{2\left(r_e + r_A\right)}{\beta^3} + \frac{6}{\beta^4} \right] \tag{3}$$

In eq 3, r_e is the effectve radius of the delocalized electron in the semiconductor, r_A is the radius of the solution-based electron acceptor (i.e., the oxidized form of the redox couple in solution), and β is the attenuation factor for the electronic coupling between the donor and acceptor. For hole transfer from a p-type semiconducting electrode, the hole-transfer rate constant, k_{ht}, is given by

$$k_{ht} = \nu_n \kappa_{el,p} \kappa_n \tag{4}$$

where

$$\kappa_{el,p} = \pi\left[\frac{2\left(r_h + r_{A^-}\right)}{\beta^3} + \frac{6}{\beta^4}\right] \tag{5}$$

In eq 5, r_h is the effective radius of the delocalized hole in the semiconductor, and r_{A^-} is the radius of the reduced form of the redox couple in solution. The nuclear term in eqs 1, 2 and 4 is invariant of the doping type and is defined as

$$\kappa_n = \exp\left\{\frac{-(\lambda + \Delta G^{\circ\prime})^2}{4\lambda kT}\right\} \tag{6}$$

where λ is the total reorganization energy for the electron-transfer process, $\Delta G^{\circ\prime}$ is the standard driving force for interfacial charge transfer, k is the Boltzmann constant and T is temperature.

The effective radius of a charge carrier in the semiconductor may be estimated by recognizing an appropriate maximum rate constant, such that $\kappa_n = 1$, and substituting reasonable values for the remaining terms. Chapter 3 describes work in this laboratory that suggests that the maximum electron-transfer rate constant, $k_{et,max}$, is 6×10^{-17} cm^4 s^{-1} at n-Si/CH_3OH contacts, and this chapter also cites several other theoretical and experimental examples indicating that $k_{et,max} = 10^{-17}$ cm^4 s^{-1}.[1] Using $k_{et} = 10^{-17}$ cm^4 s^{-1}, and substituting $\nu_n = 10^{13}$ s^{-1}, $r_A = 3 \times 10^{-8}$ cm, $\beta = 1$ $Å^{-1} = 1 \times 10^8$ cm^{-1}, and $\kappa_n = 1$ into eqs 2 and 3 yields $r_e = 1 \times 10^{-7}$ cm = 10 Å. This value for r_e implies slight delocalization of the reactant electron in the semiconductor, relative to a charge fixed on one atom within the crystal lattice.

The value of r_e = 10 Å moreover agrees in its order of magnitude with the Bohr radius of an electron in Si, 21 Å.[6] An electron and a hole in a semiconductor each have a Bohr radius, r_B, whose functional form is identical to that of Bohr's seminal description of the hydrogen atom:[6]

$$r_B = \varepsilon\varepsilon_o \frac{h^2}{\pi m^* q^2} \tag{7}$$

where ε is the dielectric constant of the semiconductor, ε_o is the permittivity of free space, h is Planck's constant, m* is the effective mass of the relevant charge carrier in the semiconductor, and q is the electronic charge. Note that the Bohr radius is independent of the doping level, and indeed even the doping type; effective masses of charge carriers and dielectric constants are properties originating strictly from the underlying semiconductor lattice. Values of effective mass, obtained either from theoretical calculations of the band structure or by direct experiment with cyclotron resonance, have been tabulated for most known semiconductors.[9] In principle, then, the Bohr radius of a charge carrier in a given semiconductor is determinable from known data. Provided that this parameter is analogous to the effective radius employed in eqs 3 and 5, the interfacial charge-transfer rate constant should increase with larger Bohr radius.

Indium phosphide represents an intriguing possibility for testing this theory, as it is a common semiconductor in which the effective masses of electrons and holes differ significantly.[9] Although almost all semiconductors possess nonequivalent electron and hole effective masses, and by extension dissimilar Bohr radii, this disparity generally falls within one order of magnitude.[9] Other materials in which electrons and holes have widely varying effective masses, such as InSb, are irrelevant to most electrochemical applications and consequently rarely studied in this context. InP combines the advantages of familiarity and favorable material qualities. Extensive research has been devoted to the electrochemical and photoelectrochemical properties of InP,[8,10-16] and the effective masses of electrons and holes in this material are sufficiently different that the predicted variation in the rate constant should be observable. The effective mass of electrons, m_e^*, is $0.077m_e$ (where m_e is the mass of an electron in vacuum),whereas the effective mass of holes, m_h^*, is $0.64m_e$.[9] Using eq 7 with the dielectric constant of InP, $\varepsilon = 12.4$, affords the Bohr radius of an electron, $r_{B,e} = 85$ Å, and the Bohr radius of a hole, $r_{B,h} = 10$ Å, in this semiconductor. Substituting this value of $r_{B,e}$ into eq 3 and assuming that the radius of the redox molecule

in solution is 3 Å yield $\kappa_{el,n} = 6 \times 10^{-30}$ cm^4. With this electronic coupling value and the estimates of $\nu_n = 10^{13}$ s^{-1} and $\kappa_n = 1$, eq 2 indicates $k_{et,max} = 6 \times 10^{-17}$ cm^4 s^{-1} for n-InP in contact with an electrolyte solution. As for hole transfer across the p-InP/liquid interface, similar calculations using the value of $r_{B,h}$ derived above and eqs 4 and 5 predict a maximum hole-transfer rate constant, $k_{ht,max}$, of 1×10^{-17} cm^4 s^{-1}.

This theoretical value for $k_{et,max}$ is corroborated by recent experimental work in this laboratory. The electrical behavior of n-InP/CH_3OH junctions, which is consistent with a second-order electron-transfer mechanism, indicated that k_{et} ranges from 10^{-17} to 10^{-16} cm^4 s^{-1}.[8] The techniques used in this work are applicable to the study of p-InP/CH_3OH junctions, and a brief outline of the measurement process follows. The interfacial barrier height, ϕ_b, may be ascertained by using differential capacitance-potential (C^{-2}-E) methods. Accurate knowledge of this parameter is required for rate constant determinations, as it relates intimately to the hole concentration at the surface of the semiconductor, p_s:[9]

$$p_s = N_v \exp\{q(\phi_b + E)/kT\} \tag{8}$$

In eq 8, N_v is the effective density of states in the valence band and E is the applied potential. Once the values of ϕ_b and p_s are established, the kinetic flux across the interface, measurable with standard current density-potential (J-E) techniques, can be used to assess the value of k_{ht} according to the second-order rate expression

$$J(E) = q\, k_{ht}\, p_s\, [A^-] \tag{9}$$

The concentration of redox donors at the interface, $[A^-]$, deviates little from its value in bulk solution,[17] and hence it is trivially quantified. Of course, successful determination of J, p_s, and $[A^-]$ does not suffice for a rate constant measurement: the second-order nature of the recombination kinetics must be demonstrated. Current density must increase proportionally with either the surface hole concentration or the redox donor concentration. These trends are confirmed by noting the bias dependence and the concentration dependence, respectively, of the current density. Despite the number of obstacles that may preclude

reliable rate constant determinations, one previous outcome is encouraging. Given the success of these types of measurements on the n-InP/CH_3OH interface,[8] it is reasonable to expect that hole-transfer rate constants at the p-InP/CH_3OH interface are also measurable.

III. EXPERIMENTAL

A. Electrodes and Solutions

The p-type InP material (zinc-doped, <100> orientation) was obtained from CrystaComm, Inc. (Mountain View, CA). The wafer had a thickness of 445 μm and a nominal dopant density of 1.1×10^{17} cm^{-3}. An ohmic contact was formed by evaporation of three metal layers, followed by annealing. The sequential depositions of 50 Å of Au, 950 Å of Zn, and 700 Å of Au were performed at pressures not exceeding 9×10^{-6} torr at any time. The resulting sandwich structure was annealed in a N_2(g)-purged quartz tube for 5 min at 500°C. The ohmic-contacted semiconductor was then adhered to a 22 AWG Sn:Cu wire (Belden Wire and Cable) using conductive Ag print (GC Electronics). Finally, the p-InP wafer and Sn:Cu wire were sealed in a glass tube through use of white epoxy (Dexter Corp.) to afford the electrodes. Photographs of the exposed InP areas were digitized and scaled with a known linear measurement from a microruler in order to determine the electrode areas, which were typically 0.1 cm^2.

Prior to each electrochemical measurement, p-InP electrodes were etched using a combination of 0.05% (v/v) Br_2 and 4.0 M NH_3 solutions. The former was prepared by dissolving 10 μL Br_2 (Aldrich) in 20 mL CH_3OH (EM Science), whereas the latter was prepared by bubbling NH_3(g) through 20 mL CH_3OH until the mass increase of the solution indicated sufficient uptake of solute. Methanol for the etching solutions was used as received. The etching protocol called for a 10-s immersion in 0.05% Br_2, followed by a 20-s immersion in 4.0 M NH_3, then 10 s in 0.05% Br_2, and finally 20 s in 4.0 M NH_3. After the p-InP was removed from either etching solution, it was rinsed with dry CH_3OH

and dried in a stream of $N_2(g)$. The Pt wire reference electrode and the Pt gauze counter electrode (Aldrich; 52 mesh, 5 cm^2) were cleaned in a 3:1 (v/v) solution of HCl(aq) (37% w/w, EM Science) and HNO_3(aq) (70% w/w, EM Science). The electrodes were then rinsed with 18 MΩ cm resistivity H_2O and dried under flowing $N_2(g)$. All electrochemical measurements were performed in a Plexiglas box that was continuously purged with $N_2(g)$, and the ambient atmosphere had less than 10 ppm of O_2 as monitored by the lack of fuming of $(CH_3CH_2)_2Zn$.

Methanol for the cell solutions was distilled over Mg prior to use. Lithium perchlorate (J. T. Baker) was dried by fusing at 280°C under active vacuum. Lithium chloride (EM Science) was dried under active vacuum for at least 6 h at 240°C. Solvent, electrolytes, and redox compounds were stored in a $N_2(g)$-purged drybox until use. The electrolyte and redox compounds were moreover maintained under $N_2(g)$ while they were loaded into the cell vessel and dissolved into the solvent. All electrochemical cell solutions contained either 1.0 M $LiClO_4$ or 1.0 M LiCl. Both the neutral and the cationic forms of the ferrocene redox couples were weighed as solid reagents. The monocation radicals of the two viologen compounds and of the diamine compound were created *in situ* via bulk electrolysis with a Pt gauze counter electrode separated from the main cell solution by a Vycor™ frit. Formal reduction potentials were taken to be the cyclic voltammetric half-wave potentials that were measured at a Pt wire in a CH_3OH-1.0 M LiCl solution containing 20 mM of the relevant viologen dication or neutral diamine. Nernstian solution potentials were monitored before and after each set of electrical measurements through use of a CH_3OH-LiCl saturated calomel reference electrode (SCE). The potential of this electrode was -0.050 V vs a standard aqueous SCE.

B. Redox Compounds

Dimethylferrocene (Me_2Fc; Aldrich) was sublimed before use, and the dimethylferrocenium salt, Me_2FcBF_4, was prepared as described previously. N,N,N',N'-tetramethyl-*p*-phenylenediamine (TMPD; Eastman Kodak Co.), available from prior work in this laboratory,[18] was purified by recrystallization. Methyl viologen dichloride hydrate (MV; Aldrich) was dried under active vacuum for 6 h at 60°C before use. The other bipyridinium compound, 1,1'-bis(diethoxycarbonylmethyl)-4,4'-bipyridinium dichloride (DCEV), was synthesized according to a preparative route[19] using the general Menschutkin reaction, in which an amine is quaternized with an alkyl halide.[20] Full details of this synthesis are reported in Chapter 3.[1]

C. Electrical Measurements

Each p-InP electrode was etched in the $N_2(g)$ atmosphere immediately before its electrochemical characterization. To ensure electrode stability, the semiconductor working electrode was cycled between -0.500 and +0.100 V vs the Nernstian solution potential $E(A/A^-)$ for 30 min under ambient room illumination before use. Any electrode that exhibited unstable electrical behavior after this point was discarded. J-*E* properties were recorded before and after the differential capacitance measurements. Both the steady-state J-*E* behavior and the differential capacitance vs potential (C^{-2}-*E*) behavior were performed in the dark. $E(A/A^-)$ was measured before and after collection of the J-*E* and C^{-2}-*E* data to confirm chemical stability of the cell solution.

J-*E* data were obtained with an EG&G Princeton Applied Research Model 273 Potentiostat and a Houston Instruments Omnigraphic 2000 X-Y recorder. The scan rate was 50 mV s^{-1} in all experiments. As described previously,[1] the dark J-*E* curves were digitized and were corrected for concentration overpotential, η_{conc}, and cell resistance, R_{cell}, by measuring the mass-transport-limited currents at a one-sided Pt foil electrode. For a given redox solution, the limiting anodic current density, $J_{l,a}$, and the limiting cathodic

current density, $J_{l,c}$, at this Pt foil electrode were used with the current densities J at a p-InP electrode to correct the InP J-*E* data:[21]

$$\eta_{conc} = \left(\frac{RT}{nF}\right)\left\{\ln\left(\frac{J_{l,a}}{-J_{l,c}}\right) - \ln\left(\frac{J_{l,a} - J}{J - J_{l,c}}\right)\right\} \qquad (10)$$

where R is the gas constant, n is the number of electrons transferrred (1 for all redox couples studied in this work) and F is the Faraday constant. The cell resistance values were extracted from the high-frequency limits of the Bode plots of the p-InP/CH_3OH junctions and were typically 50 Ω. The final corrected potential, E_{corr}, was calculated from *E*, η_{conc}, R_{cell}, and the current *i* using the equation

$$E_{corr} = E - \eta_{conc} - iR_{cell} \qquad (11)$$

The reference point of the potentials was then changed to SCE by accounting for the difference between $E(A/A^-)$ and SCE.

As observed with n-InP, p-InP electrodes in contact with methanolic ferrocene and viologen solutions exhibited stable J-*E* characteristics over the typical measurement timescale of several hours.[8] For each electrode/redox couple combination, the anodic currents at a given forward bias varied by less than 20% over the course of 2 h, or the typical duration of one set of differential capacitance experiments. Cell stability was further verified by monitoring $E(A/A^-)$, which changed by no more than 5 mV from the beginning to the end of all electrical measurements performed using a given electrode.

The differential capacitance experiments were performed according to the instrumental protocol described in Chapter 3.[1] Because the electrical behavior of the p-InP/CH_3OH contacts was similar to that of the n-Si/bipyridinium$^{2+/+}$ system, extraction of the differential capacitance (C_{diff}) values from the impedance data was accomplished using similar assumptions. The C_{diff} vs *E* results were again analyzed with the Mott-Schottky equation:[3]

$$C_{diff}^{-2} = \frac{2}{q\varepsilon\varepsilon_o N_d A_s^2}\left(E - E_{fb} - \frac{kT}{q}\right) \qquad (12)$$

where N_a is the dopant density of the semiconductor, A_s is the area of the semiconductor electrode, and E_{fb} is the flat-band potential. For each measurement frequency, the linear regression of the C_{diff}^{-2} vs E ("Mott-Schottky" or "M-S") plot was extrapolated to its x-intercept and shifted by kT/q to yield the value of E_{fb}. The flat-band potential and the barrier height of the junction, ϕ_b, are related by the equation[9]

$$\phi_b = \frac{E_{vb}}{q} - E(A/A^-) = \frac{kT}{q}\ln\left(\frac{N_v}{N_a}\right) + E_{fb} - E(A/A^-) \qquad (13)$$

The values of $N_v = 1.3 \times 10^{19}$ cm^{-3} (ref. [22]) and $N_a = 1.1 \times 10^{17}$ cm^{-3} were used in the calculations of ϕ_b.

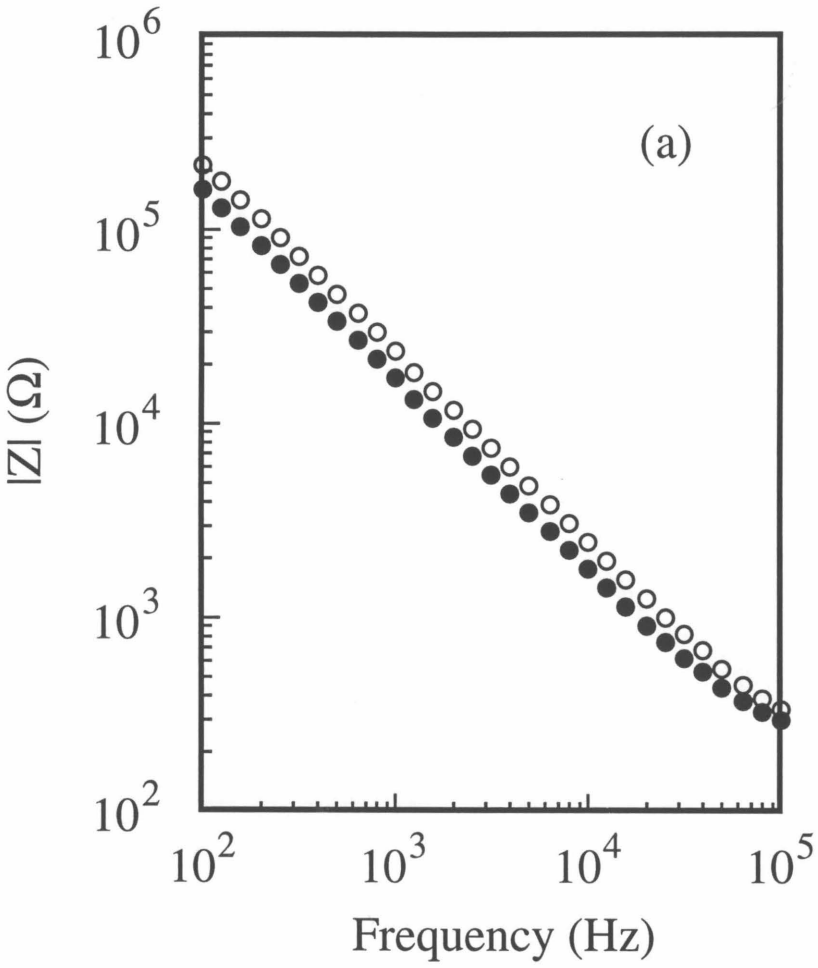
Careful attention to several experimental details afforded Mott-Schottky plots that obeyed theoretical expectations. The concentrations of donor and acceptor in the cell solution were always maintained at 10 mM or higher, in order to miminize frequency dispersion and nonlinearities in the C^{-2}-E data trends. Similarly, the measuring resistor of the impedance analyzer was maximized to provide the greatest precision for each impedance measurement and hence to improve reproducibility.

IV. RESULTS

A. C^{-2}-E Data for p-InP/CH_3OH Contacts

Figure 1 illustrates typical Bode plots for the p-InP/CH_3OH interface. Although the data shown in this figure pertain specifically to the $Me_2Fc^{+/0}$ and $DCEV^{2+/+}$ redox couples, similar behavior was exhibited by the cells containing $TMPD^{+/0}$ and $MV^{2+/+}$. Figure 1a shows representative impedance data recorded at the two reverse bias limits, -0.20 V and -0.80 V vs $E(A/A^-)$, for the experiments at the p-InP/CH_3OH-$Me_2Fc^{+/0}$ junction. At both potentials, the region of linear Bode character spanned from 100 Hz to 25.1 kHz, with a regression slope of -0.981 at -0.20 V vs $E(A/A^-)$ and a slope of -0.980 at -0.80 V vs $E(A/A^-)$. Both regression analyses yielded a correlation coefficient of 0.99998. Representative impedance data for the p-InP/CH_3OH-$DCEV^{2+/+}$ junction are shown in

Figure 1. Representative Bode plots for the p-InP/CH_3OH interface. (a) The cell solution consisted of 10 mM Me_2Fc, 10 mM Me_2Fc^+, and 1.00 M $LiClO_4$. The filled circles represent data taken at -0.20 V vs $E(A/A^-)$, whereas the open circles represent data taken at -0.80 V vs $E(A/A^-)$. (b) The cell solution consisted of 10 mM $DCEV^{2+}$, 10 mM $DCEV^+$, and 1.00 M LiCl. The filled circles indicate impedance data obtained at 0.00 V vs $E(A/A^-)$, whereas the open circles indicate impedance data obtained at -0.60 V vs $E(A/A^-)$.


(a)
|Z| (Ω)
10^6
10^5
10^4
10^3
10^2
10^2
10^3
10^4
10^5
Frequency (Hz)

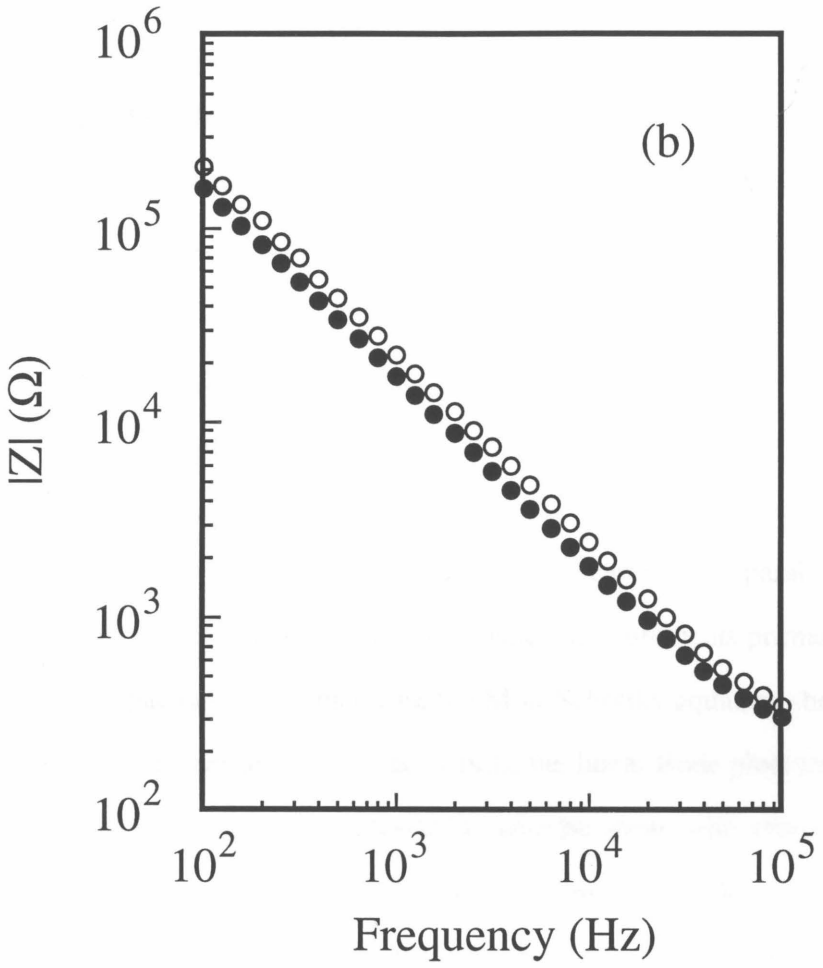
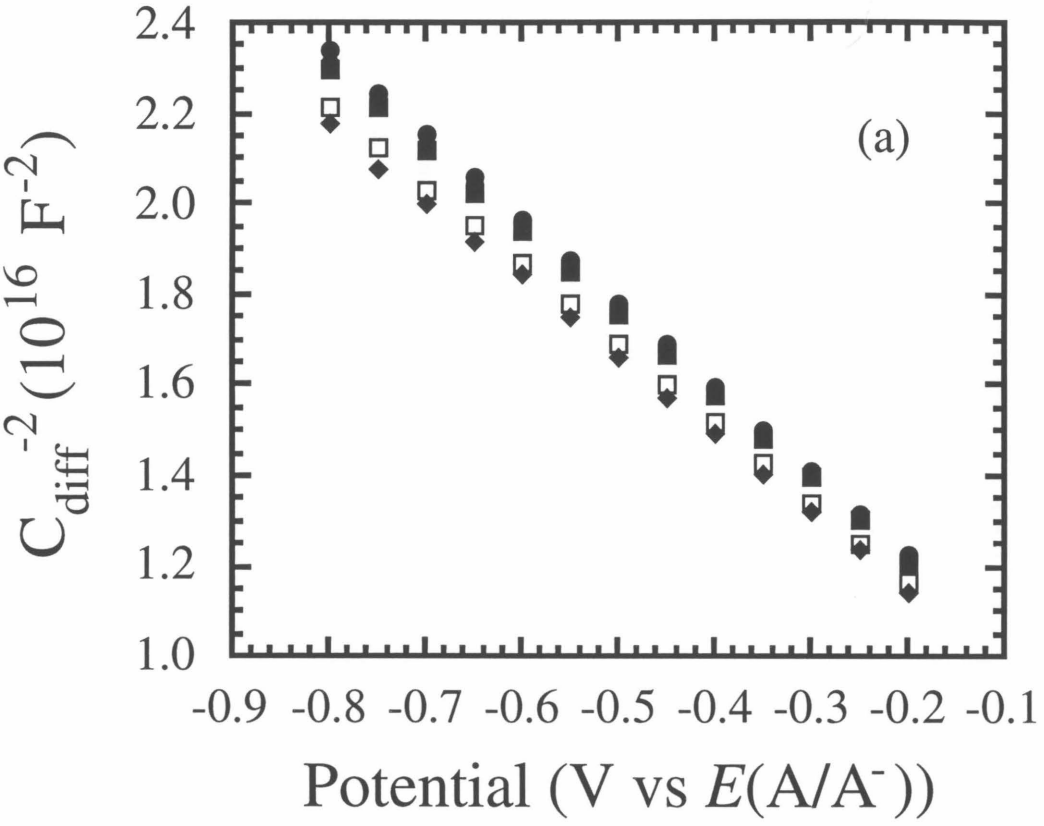

(b)
|Z| (Ω)
10^6
10^5
10^4
10^3
10^2
10^2
10^3
10^4
10^5
Frequency (Hz)

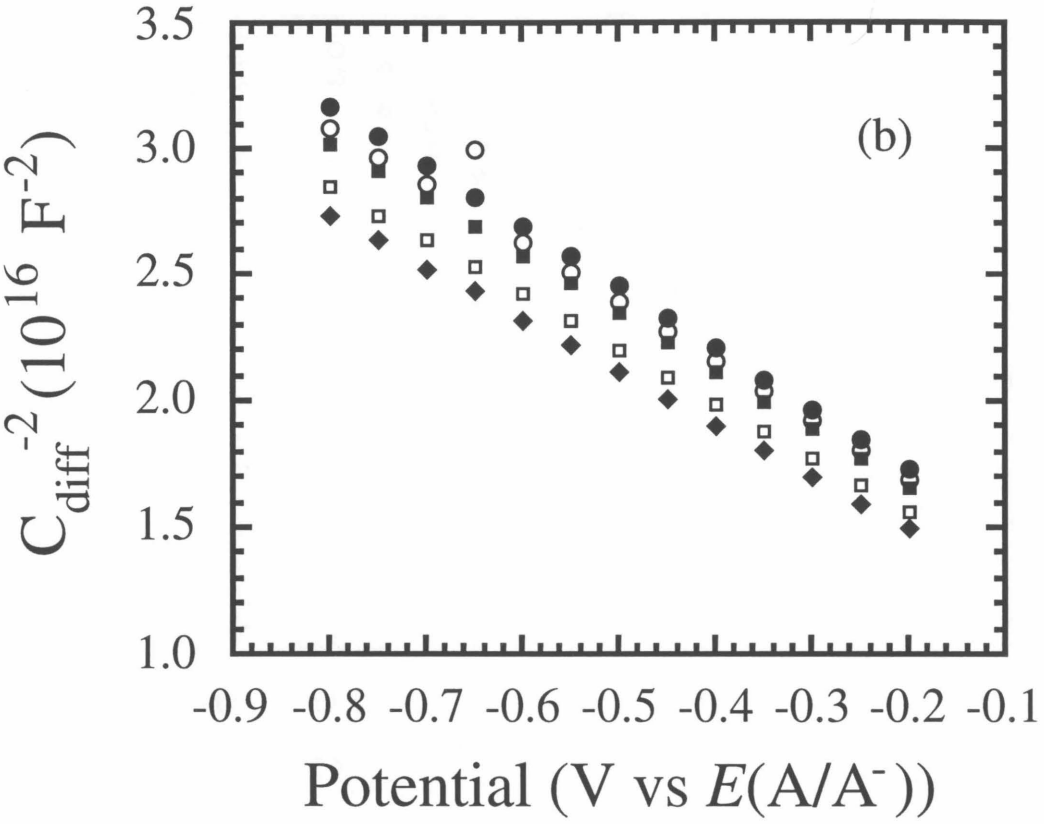
Figure 1b. Again, the frequency regime of Bode plot linearity ranged from 100 Hz to 25.1 kHz. At the lower limit of reverse bias, 0.00 V vs $E(A/A^-)$, linear regression indicated a slope of -0.966 and a correlation coefficient of 0.99998, whereas at the higher limit of reverse bias, the analysis produced a slope of -0.968 and a correlation coefficient of 0.99999. For all p-InP/CH_3OH contacts studied in this work, the Bode plots displayed excellent linearity over the frequency range of 100 Hz to 25.1 kHz, with correlation coefficients of at least 0.99990 in all cases. Under these frequency conditions, the regression slopes of all Bode plots were consistently between -0.96 and -0.99.

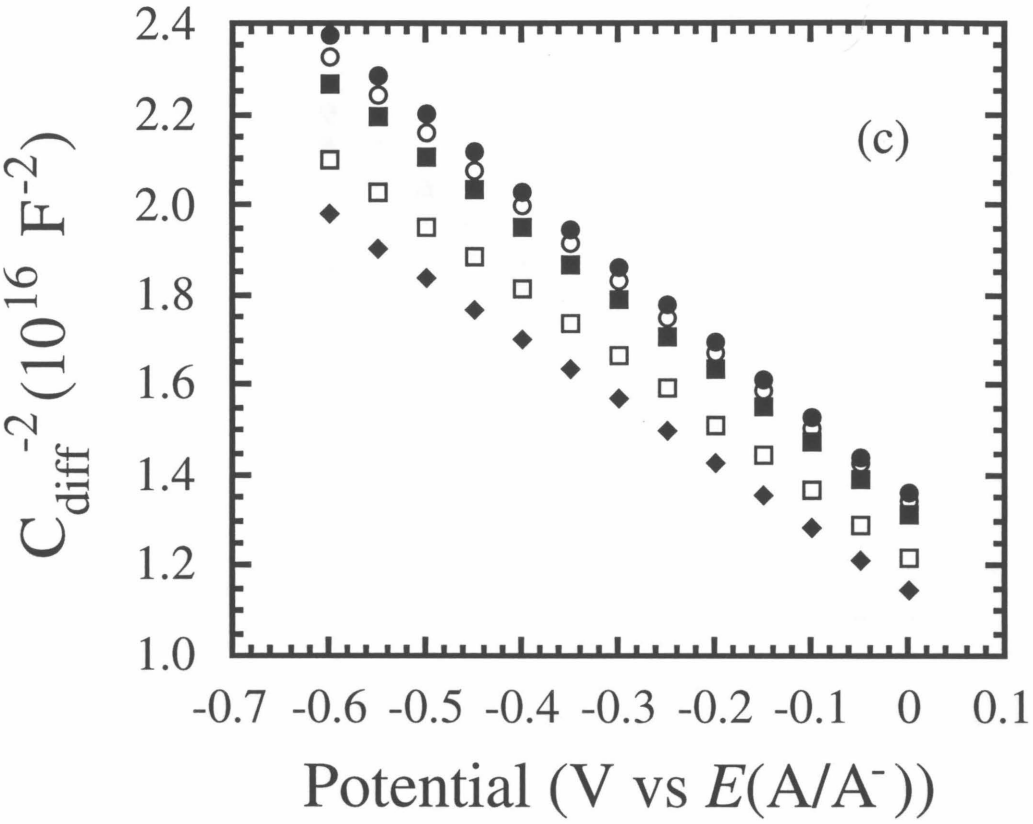
This Bode behavior indicates that, within a certain frequency range, the impedance properties of the p-InP/CH_3OH interface are principally governed by a single capacitance. The proportional trend of total impedance vs input frequency is diagnostic of capacitive character, since any decrease in frequency translates directly into an increase in the imaginary component of the impedance. Moreover, the slopes of nearly unity are consistent with an equivalent circuit model of a single capacitor in parallel with a resistor. Adherence to this model implies that the impedance measurements primarily probe the semiconductor capacitance, in which case the Mott-Schottky equation should adequately describe the junction energetics. In other words, the linear Bode plots suggest that the corresponding Mott-Schottky plots should likewise be linear, with minimal frequency dispersion and slopes that correctly reflect the measured dopant density and area of the p-InP electrodes. Accurate results of E_{fb} should therefore be extractable from these impedance data.

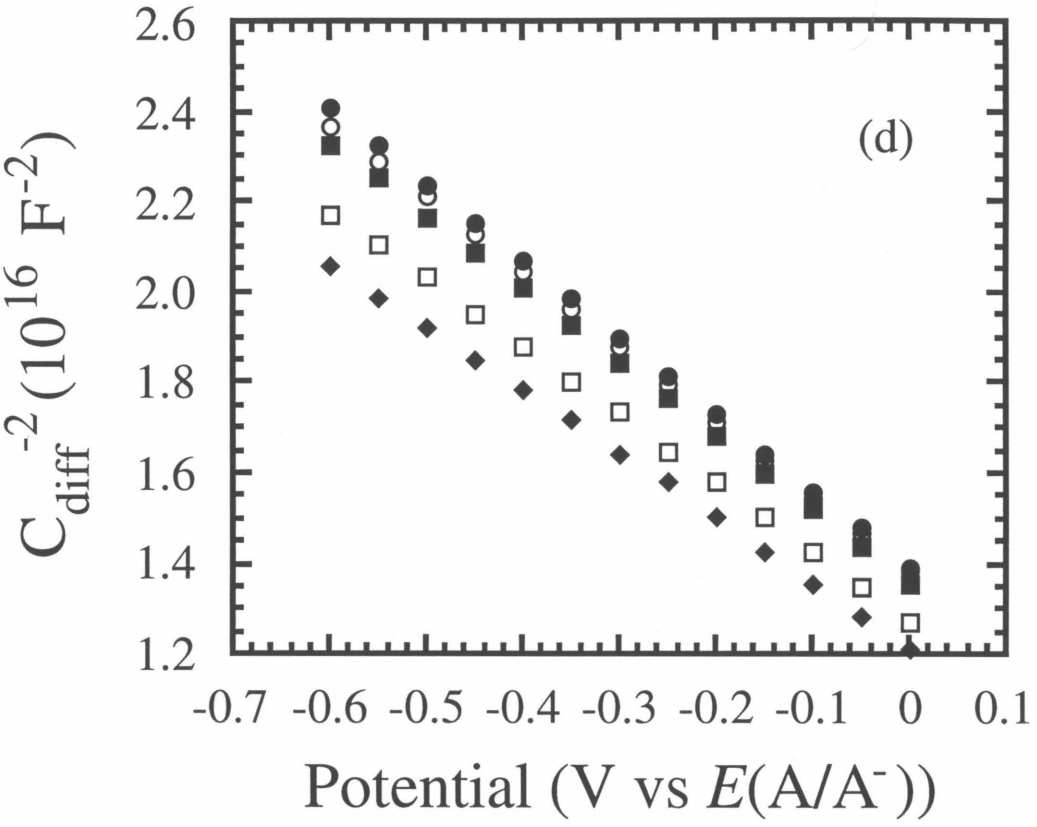
Figure 2 depicts representative Mott-Schottky plots of the p-InP/CH_3OH interface with the $Me_2Fc^{+/0}$, $TMPD^{+/0}$, $DCEV^{2+/+}$, and $MV^{2+/+}$ redox couples. Each plot shows the capacitance data derived from five different measurement frequencies, equally spaced on a logarithmic scale among the range of 1.0 kHz to 25.1 kHz. Slight frequency dispersion of the capacitance values is evident, and in some cases the measurements

Figure 2. Mott-Schottky plots of the p-InP/CH_3OH interface. Each plot shows five different measuring frequencies that span from 1.0 kHz to 25.1 kHz. Each cell solution consisted of 10 mM acceptor and 10 mM donor. The redox couples for each plot were (a) $Me_2Fc^{+/0}$; (b) $TMPD^{+/0}$; (c) $DCEV^{2+/+}$; and (d) $MV^{2+/+}$.


2.4
2.2
2.0
1.8
1.6
1.4
1.2
1.0
(a)
C_{diff}^{-2} (10^{16} F^{-2})
-0.9 -0.8 -0.7 -0.6 -0.5 -0.4 -0.3 -0.2 -0.1
Potential (V vs $E(A/A^-)$)


3.5
3.0
2.5
2.0
1.5
1.0
(b)
C_{diff}^{-2} (10^{16} F^{-2})
-0.9 -0.8 -0.7 -0.6 -0.5 -0.4 -0.3 -0.2 -0.1
Potential (V vs $E(A/A^-)$)


2.4
2.2
2.0
1.8
1.6
1.4
1.2
1.0
C_{diff}^{-2} (10^{16} F^{-2})
(c)
-0.7 -0.6 -0.5 -0.4 -0.3 -0.2 -0.1 0 0.1
Potential (V vs $E(A/A^-)$)


2.6
2.4
2.2
2.0
1.8
1.6
1.4
1.2
C_{diff}^{-2} (10^{16} F^{-2})
(d)
-0.7 -0.6 -0.5 -0.4 -0.3 -0.2 -0.1 0 0.1
Potential (V vs $E(A/A^-)$)

produced obvious outlying data points (see Figure 2b), which were discarded from the Mott-Schottky analysis. Regression of C_{diff}^{-2} against E indicated excellent linearity, with correlation coefficients always exceeding 0.999. The slopes of the linear fits agreed within 20% with the slopes expected from independent knowledge of the dopant density and electrode area. For example, the average regression slope of the five curves in Figure 2a was 1.8092×10^{16} F^{-2} V^{-1}. Since the electrode area for this particular cell was 0.080 cm^2, this slope predicts a dopant density of 9.82×10^{17} cm^{-3}, in accord with the measured dopant density of 1.1×10^{17} cm^{-3}.

Although the Mott-Schottky data points appeared to vary with frequency, the regression fits tended to converge at their x-intercepts, thus reducing the scatter of the extracted E_{fb} values. For the data presented in Figure 2a-d, the x-intercepts of the linear extrapolations fell within ranges of 13, 48, 26 and 40 mV, respectively. Under the frequency conditions stated above, the typical spread of the x-intercepts for all junctions was 40 to 50 mV. The barrier heights calculated from eqs 6 and 7 were combined to yield an average and standard deviation for each p-InP/CH_3OH junction. Initially, the barrier height values derived from the five different measurement frequencies were incorporated to give an average for a given cell. The average barriers of all cells of a given redox couple solution were then merged into a final average and standard deviation. These results are presented in Table I. Standard deviations of the barrier heights of the p-InP/CH_3OH interface were on the order of 10-20 mV, which is comparable to the analogous values found from previous applications of this experimental method.

Knowledge of the barrier height establishes the band edge positions of the semiconductor, since the solution potential can serve as an electrochemical reference point. However, the invariance of the band edge positions must be confirmed prior to any undertaking of rate constant measurements. Band edges that apparently shift depending on the solution potential confound the kinetic analysis because the first-order dependence of

the current density on the donor concentration is confirmed by holding the acceptor concentration constant while increasing the donor concentration by one order of magnitude. A shifting valence band edge would result in different hole-transfer rate constants at different redox concentrations. For the $Me_2Fc^{+/0}$ and $TMPD^{+/0}$ redox couples, the concentration ratio was varied from 10 mM donor and 10 mM acceptor (Figures 2a and 2b) to 100 mM donor and 10 mM acceptor, which shifted the Nernstian solution potential negatively by 59 mV. As with the cells of lower donor concentration, the Mott-Schottky measurements on the cells of higher concentration displayed some frequency dispersion in the data, but the linear extrapolations tended to converge at the x-intercepts. Using eq 6, the slopes of the regression fits again predicted dopant densities that were within 20% of the measured values. The energetic results for the solutions of higher donor concentration are provided in Table I. While the barrier heights at higher concentration appear to be larger than those at lower concentration, the increases in barrier height are only 24 mV for p-InP/CH_3OH-$Me_2Fc^{+/0}$ and 14 mV for p-InP/CH_3OH-$TMPD^{+/0}$, incommensurate with the 59-mV shift in $E(A/A^-)$. These nonideal shifts suggest band-edge movement for the p-InP/CH_3OH system.

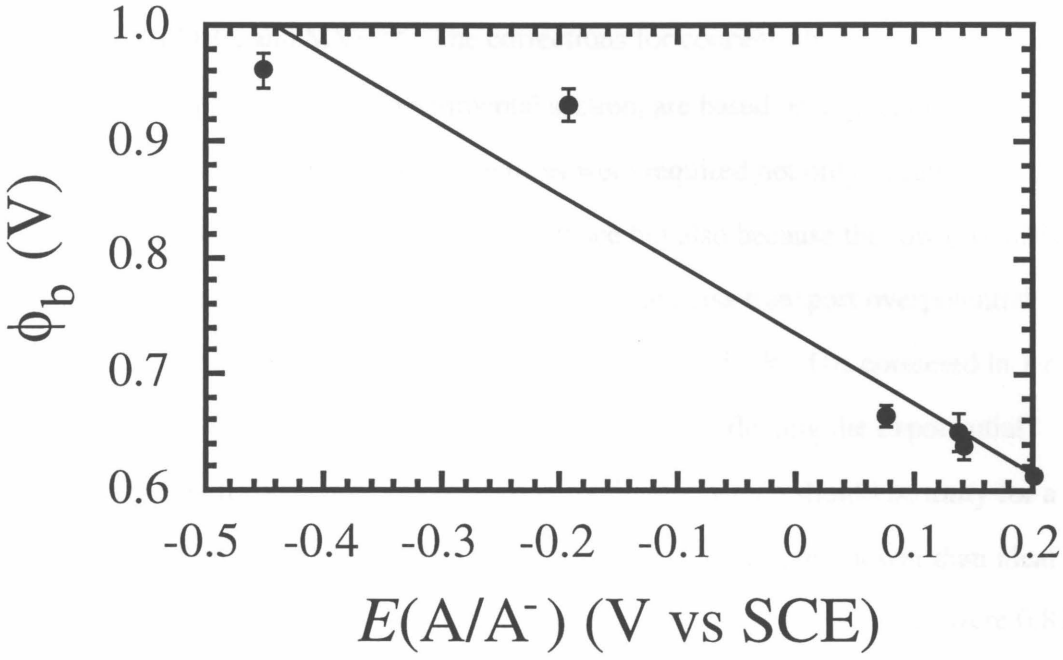
The degree of band-edge movement is illustrated vividly by Figure 3, which plots the entire set of ϕ_b results against $E(A/A^-)$. In the "ideal" case, whereby the equilibration of electrochemical potentials is accomplished solely by depletion of dopant charges, any negative shift in the solution potential induces an equivalent increase in the barrier height, assuming a p-type semiconductor. Ideal energetic control by the solution is hence observed as a slope of unity in the ϕ_b vs $E(A/A^-)$ trend. While the plot in Figure 3 does indicate some dependence of ϕ_b on $E(A/A^-)$, this response is nonideal. Linear regression analysis of these data produced a slope of -0.600 ± 0.085 and a correlation coefficient of 0.962. These energetic characteristics preclude a straightforward determination of hole-transfer rate constants at the p-InP/CH_3OH interface.

Table I. Barrier height results for p-InP/CH_3OH interfaces

Redox couple	Barrier height at $[A^-]$ = 10 mM (mV) [a]	Barrier height at $[A^-]$ = 100 mM (mV) [a]
$Me_2Fc^{+/0}$	615 ± 14	639 ± 12
$TMPD^{+/0}$	651 ± 17	665 ± 10
$DCEV^{2+/+}$	933 ± 14	------- [b]
$MV^{2+/+}$	963 ± 15	------- [c]

Each barrier height result represents an average and a standard deviation of four to eight different ϕ_b values. [a] Each cell solution contained 10 mM of the acceptor. [b] The first-order dependence of the current density on the donor concentration was tested by increasing the concentrations of both redox forms by the same proportion. [c] Not performed to date.

Figure 3. A plot of the barrier height vs the Nernstian solution potential. Each point represents an average of four to eight ϕ_b values, and the indicated error bars are the associated standard deviations. The linear regression slope was -0.600 ± 0.085, and the correlation coefficient of the fit was 0.962.


1.0
0.9
0.8
0.7
0.6
ϕ_b (V)
-0.5
-0.4
-0.3
-0.2
-0.1
0
0.1
0.2
$E(A/A^-)$ (V vs SCE)

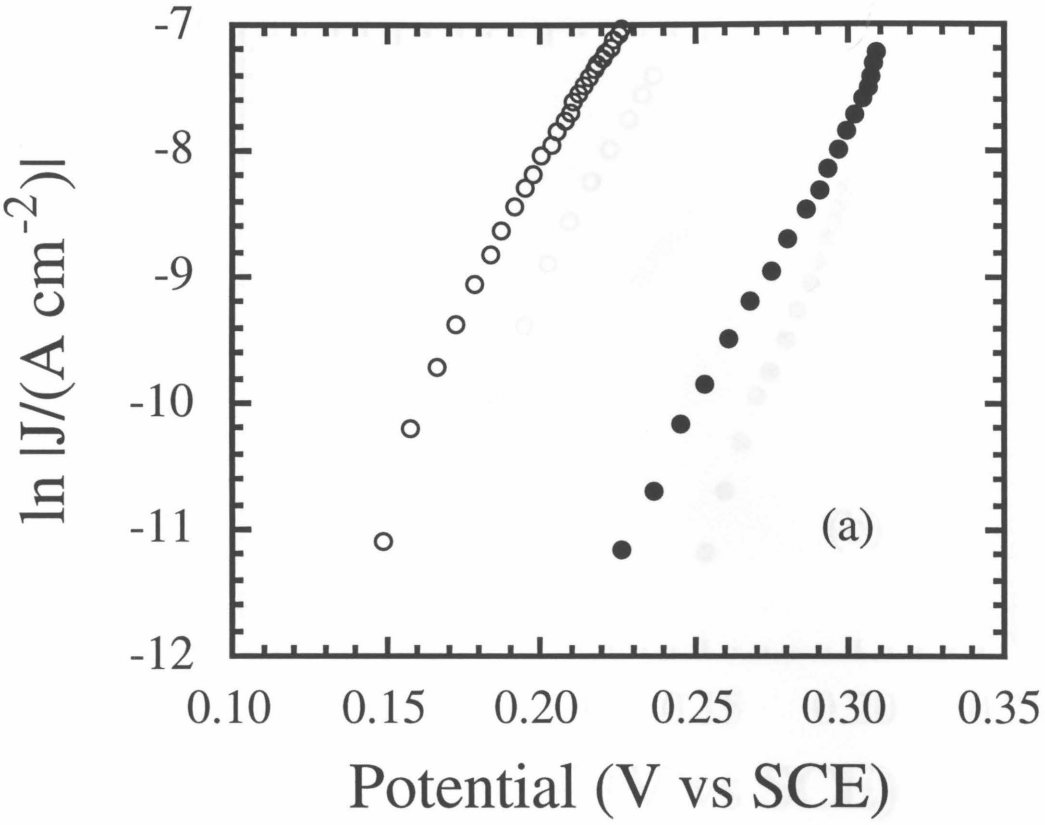
B. J-*E* Data for p-InP/CH_3OH Contacts

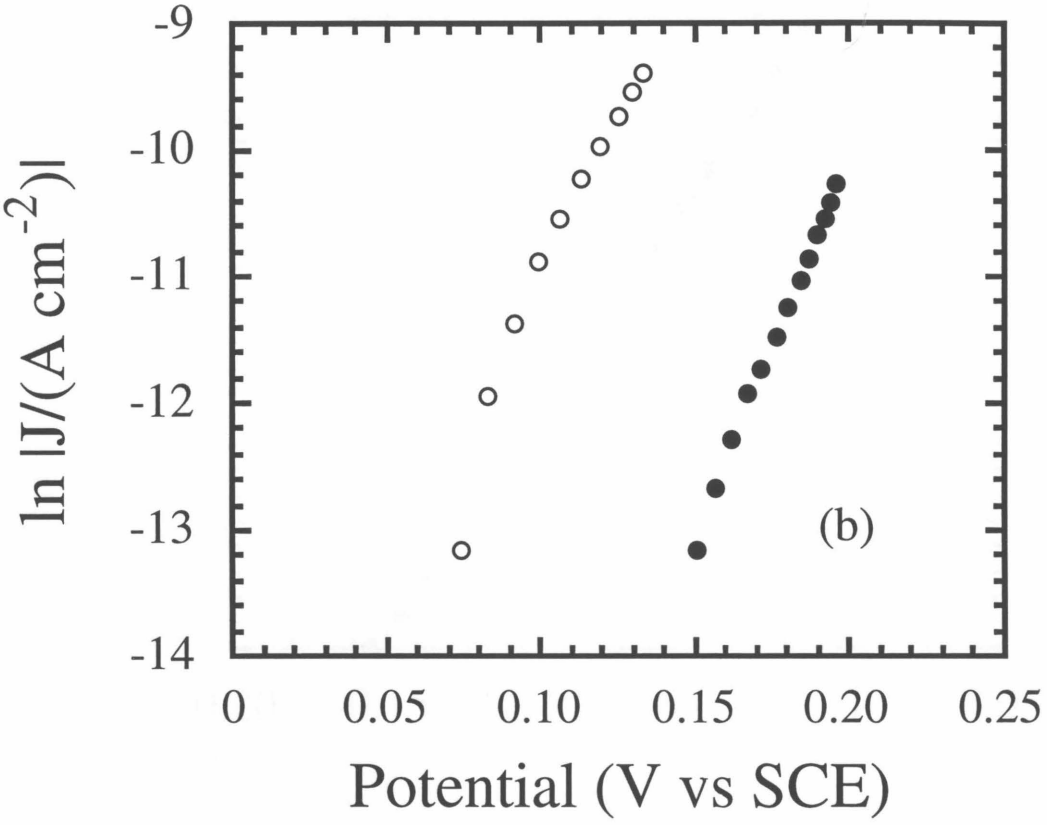
Every p-InP/CH_3OH interface exhibited rectifying J-*E* behavior, with a limiting value for the cathodic current density and an approximately exponentially increasing anodic current density as *E* was made more positive. Consistent with previous work on interfacial kinetics,[1] the current density was not limited by mass transport, as evidenced by the significantly larger currents observed at a Pt electrode in the same redox solution.

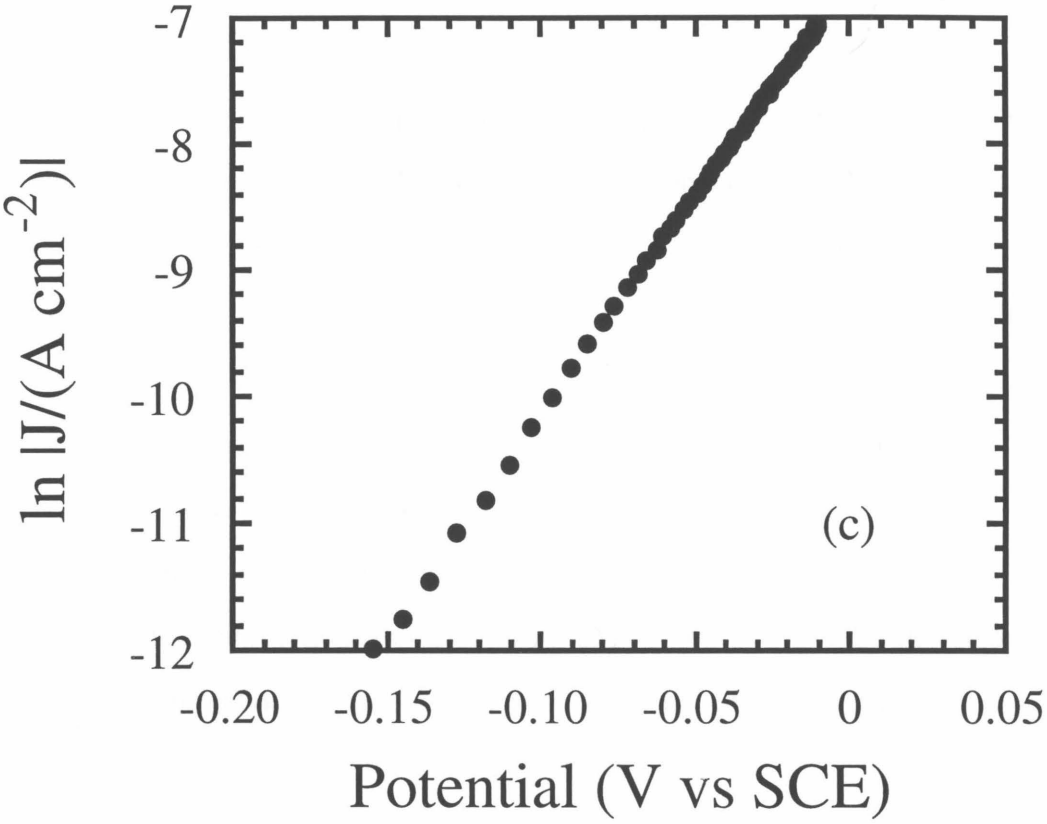
Figure 4 shows the ln |J| vs E_{corr} data for the p-InP/CH_3OH junctions with $Me_2Fc^{+/0}$, $TMPD^{+/0}$, and $MV^{2+/+}$. The corrections for concentration overpotential and cell resistance, explained in the Experimental section, are based on conventional electrochemical protocols.[21] These corrections were required not only because the nonaqueous solvent had a significant cell resistance but also because the low (10 mM) concentrations of redox species imposed nonnegligible mass-transport overpotential corrections at the highest current densities accessed in this work. The corrected ln J-*E* data yielded linear trends over most of the forward bias range, reflecting the exponential character expected for a diode. The diode quality factors, which should be unity for a purely exponentially increasing current in forward bias, were slightly lower than ideal but nonetheless roughly unity. For the curves depicted in Figure 4, the γ values were 0.87 and 0.97 for $Me_2Fc^{+/0}$, 0.90 and 1.03 for $TMPD^{+/0}$, and 1.09 for $MV^{2+/+}$. As there is no known recombination mechanism that engenders a diode quality factor of less than unity, it is probable that the corrections of *E* for overpotential and resistance effects may have introduced a residual systematic error into the J-E_{corr} curves. The diode quality factor can be interpreted as the reaction order of the surface electron concentration in determining the reaction rate, with a quality factor of 1.0 indicating a first-order kinetic dependence on n_s.

Figures 4a and 4b also depict the changes in the ln |J|-E_{corr} data for the p-InP/CH_3OH-$Me_2Fc^{+/0}$ and p-InP/CH_3OH-$TMPD^{+/0}$ junctions in response to a variation in the concentration of the donor species A^-. If the rate law of eq 1 were obeyed, increasing

Figure 4. Dark ln J-E_{corr} characteristics for representative p-InP/CH_3OH junctions. Parts (a) and (b) each depict the shift in potential as [A] is held constant at 10 mM and [A^-] is increased from 10 mM (filled circles) to 100 mM (open circles). For clarity, the potential is referenced to SCE. As mentioned in the text, a tenfold higher [A^-] with fixed [A] should decrease the potential vs SCE by 59 mV that is needed to obtain a given current density. (a) The redox couple was $Me_2Fc^{+/0}$. (b) The redox couple was $TMPD^{+/0}$. (c) The redox couple was $MV^{2+/+}$. The kinetic dependence on [MV^+] was not performed.


-7
-8
-9
-10
-11
-12
ln |J/(A cm-2)|
0.10
0.15
0.20
0.25
0.30
0.35
Potential (V vs SCE)
(a)

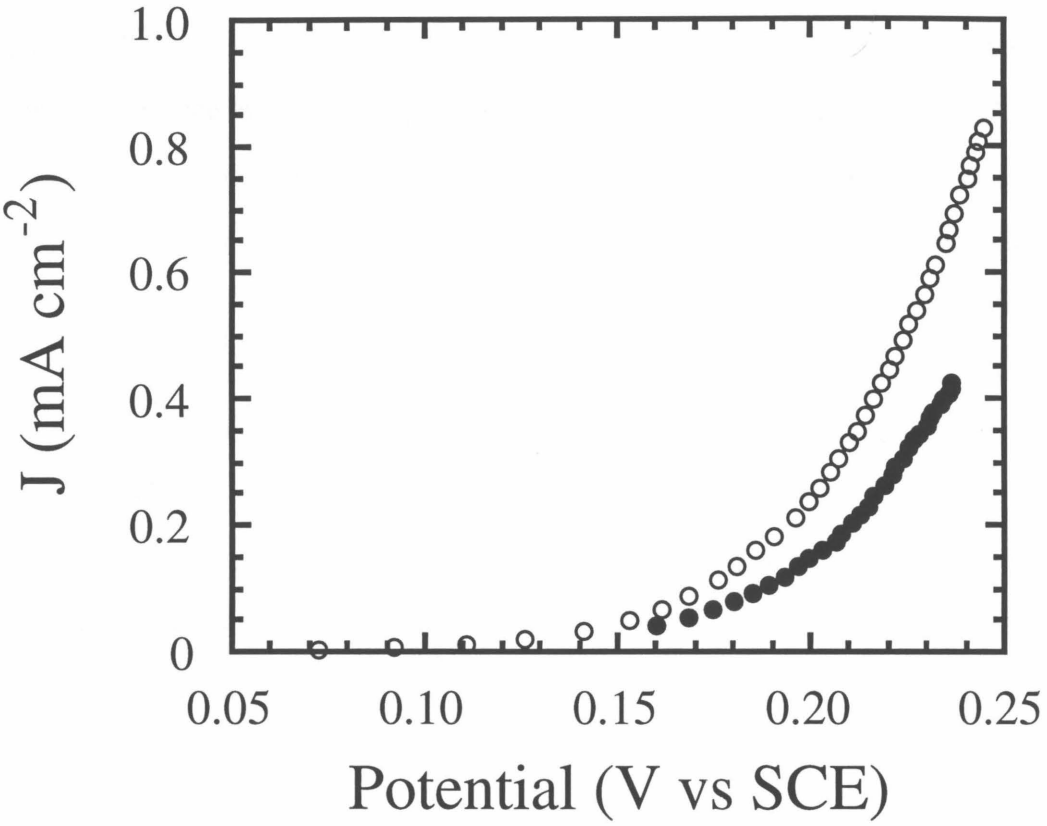

-9
-10
-11
-12
-13
-14
ln |J/(A cm-2)|
0
0.05
0.10
0.15
0.20
0.25
Potential (V vs SCE)
(b)


-7
-8
-9
-10
-11
-12
ln |J/(A cm-2)|
(c)
-0.20
-0.15
-0.10
-0.05
0
0.05
Potential (V vs SCE)

the acceptor concentration by a factor of 10 should decrease the value of E_{corr} vs a fixed reference, such as SCE, by (kT/q)(ln 10) = 59 mV needed to obtain a given current density. This behavior was observed neither for the p-InP/CH_3OH-$Me_2Fc^{+/0}$ nor for the p-InP/CH_3OH-$TMPD^{+/0}$ junction, as the potential response upon a tenfold increase in [A^-] was roughly 90 mV for both systems. This excessive shift is unlikely to be representative of a system dominated by direct hole transfer from the valence band of the semiconductor to the redox donor.

A different tactic for establishing [A^-] dependence was taken with the $DCEV^{2+/+}$ solution. Because of possible solubility limits of the monocation radical in CH_3OH, the donor concentration was not taken to 100 mM. Instead, the concentrations of both redox forms were augmented from 10 mM to 55 mM. In this case, the barrier height should remain constant, since the Nernstian potential is invariant, but the currents at all applied potentials should increase by a factor of 5.5 if in fact hole transfer from the semiconductor dominates the observed recombination currents. Figure 5 illustrates the effect of the total redox concentration on the observed kinetics for a sample p-InP/CH_3OH-$DCEV^{2+/+}$ contact. For the cell solution consisting of 10 mM donor ($DCEV^+$) and 10 mM acceptor ($DCEV^{2+}$), a current density of 0.43 mA cm^{-2} was obtained at the highest potential of 0.237 V vs SCE. For the solution of 55 mM donor and 55 mM acceptor, the current denisty at the identical applied potential was 0.68 mA cm^{-2}. Despite the invariance of the barrier height, as ϕ_b = 0.959 mV in the dilute solution and ϕ_b = 0.963 mV in the concentrated solution, the kinetics did not scale concomitantly with concentration, even after overpotential and cell resistance corrections were included. These results provide evidence against a direct hole-transfer mechanism at the p-InP/CH_3OH-$DCEV^{2+/+}$ junction.

Figure 5. Dark J-E_{corr} data for the p-InP/CH_3OH-$DCEV^{2+/+}$ system, illustrating the kinetic dependence on the total redox concentration. The filled circles indicate the current densities at a p-InP electrode in a solution of 10 mM $DCEV^{2+}$, 10 mM $DCEV^{+}$, and 1.00 M LiCl. The open circles indicate the current densities at the same electrode in a solution of 55 mM $DCEV^{2+}$, 55 mM $DCEV^{+}$, and 1.00 M LiCl. In both solutions, $E(A/A^{-})$ was -0.194 V vs SCE.


1.0
0.8
0.6
0.4
0.2
0
J (mA cm-2)
0.05
0.10
0.15
0.20
0.25
Potential (V vs SCE)

V. DISCUSSION

The results presented on the p-InP/CH_3OH interface appear incompatible with the ideal model of direct hole transfer from the semiconductor to the solution. The characterization of junction energetics was successfully accomplished by differential capacitance techniques; the quality of these data is notable in light of the frequency dispersion that has traditionally plagued such measurements on the semiconductor/liquid interfaces.[23-27] However, the junction energetics *per se* suggest the presence of electrical traps at the surface of the semiconductor. The nonideal dependence of ϕ_b on $E(A/A^-)$, specifically its slope of -0.60 instead of the expected -1.0, implies that other sources of charge participate in the initial equilibration of electrochemical potentials. Regarding the kinetic data, the diode quality factors were roughly unity, suggesting not only that the observed anodic current density has a simple exponential dependence on the applied potential, but also that the interfacial charge flux has a first-order dependence on the surface hole concentration. Unfortunately, this charge flux does not exhibit a first-order dependence on the donor concentration. In order to maintain a constant current density, the potentials at the p-InP/CH_3OH-$Me_2Fc^{+/0}$ and p-InP/CH_3OH-$TMPD^{+/0}$ cells shifted by approximately 90 mV in response to a tenfold increase in the donor concentration, significantly higher than the 59 mV shift expected under conditions of interfacial hole transfer. Increasing the concentrations of both redox forms while holding constant their ratio and thus the Nernstian solution potential likewise did not elicit proportionally larger current densities, as evidenced by the experiments on the p-InP/CH_3OH-$DCEV^{2+/+}$ junction.

The present results may be placed in the context of prior work on InP in contact with nonaqueous solutions. Pomykal and Lewis observed that for the n-InP/CH_3OH-ferrocene$^{+/0}$ interface, a change in the acceptor concentration seemed to shift the positions of the band edges.[8] The band-edge movement was attributed to possible surface state

charging or carrier inversion. Segar and Koval reported that the etching procedure for p-InP in contact with acetonitrile solutions greatly influenced its electrochemical behavior.[15] Electrodes treated with an HCl-CH_3OH etch yielded severe irreproducibility in the E_{fb} determinations due to the presence of hydrocarbon and indium oxide contamination on the surface.[15] Another etch[28] based on separate solutions of Br_2 in CH_3OH and aqueous NH_3 produced surfaces with submonolayer quantities of indium phosphates and indium hydroxides, but negligible hydrocarbons.[16] Electrochemical cells using p-InP electrodes treated with the latter protocol resulted in stable, linear Mott-Schottky plots.[15] The interfacial energetics of such junctions were discovered to be controlled by the filling of empty surface states, which are present throughout the p-InP bandgap at a density of 10^{12} cm^{-2} V^{-1}, by the redox donor.[16] Consequently, even in the case of optimal surface conditions, electrical traps dictate the energetic behavior of the interface between p-InP and a nonaqueous solution. The work presented in this chapter is fully consistent with these previous findings, as it appears that surface states play a dominant role in the electrochemistry of the p-InP/CH_3OH interface.

VI. SUMMARY

Attempts to compare the electron-transfer rate constants at n-InP/CH_3OH junctions with the hole-transfer rate constants at p-InP/CH_3OH contacts were unsuccessful. Differential capacitance measurements provided well-behaved Mott-Schottky plots, but the interfacial energetics exhibited nonideality and suggested the presence of surface electrical traps. Similar information was obtained from the kinetic studies, which indicated a roughly first-order dependence of the anodic current density on the surface hole concentration but relative independence of the current density on the donor concentration.

VI. ACKNOWLEDGMENT

This research was supported by the Department of Energy, Office of Basic Energy Sciences, Fundamental Interactions Branch.

VII. REFERENCES

(1) Fajardo, A. M.; Lewis, N. S. *J. Phys. Chem. B* **1997**, *101*, 11136.

(2) Morrison, S. R. *Surf. Sci.* **1969**, *15*, 363.

(3) Morrison, S. R. *Electrochemistry at Semiconductor and Oxidized Metal Electrodes*; Plenum: New York, 1980.

(4) Lewis, N. S. *Annu. Rev. Phys. Chem.* **1991**, *42*, 543.

(5) Marcus, R. A. *J. Phys. Chem.* **1991**, *95*, 2010.

(6) Ibach, H.; Luth, H. *Solid-State Physics*; Springer Verlag: Berlin, 1990.

(7) Koval, C. A.; Howard, J. N. *Chem. Rev.* **1992**, *92*, 411.

(8) Pomykal, K. E.; Lewis, N. S. *J. Phys. Chem. B* **1997**, *101*, 2476.

(9) Sze, S. M. *Physics of Semiconductor Devices;* 2nd ed.; Wiley: New York, 1981.

(10) Dominey, R. N.; Lewis, N. S.; Wrighton, M. S. *J. Am. Chem. Soc.* **1981**, *103*, 1261.

(11) Heben, M. J.; Kumar, A.; Zheng, C.; Lewis, N. S. *Nature* **1989**, *340*, 621.

(12) Koval, C. A.; Austermann, R. L.; Turner, J. A.; Parkinson, B. A. *J. Electrochem. Soc.* **1985**, *132*, 613.

(13) Koval, C. A.; Austermann, R. L. *J. Electrochem. Soc.* **1985**, *132*, 2656.

(14) Schefold, J. *J. Electroanal. Chem.* **1993**, *362*, 97.

(15) Segar, P. R.; Koval, C. A. *J. Electrochem. Soc.* **1988**, *135*, 2655.

(16) Segar, P. R.; Koval, C. A.; Koel, B. E.; Gebhard, S. C. *J. Electrochem. Soc.* **1990**, *137*, 544.

(17) Royea, W. J.; Krüger, O.; Lewis, N. S. *J. Electroanal. Chem.* **1997**, *438*, 191.

(18) Rosenbluth, M. L.; Lewis, N. S. *J. Am. Chem. Soc.* **1986**, *108*, 4689.

(19) Hünig, S.; Schenk, W. *Liebigs Ann. Chem.* **1979**, 727.

(20) Bird, C. L.; Kuhn, A. T. *Chem. Soc. Rev.* **1981**, *10*, 49.

(21) Bard, A. J.; Faulkner, L. R. *Electrochemical Methods: Fundamentals and Applications*; Wiley: New York, 1980.

(22) Sah, C.-T. *Fundamentals of Solid-State Electronics*; World Scientific: River Edge, NJ, 1991.

(23) Tomkiewicz, M. *Electrochim. Acta* **1990**, *35*, 1631.

(24) Nagasubramanian, G.; Wheeler, B. L.; Fan, F.-R. F.; Bard, A. J. *J. Electrochem. Soc.* **1982**, *129*, 1742.

(25) Nagasubramanian, G.; Wheeler, B. L.; Bard, A. J. *J. Electrochem. Soc.* **1983**, *130*, 1680.

(26) Nagasubramanian, G.; Wheeler, B. L.; Hope, G. A.; Bard, A. J. *J. Electrochem. Soc.* **1983**, *130*, 385.

(27) Kobayashi, H.; Takeda, N.; Sugahara, H.; Tsubomura, H. *J. Phys. Chem.* **1991**, *95*, 813.

(28) Aspnes, D. E.; Studna, A. A. *Appl. Phys. Lett.* **1981**, *39*, 316.